CHEMICAL STUDIES OF PLASMA ETCHANTS USED IN INTEGRATED CIRCUIT MANUFACTURE

DAVID CHARLES WILLIAM BLAIKLEY

A Thesis submitted for the Degree of

Doctor of Philosophy

THE UNIVERSITY OF ASTON IN BIRMINGHAM

October 1991

THE UNIVERSITY OF ASTON IN BIRMINGHAM

Chemical Studies of Plasma Etchants used in Integrated Circuit Manufacture

A Thesis submitted for the Degree of Doctor of Philosophy

David Charles William Blaikley

1991

SUMMARY

Plasma or "dry" etching is an essential process for the production of modern microelectronic circuits. However, despite intensive research, many aspects of the etch process are not fully understood. The results of studies of the plasma etching of Si and SiO_2 in fluorine-containing discharges, and the complementary technique of plasma polymerisation are presented in this thesis. Optical emission spectroscopy with argon actinometry was used as the principle plasma diagnostic.

Statistical experimental design was used to model and compare Si and SiO_2 etch rates in CF_4 and SF_6 discharges as a function of flow, pressure and power. Etch mechanisms in both systems, including the potential reduction of Si etch rates in CF_4 due to fluorocarbon polymer formation, are discussed. Si etch rates in CF_4/SF_6 mixtures were successfully accounted for by the models produced. Si etch rates in CF_4, C_2F_6 and CHF_3 as a function of the addition of oxygen-containing additives (O_2, N_2O and CO_2) are shown to be consistent with a simple competition between F, O and CF_x species for Si surface sites. For the range of conditions studied, SiO_2 etch rates were not dependent on F-atom concentration, but the presence of fluorine was essential in order to achieve significant etch rates.

The influence of a wide range of electrode materials on the etch rate of Si and SiO_2 in CF_4 and CF_4/O_2 plasmas was studied. It was found that the Si etch rate in a CF_4 plasma was considerably enhanced, relative to an anodised aluminium electrode, in the presence of soda glass or sodium or potassium "doped" quartz. The effect was even more pronounced in a CF_4/O_2 discharge. In the latter system lead and copper electrodes also enhanced the Si etch rate. These results could not be accounted for by a corresponding rise in atomic fluorine concentration. Three possible etch enhancement mechanisms are discussed.

Fluorocarbon polymer deposition was studied, both because of its relevance to etch mechanisms and its intrinsic interest, as a function of fluorocarbon source gas (CF_4, C_2F_6, C_3F_8 and CHF_3), process time, RF power and percentage hydrogen addition. Gas phase concentrations of F, H and CF_2 were measured by optical emission spectroscopy, and the resultant polymer structure determined by X-ray photoelectron spectroscopy and infrared spectroscopy. Thermal and electrical properties were measured also. Hydrogen additions are shown to have a dominant role in determining deposition rate and polymer composition. A qualitative description of the polymer growth mechanism is presented which accounts for both changes in growth rate and structure, and leads to an empirical deposition rate model.

Keywords: Plasma etch, plasma polymerisation, silicon, silicon dioxide, optical emission spectroscopy.

ACKNOWLEDGEMENTS

I am indebted to the United Kingdom Atomic Energy Authority for funding the work contained within this thesis.

I should like to thank both my university supervisors, Drs. S.J. Moss and M.S. Beevers, and my industrial supervisors, Professor J.A. Cairns (University of Dundee, formerly at Harwell Laboratory) and Dr. A. Atkinson (Harwell Laboratory) for their support, encouragement and valuable advice. I wish to express my particular gratitude to Dr. Moss for his thoughtful supervision and teaching through the full duration of this project.

I also thank Mr. C.M. Kemp for laboratory assistance during the first year of these studies, and Mr. V. Moore (Harwell Laboratory) and Dr. J.A. Busby (Johnson Matthey Technology Centre, Sonning Common) for X-ray photoelectron spectroscopy analyses.

CONTENTS

List of Tables

List of Figures

CHAPTER 1 - INTRODUCTION

1.1 Introduction

The discovery of the transistor by John Bardeen and Walter Brattain in 1947 at the Bell Telephone Laboratories, and its subsequent development by William Shockley, laid the foundation for the development of microelectronic circuits. The term transistor refers to a solid-state device, usually manufactured from silicon, which is capable of signal amplification - a property previously only associated with thermionic valves. The reductions in weight, size, power consumption and component cost achieved by the use of transistors encouraged the solid-state revolution[1, 2].

Demands for further miniaturisation of electronic components particularly for military and aerospace applications led to the conception of the integrated circuit or "chip" by Harwich Johnston of the RCA and its development in the late 1950's by Fairchild Inc. engineers. An integrated circuit may be formally defined as a circuit which is fabricated as an assembly of electronic elements in a single structure, which cannot be subdivided without destroying its intended function. The dramatic developments made possible by the introduction of this technology are exemplified by comparing two state-of-the-art computers - a 1958 Ferranti Mercury (transistor based) and a 1987 Cray 2 supercomputer. The former took 180 μs to perform an addition, required a subroutine to perform a division, and had only a 5 kbyte memory. The Cray, however, has a 4.1 ns clockcycle and 2 Gbyte memory[3]. Indeed, even most current (1990) personal computers can outperform the 1958 Ferranti mainframe by two orders of magnitude in both speed and internal memory, e.g. IBM PS/2 Model 80: 25 MHz, 4 MB RAM.

The integrated circuit has gone through various levels of complexity[4]:

SSI	Small Scale Integration	($10 - 10^2$ transistors)
MSI	Medium Scale Integration	($10^2 - 10^3$ ")
LSI	Large Scale Integration	($10^3 - 10^5$ ")
VLSI	Very Large Scale Integration	($10^5 - 10^6$ ")
ULSI	Ultra Large Scale Integration	($>10^6$ ")

Such advances have been achieved both by increasing the size of the integrated circuit, and by shrinking, or scaling, the device features thus increasing the number of transistors per unit area. These points are illustrated in Table 1 which summarises a recent review by Motorola engineers[5]. It is clear that they foresee no immediate limit to circuit complexity.

Table 1. Past and predicted integrated circuit complexity.

Date	**1984**	**1987**	**1988**	**1990**	**1993**	**1995**
Geometry (μm)	2	1.5-2	1.0	0.8-0.6	0.6-0.5	0.5-0.25
Die Size (mm)	9	12.5	14	15	16	17.5
Transistors (x1000)	190	750	1000	3000	6000	15000

Similarly, Hitachi, who currently (1990) use a minimum 0.8 μm feature size to manufacture 4-megabit DRAM (Dynamic Random Access Memory) chips, plan to use a 0.5 μm feature size to manufacture 16-megabit DRAMS in 1992[6].

Such progress in integrated circuit technology has only been possible through similar advances in manufacturing processes. One recently developed process that is now almost universally used in integrated circuit manufacture, and which is essential for the production of sub 4 μm feature sizes is plasma etching. Aspects of the chemistry of plasma etching silicon and silicon dioxide are the subject of part of this thesis.

This chapter first considers why plasma etching is essential for the production of sub 4 μm features, then outlines the basic physics of plasma etching before reviewing the chemistry of silicon and silicon dioxide etching. It is shown that PTFE-like fluoropolymers, which are often produced during etching, play a crucial role in determining etch rate, selectivity and anisotropy. Not only for this reason, but also because these polymers may have commercial value in their own right, plasma polymerisation is considered. Finally, the topics investigated in this thesis are outlined.

1.2 The Requirement for Plasma Etching

Before defining the term plasma etching and considering reasons for its requirement, it is useful to consider some of the elementary steps in integrated circuit manufacture. Some of the most commonly encountered circuit elements are shown in cross section in figure 1: (a) a NPN bipolar transistor; (b) a MOS (metal-oxide-silicon) transistor; and (c) a CMOS (Complementary-metal-oxide-silicon) transistor pair. A

CMOS pair consists of linked n- and p-type transistors and offers significant advantages in power dissipation over conventional MOS integration.

Figure 1. *Typical integrated circuit transistor types.*[7]

It can be seen that each transistor consists of a silicon substrate upon which there is a series of patterned layers of insulating and conducting materials. The layers can be applied in a number of ways including diffusion, ion implantation, chemical vapour deposition, physical vapour deposition and epitaxy. After each film is deposited, lithography and etching are used to define a circuit pattern, a succession of which builds up the complete device. The steps required for patterning each layer are essentially similar, and may be summarised as shown in figure 2[8] :-

Step 1 The film on the substrate is coated with photoresist.

Step 2 Ultraviolet light is applied through a mask; exposed regions undergo reactions, while unexposed regions are unchanged.

Step 3 Photoresist is developed by removing (or leaving) the portions exposed to light.

Step 4 The film is patterned by etching away those parts not protected by photoresist.

Step 5 The photoresist is removed, leaving the desired pattern on the film.

Figure 2. Plasma etching.

Photoresists are usually polymeric materials, containing radiation sensitive groups, which are spin-coated onto the substrate. As has been hinted in Step 3 above, they may be of two types: positive, which are rendered soluble by radiation (usually ultraviolet light); or negative which are rendered insoluble. Positive resists are used to fabricate the majority of VLSI and more complex devices[9, 10].

Most commercial positive photoresists use diazoquinone sensitisers as the photoactive component, and Novolac (cresol), or a derivative, as the film-forming resin. Exposure of the diazoquinone to ultraviolet light (350-450 nm) yields indenecarboxylic acid as the photolysis product. This product and the novolac are alkali soluble and may readily be removed during development. However, the Novolac solubility is limited by the unconverted photoactive component and these portions remain in place.

The minimum feature size which may be defined by such systems is about three times the wavelength of the radiation used, i.e. for ultraviolet light, about 1 μm. In reality this is hard to achieve with adequate resolution, mainly because of the reflectivity of the substrate, and diffraction effects at feature edges. Multilayer resist processes have been introduced in order to overcome this and other problems. It follows that shorter wavelength exposure systems are needed to define submicron features. Techniques using deep ultraviolet light (190-250 nm; provided by excimer lasers), electron beams and X-rays have been developed. Electron beam and X-ray lithography are capable of defining features a few nanometres in size.

Historically, wet-chemical etchants have been used to pattern those parts of the film not protected by photoresist. The technology potentially offers high etch rates, high film to substrate etch rate ratios and minimal substrate damage, together with relative simplicity of apparatus and therefore low capital costs. However, liquid etchants tend to

remove material in all directions with equal efficiency yielding an isotropic etch profile. This was not a problem for early integrated circuits, but for VLSI devices with feature sizes of 2 μm or less, i.e. features of an approximately similar size to the thickness of the film being etched, an anisotropic or directional etch is required in order to achieve adequate pattern transfer fidelity. This is possible with plasma or "dry" etching.

A plasma is defined as an ionised gaseous discharge in which there is no resultant charge, the number of positive and negative charges being equal, in addition to unionised molecules or atoms. Plasma etching occurs when chemically reactive species generated in the discharge, e.g. atomic fluorine, interact with a solid substrate, e.g. silicon to produce a volatile etch product, e.g. silicon tetrafluoride. This chemical process is often accompanied by, and assisted in a number of ways by ion bombardment.

The earliest application of plasmas for etching occurred in the 1960's with the use of oxygen plasmas to remove carbon-containing films (e.g. photoresist). By the middle of the decade, fluorine- and chlorine-containing discharges were being explored for etching silicon. The first patent describing the use of CF_4 and O_2 mixtures for etching silicon was filed in 1969 and granted in 1971[8].

1.3 Plasma Physics

A plasma has already been defined as a partially ionised gas with equal numbers of positive and negative charges. The positive charges are ions and the negative charges predominantly electrons, although in some discharges, e.g. SF_6, negative ions may be significant.

Plasma formation may most readily be understood by considering the case of a simple gas, argon, at reduced pressure and between two parallel electrodes. If a large negative potential is applied to one electrode whilst the other is held at earth potential, then the few free electrons that always exist are accelerated by the electric field and gain energy. These electrons may undergo elastic collisions with the neutral species (with no energy loss, due to the large mass difference), or, if they have sufficient energy, inelastic collisions such as excitation, causing the plasma to "glow", or ionisation. The newly produced electrons are also accelerated and ionise further neutrals. This is often referred to as a "cascade" or "avalanche" process.

The ions are accelerated towards the cathode, strike it and produce secondary electrons which sustain the process. If the applied voltage is high enough, the number of electrons and ions increases until an equipotential cloud - the plasma - is formed (figure 3). (Since the plasma is electrically conducting and neutral it tries to exclude any electric field from itself, as will be discussed.) There is a continuous loss of electrons and ions from the plasma. (Note that a third body, usually the chamber wall, is required for simple recombination of small species to occur.) As the plasma is equipotential the cascading process can only occur in the cathode sheath, and cannot generate enough ions to sustain the required secondary electron current. However, a sufficient number of

electrons within the plasma will have a high enough energy to assure the required ion generation rate.

Due to the large mass difference between electrons and ions, electrons attain much higher mean speeds and therefore also much higher temperatures than ions. Typical values[11] for an argon discharge are shown in table 2.

Table 2. Particle mass, speed and temperature values for an argon plasma.

Species	Mass (g)	Speed (ms^{-1})	Temperature (K)
Electron	9.1×10^{-28}	9.5×10^{5}	23200
Ion	6.6×10^{-23}	5.2×10^{2}	500
Neutral	6.6×10^{-23}	4.0×10^{2}	300

If an electrically isolated substrate were suspended in the plasma it would be struck by both ions and electrons. As the average speed of the electrons in a plasma is higher than that of the ions, and their concentrations are equal, the electron flux to the substrate will be higher than the ion flux. It will charge negatively until the two fluxes are equal. The substrate is then said to have developed a floating potential, V_f, which is negative with respect to the plasma potential, V_p. The potential difference V_p-V_f will repel electrons leaving a net positive charge, a sheath, around the substrate. There will therefore be fewer electrons to cause excitation by electron impact, and the plasma will glow less brightly - the substrate is surrounded by a dark space. Similarly, sheaths are formed at both electrodes (figure 3).

Figure 3. *Voltage distribution in a d.c. discharge.*[11]

If the cathode in a d.c. discharge were covered with an insulator, the insulator would start to charge positively (through neutralising positive ions) and the plasma would be extinguished at the threshold voltage.

At RF frequencies the ions (massive) may be regarded as stationary, and the electrons (light) as oscillating between, but not necessarily reaching, the electrodes. The electrons may gain sufficient energy in their oscillations to cause ionisation, removing the dependence on secondary electron emission. Further, the ionisation process becomes more efficient with increasing frequency allowing lower operating pressures. Most commonly a frequency of 13.56 MHz (an allocated frequency) is used.

At even higher, microwave (2450 MHz), frequencies the a.c. field cannot produce significant displacement of electrons or ions. For a given absorbed power density in the plasma the yield of ions, electrons and free radicals is significantly higher than at RF

frequencies[12]. As ion lifetimes are short with respect to free radicals, microwave systems are often used as a source of free radicals for the chemical etching of substrates downstream of the discharge. However, much lower operating pressures (10^{-5} torr) are possible with microwave discharges. Charged particle recombination then becomes slow with respect to diffusion and flow, and in this case ions may be magnetically or electrically extracted from the plasma, and made to impinge on the substrate at controlled energies[13].

Typical plasma characteristics of a parallel plate electrode system are given in table 3[8].

Table 3. Typical plasma characteristics.

Number density of ions and electrons	10^{8}-10^{11} cm^{-3}
Fractional degree of ionisation	10^{-6}-10^{-4}
Electron mean energy	0.1-10 eV
Ion and neutral mean energy	0.03-0.05 eV
Pressure	10^{-3}-10 torr
Electrode separation	1-10 cm
Frequency	50 kHz-50 MHz
Power dissipation	0.01-1 Wcm^{-3}

In most commercial RF plasma systems power is applied to the driven electrode via a blocking capacitor in order to protect the power supply. A d.c. self-bias then develops across the capacitor, the magnitude of the bias being inversely proportional to

the relative size of the two electrodes. Two geometric arrangements, viz. (i) equal area electrodes, and (ii) an asymmetric design with the driven electrode smaller than the ground electrode, are represented in figures 4(a) and (b) respectively[14], together with the instantaneous voltages and the time-averaged plasma potential.

Figure 4. *Voltage distributions in RF plasma discharges.*

The material to be etched may be placed on either the earthed or the driven electrode. Confusingly, the term plasma etching is used to describe not only dry etching in general, but also more specifically the case where the material is placed on the ground electrode of a parallel plate system. However, if it is on the smaller driven electrode in the asymmetric design this is referred to as Reactive Ion Etching (RIE). In RIE a combination of the asymetric design and the capacitive coupling of the power supply allows a significant negative d.c. self-bias to develop. Highly directional positive ion bombardment (present in either configuration) then plays a considerably more significant role in the etch processes.

1.4 Silicon and Silicon Oxide Etching in Fluorine-Containing Plasmas

1.4.1 Thermodynamics

It has already been noted that plasma etching is said to occur when chemically reactive species generated in a discharge interact with a solid substrate to produce a volatile etch product. The two necessary conditions for the *spontaneous* chemical etching of silicon are: (i) the formation of a volatile reaction product; and (ii) an exothermic reaction[15].

The volatility of a substance is controlled by its vapour pressure, P_v, with a temperature dependence given by[16]:

$$\log P_v = -\Delta H_v/2.3RT + \text{constant} \qquad (1.1)$$

where ΔH_v = heat of evaporation

R = gas constant = 8.314 $JK^{-1}mol^{-1}$

At first sight, it follows that if evaporation/desorption of an etch product was the sole criterion for successful etching, then lowering operating pressures and using elevated temperatures would be beneficial. In reality, it is the partial pressure of the product that is the key factor; this is reduced by reducing the residence time. Many other factors such as supply of reactant and photoresist damage must also be taken into account.

Returning to the specific case of silicon and considering possible volatile reaction products the following candidates, in table 4, may be identified[17]:

Table 4. *Boiling points of selected silicon compounds.*

Compound	Boiling point (°C)
SiH_4	-111.8
SiF_4	-86
$SiCl_4$	57.57
$SiBr_4$	154
SiI_4	287.5

Whilst the first three compounds may readily be considered volatile, this is also the case for $SiBr_4$ and SiI_4 which have vapour pressures of 10 and 7×10^{-3} torr respectively at room temperature, and considerably higher vapour pressures at elevated temperatures.

The other condition for spontaneous etching is that the volatile products must be more stable than the reactants products. Silicon is etched according to the complete reaction

$$Si + 4X \rightarrow SiX_4$$

where X (= H, F, Cl, Br, I) is supplied by the discharge.

The requirement is therefore for the breaking of an -Si-Si- bond in bulk silicon and the formation of an Si-X bond to be exothermic. Consideration of the bond strengths in diatomic molecules[17], table 5, shows that this is the case for all of the halogens. Thus as SiF_4 is the most volatile of the silicon halides, and its formation the

most exothermic it is not surprising that fluorine chemistry is frequently used for the plasma etching of silicon. However, chlorine chemistry is in fact most widely used due to control of other factors such as selectivity, anisotropy, damage etc.

Table 5. Selected silicon diatomic-bond strengths.

Bond	Bond strength ($kJ.mol^{-1}$)
Si-Si	226[18]
Si-O	465[18]
Si-H	298
Si-F	540
Si-Cl	456
Si-Br	343
Si-I	339

Atomic hydrogen is theoretically also a possible silicon etchant. However, the product, silane, though volatile is highly unstable in air:

$$SiH_4 + 2O_2 \rightarrow SiO_2 + 2H_2O \qquad \Delta H^{\circ}_{298} = -1279\ kJ.mol^{-1}$$

In contrast, while SiO_2 reacts with fluorine it cannot be spontaneously etched by other halogens. However, the plasma etching of SiO_2 by both chlorine and bromine is possible in the presence of ion bombardment, showing that non-equilibrium processes occur during plasma etching[18,19]. Finally, although thermodynamic equilibrium may specify the stable end products of a given reaction, it gives no indication of the reaction kinetics.

1.4.2 Fundamental Mechanisms of Silicon Etching

The plasma etching of silicon and its compounds in fluorine-containing plasmas to produce the stable, volatile etch product silicon tetrafluoride is the longest established plasma-etch technology. The mechanisms of silicon dry etching by fluorine in the presence and absence of ion bombardment have been studied extensively. Even so, disagreement as to the exact mechanism still exists. This section considers only the most instructive and significant of the voluminous published studies.

Coburn and Winters[20] used well-controlled ultra-high-vacuum experiments to study silicon etching with XeF_2 as a convenient residue free source of fluorine. A clean silicon surface was subjected to separate beams of Ar^+(450 eV) and XeF_2. The etch rates for each beam, measured by quartz crystal microbalance, were found to be relatively low (figure 5). However, the etch rate for both beams incident simultaneously far exceeded the sum of either individually. These experiments clearly showed both that spontaneous silicon etching occurred in the absence of ion bombardment (with SiF_4 as the only etch product), and that ion bombardment increased the etch rate by an order of magnitude indicating a synergistic effect.

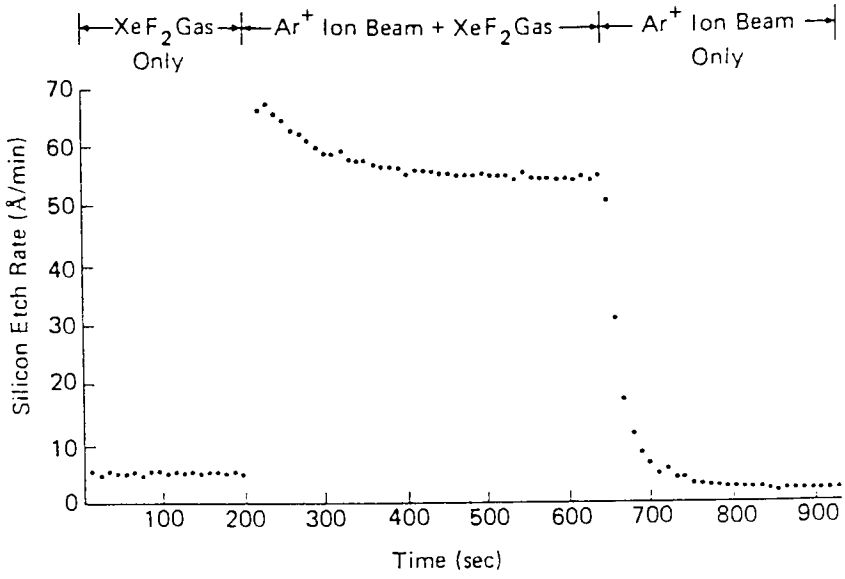

Figure 5. Ion-assisted gas surface chemistry.

Kay[21], and many others, have noted that results of this and similar experiments allow the connection between ion-enhanced etching and etch directionality to be understood. If, as in figure 6(a), a silicon surface was subjected to orthogonal ion bombardment through an opening in a mask, then physical sputtering would give a highly directional etch feature. Whereas neutral etchant species (F-atoms), figure 6(b), arriving in all directions from above the mask would etch isotropically. If ion bombardment and neutral F-atom etching were combined, the very much faster downward than lateral etching would give the anisotropic etch profile shown in figure 6(c).

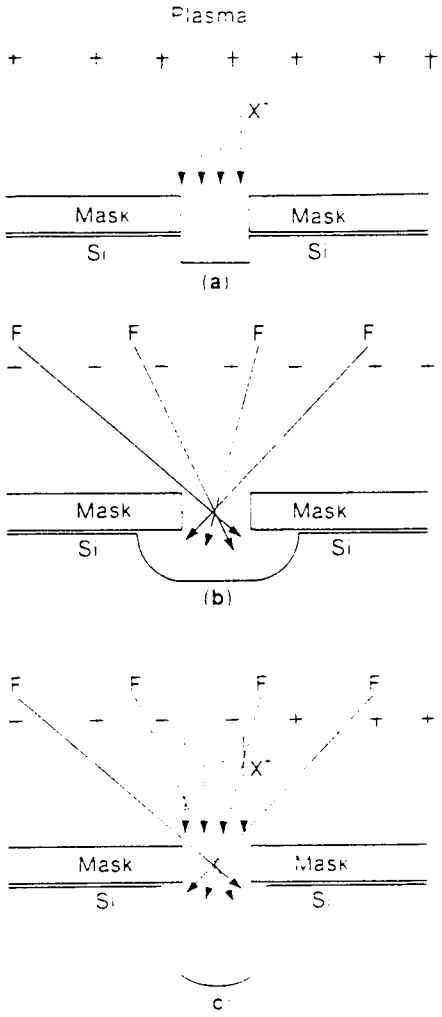

Figure 6. Silicon etch directionality.

Yarmoff and McFeely[22] used X-ray Photoelectron Spectroscopy (XPS) to examine the surface of silicon samples etched under the same conditions. A silicon surface was first exposed to sufficient XeF_2 to reach a steady state regime, and studied by XPS. Peaks were identified in the Si $2p_{3/2}$ spectrum corresponding to bulk silicon and each of SiF_x, (x=1-4). The surface was then treated to incremental doses of argon ions, and photoemission spectra recorded after each dose. The SiF_3 peak intensity declined with increasing Ar^+ dose, whereas all the other silicon peaks increased. These results are consistent with the ion beam driving a disproportionation reaction in which SiF_3 species are converted into SiF_2 plus SiF_4. The SiF_4 molecules then desorb from the surface as the major reaction product. Thus the conversion of SiF_3 into products is the rate determining step.

Flamm et al.[23] studied the gas-phase chemiluminescence at 632 nm accompanying the spontaneous etching of silicon downstream of a fluorine discharge. In separate studies of an SiF_4 discharge, the chemiluminescence had previously been assigned to the decay of excited state SiF_3 formed by the interaction of gaseous SiF_2 and F_2. They found that the silicon etch rate and chemiluminescence exhibited the same activation energy and concluded that the formation of SiF_2 was a rate-limiting step. In contrast to Coburn and Winters, they proposed a silicon etching model with SiF_2 as a direct product, and a single-reaction branching mechanism to account for the presence of SiF_4. They also showed[24] that "under equivalent conditions, chosen to more nearly simulate those encountered in plasma etching", there is a dramatic difference between F-atoms and XeF_2 etching of silicon. The F-atoms/silicon reaction displayed an Arrhenius type behaviour over the entire temperature range studied, unlike the XeF_2/silicon reaction.

Pelletier[25] has recently proposed a model for the halogen-based plasma etching of silicon. It takes into account the above and other results, and provides a conceptually useful description of silicon etching. The model equates steady-state fluorine adsorption to fluorine loss in volatile etch products, and considers both spontaneous chemical etching and ion-assisted processes.

Fluorine adsorption by silicon is controlled by repulsive, lateral interactions between neighbouring fluorine adatoms. This gives rise to the four-stage sequential adsorption mechanism depicted in figure 7.

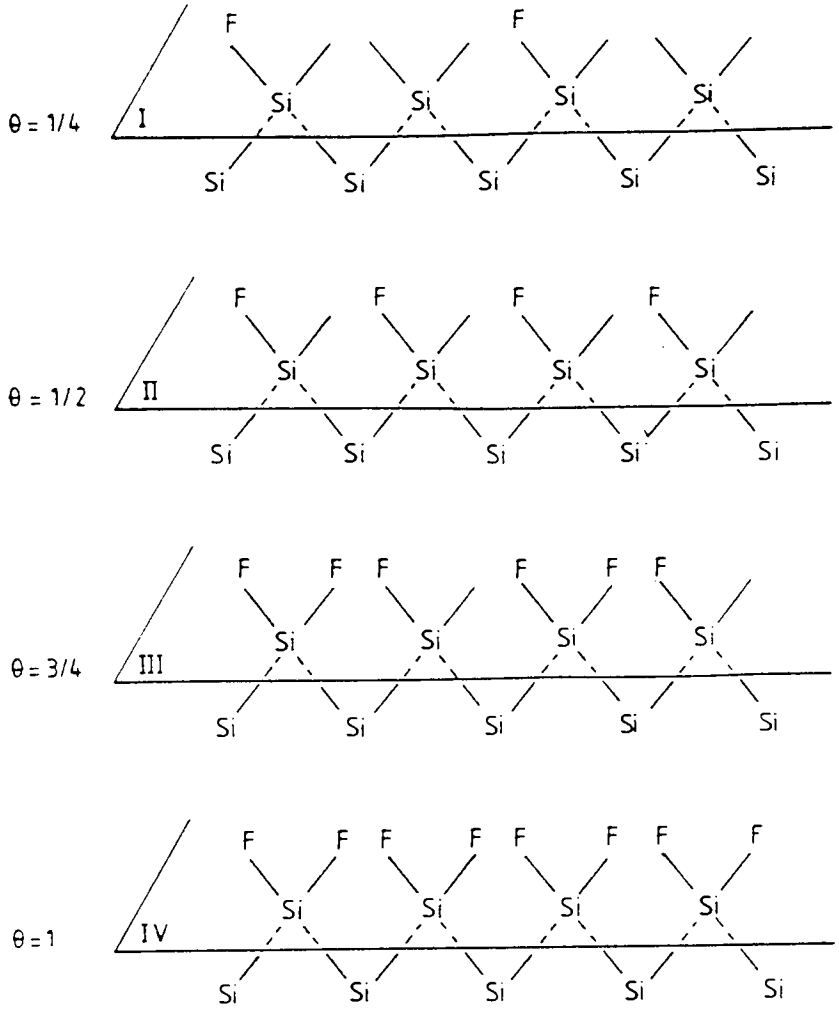

Figure 7. *The sequential mechanism of adsorption as a function of fluorine coverage θ on Si(100).*

Fluorine from XeF_2 or molecular fluorine adsorbs by dissociative chemisorption. This requires two empty nearest-neighbour sites. At low temperatures this is limited to $\theta = 0.5$, i.e. an SiF layer. At room temperature there is sufficient thermal energy for fluorine to break Si-Si back-bonds. Thus, there is the possibility of two nearest-neighbour adsorption sites on each silicon surface atom - an SiF_3 layer is formed ($\theta = 1.5$).

Atomic fluorine uptake by silicon is considerably greater than molecular fluorine. Pelletier considers that this could be due to two factors: (i) improved penetration of the silicon lattice; and (ii) atomic fluorine adsorption may continue as long as empty adsorption sites are available in the bulk.

Two routes to SiF_4 desorption are envisaged: (i) successive fluorination of the silicon surface up to the formation of SiF_4 which desorbs in a physi-sorbed state; and (ii) bimolecular reactions between SiF_2 and SiF_3 species (associative desorption). Evidence from the literature supports the latter (cf. ref. 22 for XeF_2 in the presence of Ar^+ ion bombardment).

In the presence of ion-bombardment, fluorine-atom adsorption continues to be the main adsorption process, and SiF_4 the major product. Ion bombardment is envisaged as assisting the etch process by inducing chemical reactions to form weakly bound species that desorb from the surface. It also destroys the short range order shown in figure 7, allowing the possibility of etching for $\theta < 0.75$.

Pelletier's model shows the silicon etch rate to be proportional to fluorine partial pressure for both chemical and ion-assisted etching. With ion-assisted etching anisotropy may be achieved by keeping $\theta < 0.75$ through the use of high ion current densities and/or low fluorine partial pressures.

1.4.3 Silicon Etching in Fluorocarbon Plasmas

In practice, fluorocarbons are commonly used as a stable, non-toxic, non-corrosive source of fluorine; the highest fluorine-to-carbon ratio is obtained with CF_4. The principal neutral plasma-species formed are F-atoms, and CF_x radicals (precursors to "PTFE-like" polymers). Measurement of the reaction rate coefficient for both CF_3 and CF_2 with atomic and molecular fluorine showed that CF_2 is the major CF_x radical[26]. CF_3^+ is the major ion[27].

Kay[27] has summarised the reactions occurring at a silicon surface in a CF_4 plasma, all enhanced by energetic ion bombardment, as follows:

(i) Etching of silicon by F-atoms.

$$Si(s) + xF(g) \rightarrow SiF_x(g)$$

(ii) Polymer deposition.

$$(CF_2)_n(g) \rightarrow (CF_{2-x})_n(s) + nxF(g)$$

(iii) Etching of polymer by F-atoms.

$$(CF_{2-x})_n(s) + (nx+2)F(g) \rightarrow C_nF_{2n+2}(g)$$

(iv) Sputtering of polymers and SiF_x.

During RIE, the bottom of a silicon feature will be subjected to high energy ion-bombardment, and the sidewalls to low energy ion-bombardment from back-scattered particles. Low energy bombardment favours deposition mechanism (ii), whereas high energy bombardment favours (iii) and (iv). Therefore, etching dominates

at the bottom of the feature, whereas carbonaceous deposition slows down sidewall reactions by blocking, so producing an anisotropic profile.

Oxygen additions to fluorocarbon plasmas

It follows that silicon etch rates may be increased by increasing the F-atom concentration, by decreasing the concentration of CF_x radicals in the plasma, and by removal of protecting deposits. This is most conveniently achieved for the CF_4 system by the addition of oxygen, giving rise to reactions of the form:

$$CF_x + O \rightarrow COF_{x-1} + F \quad (28)$$

A maximum in the silicon etch rate has been observed for the addition of ~16% O_2[29], which corresponds to an order of magnitude increase in F-atom concentration and halving of CF_2 radical concentration[30]. However, a maximum in the fluorine concentration is seen with the addition of ~23% O_2 to a CF_4 plasma. These results are represented pictorially in figure 8. A simple quantitative model which describes a competition between F-atoms and O-atoms for silicon surface sites can explain this difference for plasma-mode etching. For RIE the situation is more complex as any quantitative model must account for both chemical and ion-bombardment enhanced etching[31,32]. In situ XPS recently confirmed that oxidation of the silicon surface limits the etching reaction[33]; a SiF_xO_y layer was detected. Further, this layer was at its thinnest when the Si etch rate was highest.

Figure 8. *Etch rate of silicon versus fluorine-atom concentration*[29].

CO_2[34] and N_2O[35] are alternative sources of atomic oxygen. A comparison between the CF_4-CO_2 and CF_4-O_2 systems revealed that under similar conditions a higher concentration of CO_2 than O_2 was needed to reach the maximum silicon etch rate and that this maximum was lower with CO_2 than O_2.

In contrast, a higher silicon etch rate was achieved with a CF_4-N_2O mixture than CF_4-O_2; although the CF_4-N_2O system had lower F-atom concentrations than the CF_4-O_2 system, the much lower O-atom concentration in the N_2O plasma resulted in a relatively higher proportion of F-atoms reaching silicon surface sites. Similar relative results were observed in a comparison of SF_6-O_2 and SF_6-N_2O[36]. However, in both cases, higher etch rates could be obtained with O_2 additions than N_2O by altering the plasma conditions. With CF_4 this occured at higher d.c. bias levels and was ascribed to enhanced surface cleaning. In the case of SF_6 a higher relative F:O was achieved with O_2 than N_2O at high RF power levels.

Hydrogen additions to fluorocarbon plasmas

Conversely, increasing the CF_2:F ratio enhances polymer deposition on silicon. Two common methods are:

(i) increasing the C:F ratio in the fluorocarbon gas,

e.g. by the use of C_2F_6 or C_3F_8 instead of CF_4,

(ii) the addition of hydrogen to CF_4 in an analogous fashion to the oxygen additions, which consumes F-atoms and creates CF_2 radicals:

$$F + H_2 \rightarrow HF + H$$

$$CF_3 + H \rightarrow CF_2 + HF$$

CHF_3 often serves as a useful single substitute for CF_4/H_2 mixtures. It is interesting to note that polymer produced from CHF_3 has a higher thermal stability than that from C_3F_8[37]; XPS studies confirmed that both polymers were "PTFE-like" in nature (C, C-CF, C-F, CF_2, CF_3 were identified), but that the one from CHF_3 had many more cross-links.

Hydrogen additions to a CF_4 plasma may lead to a highly anisotropic silicon etch profile through an increase in CF_2 concentration, and enhanced sidewall protection (as already discussed). However, increased competition between polymer deposition and etching at the bottom of a silicon feature also reduces the vertical etch rate so that etching ceases for additions of ~40% hydrogen[38].

A detailed examination of silicon surface residues and sub-surface damage after RIE in CF_4/H_2[39] revealed a 3.5 nm thick fluorocarbon film on top of a 3.0 nm layer of

heavily disordered silicon. Sub-surface silicon-carbon bonds were found in this region. Hydrogen had diffused into the silicon to depths greater than 30.0 nm. Time resolved studies showed that the fluorocarbon film had reached a steady-state thickness after 5 minutes (for the particular plasma conditions used), and other studies found that the silicon etch rate showed an inverse correlation with the film thickness. It was concluded that when the silicon was first exposed to the plasma it was not initially covered with a fluorocarbon film and the etch rate was therefore high. Until the film reached a steady-state thickness, the silicon etch rate decreased continuously to a steady-state value. This is consistent with etching by a diffusion-limited supply of fluorine across the fluorocarbon film and out diffusion of the product.

1.4.4 Silicon oxide etching

Heinecke[40] first noted that selective etching of silicon oxide with respect to silicon could be achieved in a fluorine-deficient discharge, e.g. CF_4/H_2, CHF_3 or C_3F_8. (In fact he discarded CF_4/H_2 and CHF_3, now industry standards, as they "produced relatively high concentrations of HF which made the exhaust gases extremely toxic and raised problems of corrosion".) The precise mechanism of oxide etching still remains unclear. Selectivity is achieved by a reduction in the silicon etch rate through the deposition of an etch-inhibiting polymer, as already described, rather than an increase in the oxide etch rate. Reactions between oxygen of the silicon dioxide and the polymer carbon both keep the oxide clean and probably assist the etch process. Oxide etch rates are largely insensitive to gas phase chemistry, i.e. they vary little with a wide range of additions of oxygen or hydrogen to CF_4 when compared to silicon.

F-atoms[41, 42], CF_2 radicals[43, 44], CF_3^+ ions[45] and even anhydrous HF[37, 46] have variously been considered active oxide etchants. Direct etching by HF from the gas phase is too slow[47]. The small variation in etch rate with oxygen additions to a CF_4 plasma was observed to be proportional to the F-atom concentration (unlike silicon where a maximum in etch rate is observed for a lower oxygen concentration than that which gives the maximum F-atom concentration). It was therefore concluded that F-atoms are a major oxide etchant.

Mass spectroscopy and laser induced fluorescence[43] and infrared absorption measurements[44] of CF_2 radicals formed in a CF_4 plasma indicated that oxide is etched through the reaction:

$$SiO_2 + 2CF_2 \rightarrow SiF_4 + 2CO$$

Measurements of oxide etch rate as a function of RF power density demonstrated that etching occurs by an ion assisted process[48]. In another reactive ion etch study, oxide etch rates in CHF_3-O_2 plasmas were dependent only on the measured ion density. Further, a comparison of plasma and reactive ion beam etching showed that, at a fixed ion energy, the estimated etch yields per ion were independent of the radical flux to the substrate (the radical:ion flux ratio varied by four orders of magnitude). This led the authors to the conclusion that the ions themselves were the etchants[45].

More recent work[49] has combined the purely chemical and reactive ion mechanisms with a proposal that at low F-atom concentrations direct reactive ion etching dominates, whereas at high F-atom concentrations the etching is ion enhanced with F-atoms as the main neutral reactants.

1.5 Plasma Polymerisation

1.5.1 Introduction

The formation of fluoropolymers in fluorocarbon discharges during the etching of silicon and silicon dioxide plays a crucial role in determining etch rate, selectivity and anisotropy. Indeed, under certain plasma conditions net polymer deposition can occur, permitting the formation and study of a novel class of thin-film polymeric-materials. This is equally true for a wide range of organic monomers.

In general, plasma polymerisation is a technique used for the room-temperature deposition of uniform, organic films of, in principle, controlled physical and chemical properties onto almost any solid substrate from precursors generated in the gas phase. Strongly adherent films are often formed. World interest in plasma polymerisation is reflected in the ~ 1500 entries in Chemical Abstracts in the last 5 years, and over 600 entries in the World Patent Index since 1981.

Plasma polymers deposit from a wide range of organic compounds including conventional monomers used in industrial polymerisation processes. In most cases, the polymers are highly branched and cross-linked, differing markedly from conventionally produced polymers. The recent adoption of plasma etching by the microelecrtronics industry provides further impetus for the study of plasma polymerisation.

1.5.2 Influence of Machine Parameters

Parallel-plate plasma systems are most commonly used. Here, an RF power supply (13.56 MHz) is capacitively coupled to one electrode, and the other is earthed. In an asymmetric reactor design, with the driven electrode smaller than the ground, the capacitive coupling of the power supply allows the smaller electrode to develop a negative dc self-bias. Plasma polymers may be generated on **all** surfaces. However, in the asymmetric design positive ion bombardment plays a considerably more significant role in the deposition process at the driven electrode.

The deposition process is very sensitive to the process parameters[50]; completely different chemical properties can be obtained from the same starting material. For a given monomer, the deposition rate usually increases with increasing flow rate, passes through a maximum and then decreases slightly. The deposition rate increases monotonically with pressure and then saturation or even a decrease takes place at high values. A similar dependence on power is observed except that significant sputtering of the polymer may occur at high powers[51].

1.5.3 Conventional Commercial Fluoropolymers

World War II gave a major incentive for the development of many new synthetic polymers, and the ten years from the mid 1930's to the mid 1940's produced several major materials including polyethylene, polytetrafluoroethylene (PTFE), polyethyleneterephthalate, the silicones and new synthetic rubbers. PTFE was discovered in 1938 by R.J. Plunkett and semi-commercial production began in the early 1940's[52,53].

Polymerisation of the monomer, $CF_2=CF_2$, to produce PTFE occurs by free radical initiation in the presence of a small amount of oxygen. Pressures of about 7×10^6 Nm^{-2} (70 atm) are needed with temperatures of 50-200 °C. Such PTFE is a highly crystalline, linear polymer with an average relative molecular mass greater than 10^6. It is best known for its low surface friction, high thermal stability and chemical inertness. It has a melting point of 327 °C, reacts with molten alkali metals below the melting point, is soluble only in perfluorokerosene above 300 °C, absorbs no water, and has excellent electrical insulation properties (dielectric constant 2.2; resistivity 10^{14} Ωm). However, these very properties make processing difficult - most commonly the powdered polymer is pressed into the desired shape and then sintered at 325-370 °C. The main applications in microelectronics include corrosion-protective coatings, heat shrinkable tubing and sleeves for capacitor and resistor protection.

The difficulties in processing PTFE have led to the development of thermoplastic fluoropolymers such as fluorinated ethylene-propylene (FEP), fluoroelastomers and thermosetting fluoropolymers albeit with the loss of specific aspects of the performance of PTFE. Nonetheless world fluoropolymer production (1987) remains low at 54×10^3 tonnes per annum, cf. polyethylene, 25×10^6 tonnes per annum.

The use of polymers as interlayer dielectrics and passivating layers in microelectronic circuits is gaining popularity. Polyimide is most widely used. The polymer precursor is applied to the substrate in liquid form by spin coating and then baked. These films have similar dielectric properties to SiO_2, are stress free and resistant to chemical dissolution, but allow rapid diffusion of moisture.

Clearly, fluoropolymers might in many respects offer a superior performance to polyimide - better electrical characteristics (lower dielectric constant), almost total chemical inertness and reduced diffusion of moisture. However, the problems of polymer processing compatible with microelectronic circuitry have to be met. Du Pont chemists have recently developed a range of amorphous fluoropolymers - "Teflon AF" - which are of limited solubility in perfluorocarbon solvents and can be spin deposited onto wafers. Teflon AF has a low dielectric constant (1.89-1.83) but suffers from poor adhesion to substrates[54]. It is claimed to provide "the critical electrical properties for the next generation of computer chips"[55] which will have higher processing speeds and smaller circuitry. Potential applications envisaged include use as a dielectric for high-density and hybrid integrated circuits, as a passivation layer, and for encapsulation for hybrid/sandwich integrated circuit packaging.

A dry, room temperature alternative has long been envisaged using plasma generated fluorocarbon polymers. This would be fully compatible with the dry etch processes used, and offer advantages of low temperature deposition and ease of automation. The high cost of conventional fluoropolymers increases the commercial viability of a process requiring significant capital investment in plasma equipment.

1.5.4 Plasma Polymerised Fluorocarbons

Fluorocarbon polymers generated from CF_x radicals (mainly CF_2[26]) in CF_4 plasmas play a crucial role in the control of many microelectronic etch processes. They are, themselves, subject to etching by the F-atoms simultaneously produced from CF_4. Thus, the propensity for polymer deposition may be increased by increasing the CF_2:F ratio in the gas phase. This may be achieved in two ways:

(i) By increasing the C:F ratio in the fluorocarbon gas, e.g. by the use of C_2F_6 or C_3F_8;

(ii) By the addition of hydrogen to CF_4 to consume F with the production of HF. CHF_3 often serves as a useful single substitute for CF_4/H_2 mixtures.

XPS studies have shown that these polymers are "PTFE-like" in nature - C, C-CF, C-F, CF_2 and CF_3 groups are all usually present.

Films of plasma polymerised CF_4 were grown on sodium chloride and cesium iodide crystals used as infrared windows[56]. Films 1μm thick gave moisture protection to crystals exposed to 88% RH at room temperature. They have a low refractive index (1.35) near to that of PTFE, giving improved transmission.

Published properties of plasma polymerised halocarbon films have been compared to those of PTFE[57] and are summarised in table 6.

Table 6. Comparison of properties of plasma fluoropolymers and PTFE.

Property	**PTFE**	**Plasma polymer**	**Monomer**
Coefficient of friction	0.08	0.34	CF_4
Resistivity (Ωm)	10^{14}	3×10^{11}	CF_3Cl
Dielectric strength (Vcm^{-1})	1.1×10^6	3×10^6	cyclo-C_4F_8

1.5.5. Metal/Fluorocarbon Polymers

Work by Biederman[58] is typical of studies of the production of metal/fluoropolymer films. A metal (gold) target was placed on the driven electrode in a planar magnetron and was therefore subject to sputtering. A composite polymer/metal film was grown on a grounded surface. The films obtained possessed a sheet resistivity ranging from a few ohms per square to one thousand with the least resistive films having a high gold content. The optical transmission of these films is also a function of metal content and a wide range of film colours may be systematically produced (pink, red, violet, blue). Proposed applications include large area optical filters and decorative coatings.

1.6 Scope of this Thesis

It has been demonstrated in this introduction that plasma etching is an established, essential technology for the production of VLSI and ULSI devices. Further no immediate limit to device complexity due to limitations imposed by the etch process itself is foreseen. However, it has also been shown that, surprisingly, the precise etch mechanisms of silicon and silicon dioxide in fluorine containing discharges are far from fully understood.

When either developing a new plasma etch process, or simply optimising an existing process, the engineer has a bewildering number of parameters to consider, e.g. reactor geometry, reactor materials, substrate temperature, substrate bias, choice of gas(es), gas flow rate, gas pressure, excitation frequency, applied power density. These variables may interact in a complex fashion to control the etch "quality" defined in terms of etch rate, anisotropy, selectivity, substrate damage, etch residues and contamination (particulate and chemical). A potential link between the process parameters and etch quality is most readily provided through an understanding of the plasma chemistry - both gas-phase chemistry and gas-surface interactions.

This thesis reports studies of aspects of the chemistry of plasma etching of silicon and thermally grown silicon dioxide in fluorine containing discharges, including polymer formation in such discharges.

Among the topics investigated are:-

a) Source of fluorine.

Many gases, e.g. F_2, XeF_2, NF_3, SF_6, C_xF_{2x+2} (x=1-4) and chlorofluorocarbons, have been used as a source of atomic fluorine for the plasma etching of silicon and its compounds. In detailed studies much mechanistic information has been gained. However, although a considerable body of relevant chemical literature exists, it is, in the author's experience, often limited to single systems. Direct comparisons of the available data are most often not possible due to differences in other process parameters. Thus a potential wealth of information, to be gained from the comparison of gas systems, has been lost. Here, the plasma etching of silicon and silicon dioxide has been studied in CF_4 and SF_6 as a function of gas flow rate, chamber pressure and applied RF power (the major machine parameters). Response surface methodology was used to model the silicon and silicon dioxide etch rates as a function of machine parameter setting. Optical emission spectroscopy (OES) was used to study changes in the corresponding gas-phase chemistry.

b) Influence of additives : Oxygen

Similarly, it is clear that F, O and CF_2 play a crucial role in determining the etch rates of silicon and silicon oxide in fluorocarbon plasmas. Furthermore, each can be readily detected by OES and changes in their relative concentration measured. The CF_4-H_2 and CF_4-O_2 systems have been extensively studied, i.e. systems in which either atomic-O or CF_2 radicals are of major importance to the plasma chemistry. Systems such as C_2F_6-O_2 and CHF_3-O_2, i.e. where F, O and CF_2 can all be expected to be important to the plasma chemistry, have received less attention.

A matrix of experiments has been undertaken to determine the etch rates of silicon and silicon oxide in CF_4, C_2F_6, CHF_3 and SF_6 with additions of each of O_2, CO_2 and N_2O. The corresponding optical emission spectra were recorded also. SF_6 was chosen to represent a polymer/CF_x-free system. CO_2 and N_2O served as alternative sources of oxygen, in order to gain further insights into the role of oxygen.

c) Influence of electrode material

Of the many plasma parameters, one that has received less attention in the literature is choice of electrode material. The influence of a wide range of electrode materials on the etch rate of silicon and silicon oxide in CF_4 and CF_4/O_2 plasmas has been studied.

d) Fluorocarbon plasma polymerisation

It has been shown that fluorocarbon polymers often play an essential role in controlling both etch anisotropy and etch selectivity. Further, these polymers offer significant commercial potential in their own right.

Studies of the influence of plasma chemistry on polymer deposition rate, polymer chemistry and polymer properties have been undertaken for a wide range of plasma chemistries - each of CF_4, C_2F_6 and C_3F_8 with additions of hydrogen, and CHF_3.

CHAPTER 2 - EXPERIMENTAL

2.1 Plasma Etcher

2.1.1 Introduction

The researcher is faced with a wide choice of types of plasma etcher, e.g. parallel-plate, magnetron, triode, microwave, electron cyclotron resonance systems, all of which are commercially available from a variety of specialist manufacturers worldwide[54]. The plasma etcher used throughout these studies was a Plasma Technology RIE80 operating in reactive ion etch mode. The RIE80 was one of the first UK machines to be designed specifically for research use (1985), and has enjoyed high worldwide sales. The reactive ion etch configuration was chosen in order to provide both maximum compatability with the literature and relevance to industry. The RIE80 is shown schematically in figure 9, and may be described in terms of a number of discrete components.

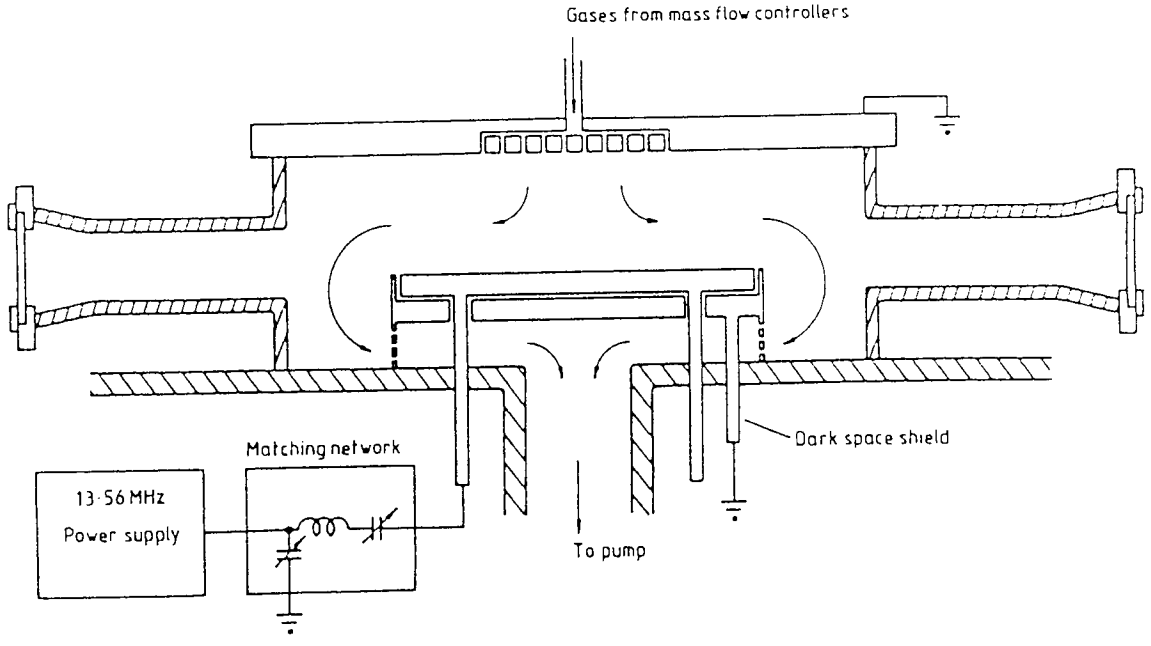

Figure 9. Schematic diagram of Plasma Technology plasma etcher.

2.1.2 Components of Plasma Technology RIE80 Plasma Etcher

a) Plasma chamber

The RIE80 is a parallel plate etching system set up in reactive ion etching (RIE) mode, i.e. with RF power applied to the lower electrode and the upper electrode grounded. Both electrodes were water cooled and made of anodised aluminium. The upper electrode was 282 mm in diameter and the lower 170 mm, giving an area ratio of 2.75:1 - neglecting contributions to the ground electrode from the chamber walls and base. Thus the lower driven electrode adopted a negative d.c. bias during etching causing positive ion bombardment. The interelectrode gap was 53 mm. The plasma chamber itself was made of pyrex, dimensions: internal diameter 282 mm, height 108 mm. The chamber volume was therefore ~7 dm^3, giving a gas residence time of ~1.5 s at 20 sccm flow and 60 mtorr chamber pressure. For optical emission spectroscopy studies a modified pyrex chamber with three side-arms with quartz windows was used.

b) Pumping system

It has been noted[59] that when choosing a pump for a semiconductor process, one must consider process contamination (the effect of the vacuum pump on process contamination), vacuum pump deterioration (the effect of the semiconductor process on the vacuum pump), and most importantly operator safety. Not all of the primary gases used in plasma etching, e.g. halocarbons, are toxic but many of their by-products are dangerous to breathe[60]. Some gases, e.g. oxygen, pose a hazard (explosion) when in contact, in high concentration, with hot hydrocarbon oils. Some by-products, e.g. HF,

may readily cause pump corrosion, and the chemistry of by-product/hydrocarbon pump oil interactions is essentially unknown. For these and other reasons inert synthetic pump fluids - perfluoropolyethers - and oil-free ("dry") pumping systems are often employed[61].

The RIE 80 was equipped with an Edwards E2M40 rotary, EH250 roots blower pump combination, running on conventional mineral oil. The rotary pump was ballasted with 2 dm^3min^{-1} dry nitrogen in order to purge the pump of contaminants etc. Oil condition was assessed by visual inspection at the sight glass, and the oil was then changed when required. The pumps were capable of bringing the chamber from atmospheric pressure to <5% of the operating pressure, e.g. from atmospheric pressure to <3 mtorr prior to an operating pressure of 60 mtorr, in 5-10 mins.

c) Pressure measurement and control

Pressure measurement was by a high resolution MKS Baratron absolute pressure transducer with pressure control by a VG automatic pressure controller situated between the chamber and pumps.

The Baratron is a diaphragm gauge and measures pressure differences by the deflection of a metal diaphragm. Changes in the position of the diaphragm are detected electrically by measuring the capacitance between the diaphragm and a fixed flat electrode. The gauge measures total pressure, and the reading is independent of the type of gas used. The calibration of the Baratron used in these studies was checked by comparison with readings obtained from a similar gauge.

d) Mass flow controllers

The gas supply to the RIE80 was introduced through a gas shower in the centre of the upper electrode, which also serves as the chamber lid. The gas flow rate was controlled using three Tylan FC260 mass flow controllers - 0-10, 0-30 and 0-100 sccm (standard $cm^3.min^{-1}$) N_2 respectively.

The calibration of the mass flow controllers was checked at ten points over their entire range using a bubble flow meter. Due correction was made for room temperature, but errors due to variations in atmospheric pressure were ignored. The conversion factors applied for use of gases other than the calibrants were those supplied by the manufacturer, (these are a direct function of the heat capacity of the gases).

e) Power supplies, matching network and d.c. bias measurement

RF power was supplied by a 300 W, 13.56 MHz generator - ENI Model HF-300 or ENI Model ACG-3, as available. In both cases the generator-indicated power output was checked with a Bird in-line wattmeter, whilst the generator was coupled to a 50 Ω dummy load, and was found to be accurate. The generator-indicated power output was then relied upon for all experimental work.

A matching network was placed between the power supply and the electrodes in order to increase the power dissipation in the discharge, and to protect the power supply. the network was used to match the generator impedance to the discharge impedance. It contained two variable capacitors, in a Π configuration, which were adjusted manually to give maximum forward and minimum reflected power.

The d.c. bias developed by the lower, driven electrode was measured across a load and displayed on a 0-5 V voltmeter, where 5 V represented 1 kV d.c. bias.

2.1.3 Operation of Etcher

Prior to any new series of experiments, and especially after severe contamination, e.g. polymer formation, the plasma chamber was stripped into its component parts, i.e. top electrode, gas shower, chamber glass, driven electrode, dark space shield, vacuum feed throughs etc., for cleaning. Cleaning was performed by the use of detergent/abrasive cloth, followed by rinsing in distilled water and acetone, and finally oven drying. After reassembly, all visible surfaces were wiped with propanol-damped cloth. Trace carbonaceous material was then removed by striking an oxygen discharge - the plasma colour changed from blue (characteristic of CO/CO_2 species) to yellow when the chamber was clean. The propanol/oxygen plasma treatment sufficed for minor contamination.

Up to three process gases could be used - invariably, a fluorinated gas, an additive and argon. When any new process gas was selected, or after a gas cylinder was changed, the gas line between the relevant mass flow controller and gas cylinder was always evacuated. This procedure served the dual purpose of both removing trace contaminants, and leak checking the line prior to pressurisation with a process gas.

The steps necessary prior to striking a plasma were:-

(i) evacuation of chamber to base pressure (5-10 mins.);

(ii) leak checking - manufacturer recommends a maximum chamber pressure rise of 6 mtorr.min^{-1} from base pressure;

(iii) admittance of process gases;

(iv) pressure adjustment;

(v) stabilisation of flow and pressure (2-3 mins.);

(vi) setting of forward RF power level;

(vii) coolant flow check.

When the chamber was to be used for the first time after cleaning, "conditioning" was necessary before spectroscopic measurements or sample treatments could be carried out. This involved running a plasma of the desired process parameters for ~15 mins. Samples for plasma treatment were generally placed at the midpoint between the centre and edge of the driven electrode. Treatment times were controlled automatically when using the ENI Model HF-300 power supply, and manually ($\pm$ 1 s) when using the ENI Model ACG-3 power supply. In either case tuning was accomplished within ~15 s.

Finally, the plasma chamber was fully evacuated after any discharge in order to remove potentially noxious gases. Dry nitrogen was used to vent the chamber.

2.2 Optical Emission Spectroscopy

2.2.1 Introduction

Optical emission spectroscopy (OES) is one of several optical diagnostic techniques for plasma discharges[62, 63]. Others include laser induced fluorescence, absorption spectroscopy and optogalvanic spectroscopy. It has the advantages of being non-invasive, capable of operating in real-time, and of being relatively straightforward to implement. The emissions from a plasma are characteristic of those species present in an excited state. OES is used to record the intensity of those emissions as a function of wavelength, most usually in the uv/visible region. The resultant spectra may, if they have a suitable emission, be fully analysed to unequivocably identify atoms, ions, free radicals and molecular species present in the plasma, and even yield information on their temperature[64] and excitation mechanisms[65]. However, the vast majority of species are present in their ground state, and the relationship between emission intensity and ground state concentration is not straightforward. One technique which has been devised to overcome this problem is actinometry.

2.2.2 Actinometry

Harshbarger et al.[66] first used OES to study silicon and silicon nitride etching in CF_4-O_2 mixtures. They found that oxygen additions to a CF_4 plasma enhanced the etch rate of these materials by the liberation of atomic fluorine. Their results, though, were qualitative as the emission intensity of an excited species is a function of both its ground state concentration and the electron energy distribution function (eedf) of the plasma. The eedf may vary with changes in the plasma parameters. In order to overcome this

problem, Coburn and Chen[67] devised a method, referred to as "actinometry", for correlating emission intensities to reactive particle density. It involves the deliberate addition of a small constant amount of a noble gas, the actinometer, to a plasma and monitoring the noble gas emissions concurrently with those of the reactive particle. If the excited state responsible for the noble gas emission matches closely in energy with the level of the reactive particle, then the same group of electrons will be responsible for the excitation of both levels. By comparing the emission intensities from the actinometer and reactive particle, the relative changes in ground state concentration of the latter can be assessed. Ideally the excited states should also be produced by direct electron impact only, and decay exclusively by photoemission. Coburn and Chen applied their method to atomic-F (703.7 nm; 14.5 eV) with argon as an actinometer (750.4 nm; 13.5 eV) (see figure 10).

In practice, it may be possible for actinometry to be used even when the above conditions are violated. For example, d'Agostino et al.[68] studying the CF_4-O_2 system validated the use of argon actinometry for the measurement of F, O, CO and CO_2 concentrations from emitting levels in the range 8-20 eV by comparing two actinometers Ar (750.4 nm; 13.5 eV) and N_2 (380.5 nm; 11.5 eV). The trends in the two actinometers were coincident, implying that their relative emission intensities were proportional to the electron density in a broad energy range. The technique was similarly extended to CF_2 (4.5 eV)[69].

Argon actinometry for the determination of O-atom concentrations in CF_4-O_2 plasmas has been tested directly using two-photon laser induced fluorescence (LIF) by Walkup et al.[70]. They found that at high O_2 concentrations the O(844.6 nm)/Ar(750.4 nm) intensity ratio followed the changes in O-atom concentration observed by LIF but the O(777.4 nm)/Ar(750.4 nm) ratio did not . Both O(777.4 nm)

and O(844.6 nm) are produced by direct electron impact excitation of atomic oxygen and dissociative excitation of molecular oxygen. However, the O(844.6 nm) emission line is a much better indicator of O-atom concentration than the O(777.4 nm) emission line because the cross section for direct excitation of O(844.6 nm) is much larger than that for O(777.4 nm) whereas the opposite is true for the dissociative excitation cross sections.

Coburn and Chen also used OES with argon actinometry to study changes in relative fluorine-atom concentration in a CF_4 discharge as a function of pressure and flow rate[71]. In their pressure dependence studies, they kept the CF_4 and Ar flow rates constant and varied the chamber pressure by adjusting the pumping speed. The procedure ensured that the percentage of Ar in CF_4 remained constant, but allowed the total Ar pressure to increase with the CF_4 pressure. In order to have a reference Ar emission at constant Ar density the Ar emission data was divided by the Ar pressure.

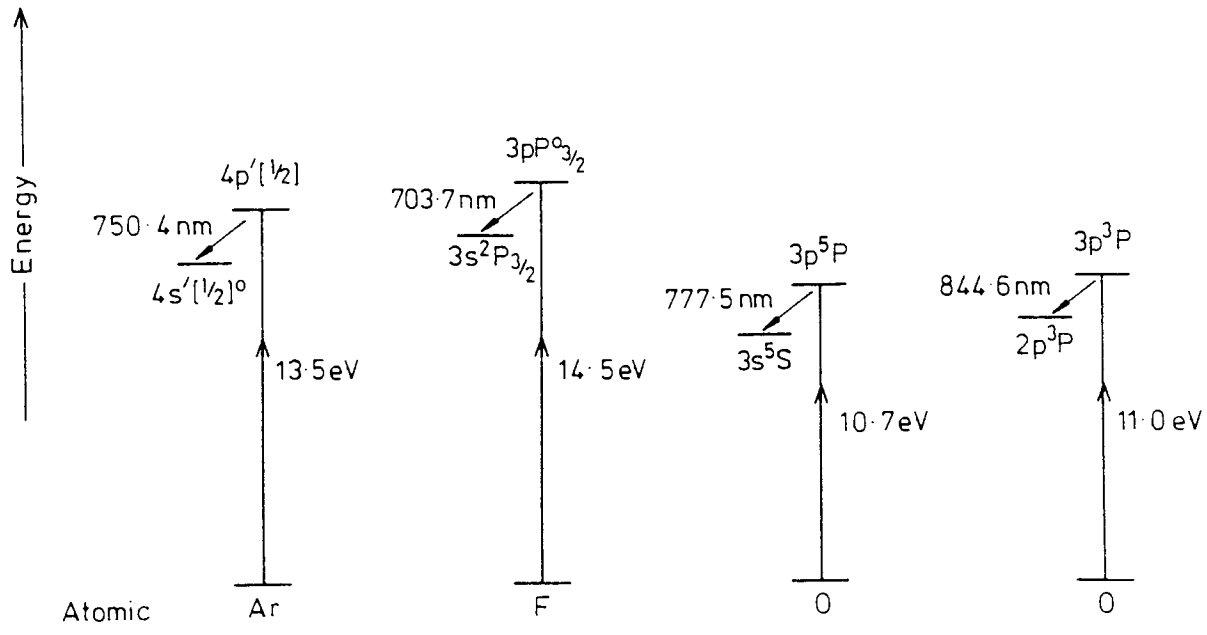

Figure 10. Energy level diagram for atomic argon, fluorine and oxygen.

2.2.3 Spectrometer

A diffraction grating is most commonly employed as the dispersion element in an optical emission spectrometer[72]. In modern instruments subsequent analysis of light intensity as a function of wavelength is carried out in one of two ways: (i) the grating is rotated to scan the spectrum, and the dispersed light is sampled at a fixed position; or, (ii) the grating is stationary and the light falls on a diode array. The former potentially offers high resolution at the expense of relatively lengthy scan times, and the latter rapid response but lower resolution even when used over a narrower spectral range - there are typically 1024 diodes in an array. The requirement for high resolution (0.2 nm) over a wide spectral range (200-850 nm) made the use of a scanning instrument essential for these studies. It is worth noting that a rapid scanning monochromator has been developed (Monolight Instruments Ltd.) which is highly competitive with the speed and resolution of diode array systems whilst covering the full spectral range. However, its resolution (1-2 nm) was not adequate for the present work[73].

The spectrometer used was a Spex 1870C 0.5 m scanning monochromator, controlled by a Spex CD2 compudrive. The spectrometer contained a 1200 groove/mm grating blazed at 300 nm, and was coupled to a R928 photomultiplier and Optronic model 730-H1 radiometer. Output was to a chart recorder. Quartz, rather than glass, optics were used in order to be able to study emissions in the region 200-320 nm. The spectrometer was aligned for maximum signal intensity, i.e. no attempt was made to gain spatial information from the discharge.

2.2.4 Method

The spectrometer was calibrated with a Hg-lamp, and its resolution determined by scanning a Hg doublet at 313.1 nm. The system was capable of 0.018 nm resolution, but was operated at ~0.2 nm resolution (150 μm entrance and exit slits). This represented a compromise between resolution and signal to noise ratio. Scan rates of 0.25 nm/s were used. Higher rates gave a significant loss of signal (> 10%). Full spectral scans, 200-850 nm, therefore took almost 45 minutes.

A number of plasma emissions from both atomic and molecular species were unequivocally identified, and, where appropriate, their relative intensities were routinely measured. The species are given in table 7[74-76], and typical spectra are shown in appendix 2. In the case of CF_2(251.9 nm) the signal intensity was taken as the peak height above the background continuum.

Table 7. *Atomic and molecular species observed in the plasma emission, corresponding wavelengths and transitions.*

Species	Transition	Wavelength (nm)
CO^+	$B^2\Sigma^+ - X^2\Sigma^+$	219.0 (0,0)
		230.0 (0,1)
CF_2	$A^1B_1 - X^1A_1$	251.9 ((0,5,0),(0,0,0))
CO	$b^3\Sigma - a^3\Pi$	283.3 (0,0)
		297.7 (0,1)
CO_2^+	$A^2\Sigma^+ - X^2\Pi$	288.3
		289.6
Ar	$4s[\frac{1}{2}]^0 \leftarrow 5p[\frac{1}{2}]$	470.2
Ar^+	$4s\ ^4P_{3/2} \leftarrow 4p\ ^4P_{5/2}$	480.6
H	$2p^2P^0_{3/2} \leftarrow 3d^2D_{3/2}$	656.3
F	$3s^2P_{3/2} \leftarrow 3p^2P^0_{3/2}$	703.7
Ar	$4s[\frac{1}{2}]^0 \leftarrow 4p[\frac{1}{2}]$	750.4
O	$3s^5S \leftarrow 3p^5P$	777.4
O	$3s^3S \leftarrow 3p^3P$	844.6

2.3 Ex-situ Diagnostic Techniques

2.3.1 Profilometer

Substrate materials to be etched or coated with plasma polymer were partially masked with smaller samples of the same material, to give a reference level, prior to processing. Plasma etch and deposition rates were then calculated from step height measurements made using a Dektak IIA profilometer manufactured by Sloan Technology.

The profilometer works by moving the sample surface beneath a diamond-tipped stylus. Vertical stylus movement, caused by variations in the sample surface, is sensed by a transducer, digitized and stored for subsequent analysis. Vertical resolution is 0.5 nm, and the diamond tip 12.5 μm in diameter.

2.3.2 Infrared

Fluorocarbon plasma-polymer films on aluminised silicon wafers were characterised by infrared using a Perkin Elmer 983 G Infrared Spectrophotometer with variable angle specular reflectance accessory.

The absorbance of a component in the sample is proportional to its concentration[77, 78]. The absorbance, A, is defined as

$$A = \log(I_o/I) = \log (1/T) \qquad (2.1)$$

where I_o and I are the intensities of the light before and after interaction with the sample, and T is the transmittance of the sample.

Thus for quantitative work band intensities should be measured as a function of absorption, as a small inaccuracy in the measurement of percentage transmission could correspond to a large inaccuracy in the measurement of absorption. The absorbance of a particular band may be measured by drawing a tangent line to the absorption minima either side of the band. The point on the tangent line at the absorbance maximum of the analytical band is taken as the background absorbance, A_o. This may be subtracted fom the total absorbance to yield a "true" absorbance. More accurate measurements of absorbance, which take into account variations in band width, may be made by considering peak areas.

2.3.3 X-ray Photoelectron Spectroscopy and X-ray Induced Auger Electron Spectroscopy

The processes occuring in these techniques are summarised in figure 11. In X-ray photoelectron spectroscopy (XPS) the sample is irradiated with X-rays of characteristic energy, e.g. Mg K_α, and the resultant photoelectrons escaping from the outer atomic layers (~5 nm depth) of the sample are recorded as photoelectron intensity versus kinetic energy. The information from such plots allows an elemental analysis of the surface and in many cases bonding states of the surface can be identified. The process may be accompanied by the emission of Auger electrons. The Auger electrons are recorded as electron intensity versus electron kinetic energy. A quantitative analysis of the spectrum is possible and chemical bonding identification of a number of elements is feasible, but as yet is not so extensive as for XPS.

XPS has proved particularly useful for the study of fluorocarbon polymers[80, 81]. The high electronegativity of fluorine causes shifts in the binding energy of the associated C 1s peak according to the degree of fluorination of the carbon atom. In a carbon-fluorine chemical environment of mixed stoichiometry in a polymer surface layer, resolvable peaks may be detected within the C 1s peak and attributed to C or C-H, C-CF, -CF, $-CF_2$ and $-CF_3$ components.

Samples were analysed either in a Vacuum Generators ESCALAB II at Harwell Laboratory (V. Moore), or in a Kratos XSAM 800 at Johnson Matthey Technology Centre, Sonning Common, Reading (J.A. Busby). These instruments had facilities for both AES and XPS.

Figure 11. X-ray photoelectron spectroscopy[79].

2.3.4 Thermal Analysis of Polymers

Fluorocarbon polymers produced by plasma polymerisation were characterised by thermal analysis. Two complimentary techniques were used: (i) thermogravimetric analysis (TGA), weight change with respect to temperature; and (ii) differential scanning calorimetry (DSC), heat flow with respect to temperature.

TGA was performed using a DuPont Instruments 951 Thermogravimetric Analyser coupled to a 1090 Thermal Analyzer, and DSC using a DuPont Instruments 910 Differential Scanning Calorimeter coupled to a Thermal Analyst 2000. For both instruments typical operating conditions were: sample weight, 5-15 mg; temperature range, room temperature - 600 °C; heating rate, 10 $^{\circ}Cmin^{-1}$ in flowing air. The sensitivity of the TGA was 5×10^{-6} g, and the DSC 6×10^{-6} W.

2.3.5 Electrical Properties of Polymers

The electrical properties of plasma polymers - bulk resistivity and relative dielectric constant - were measured as a function of frequency. A thin polymer film sandwiched between two electrodes was represented by an equivalent circuit of a parallel combination of a pure resistance and a pure capacitance, and the values of the two components determined. The response of the equivalent circuit to an applied voltage is described below[82].

In an a.c. field of period ω the voltage, V, and current, I, at time, t, are represented by,

$$V = V_o(\cos \omega t + i \sin \omega t) \qquad (2.2)$$

and $$I = I_o(\cos \omega t + i \sin \omega t) \qquad (2.3)$$

where $i=\sqrt{(-1)}$. The real parts of the two equations represent dispersion and the imaginary parts loss.

If the alternating voltage is applied across a pure resistance, R, then the current at any time is given by Ohms Law,

$$I = V/R = V_o(\cos \omega t + i \sin \omega t)/R \qquad (2.4)$$

In this case the current is in phase with the applied voltage.

For a pure capacitance, C, the relationship between applied voltage and stored charge, Q, is,

$$Q = CV \qquad (2.5)$$

thus, $I = dq/dt = C\, d(V_o \cos \omega t + V_o \sin \omega t)/dt$

$$= -\omega C V_o \sin \omega t + i\omega C V_o \cos \omega t$$

$$= i\omega CV \qquad (2.6)$$

The current leads the applied voltage by a phase angle of 90°.

Both current equations (2.4 and 2.6) have the form $I = V/Z$ where the modulus of Z is known as the electrical impedance of the component (measured in ohms) and is equal to R and $1/i\omega C$ for a resistor and capacitor respectively. The form of a complex impedance may be generalised to

$$Z = Z' - iZ'' \qquad (2.7)$$

Similarly, admittance, Y, may be defined as

$$Y = 1/Z = Y' + iY'' \qquad (2.8)$$

For a resistor and capacitor in parallel

$$Z = (1/R + i\omega C)^{-1}$$

$$= R/(1 + i\omega CR)$$

$$= (R - i\omega CR^2)/(1 + \omega C^2R^2)$$

$$= R/(1 + \omega^2C^2R^2) - i\,(\omega CR^2/(1 + \omega^2C^2R^2))$$

Thus, $|Z| = R/\sqrt{(1 - \omega^2C^2R^2)}$ (2.9)

$$Y = 1/Z = 1/R + i\omega C \quad (2.10)$$

Impedance data is obtained experimentally as simultaneous values of resistance and capacitance at a particular frequency. In this work, the values were calculated automatically using a Gen Rad 1689 Precision RCC Digibridge over the frequency range 0-100 kHz. The polymer volume resistivity, ρ (Ωm), was calculated from the relationship

$$\rho = RA/d \quad (2.11)$$

where d is the polymer thickness, and A the contact area.

The polymer relative dielectric constant, ϵ_r, was calculated from the capacitance defined by

$$C = \epsilon_o\epsilon_r A/d \quad (2.12)$$

where ϵ_o is the permittivity of free space.

The total polymer dielectric constant ϵ can be expressed as a complex quantity composed of real and imaginary parts:

$$\epsilon = \epsilon' + i\epsilon'' \quad (2.13)$$

where $\epsilon' = \epsilon_r\epsilon_o$

The two parts are related by the dissipation factor, D:

$$\epsilon' = \epsilon''D \quad (2.14)$$

where $D = 1/(\omega RC)$ (2.15)

thus $\epsilon' = \epsilon''\omega RC$ (2.16)

2.4 Materials

2.4.1 Silicon and Silicon Dioxide

Although the plasma etch rate of silicon in fluorine systems shows some dependence on dopants in heavily doped materials, it is independent of both crystallographic structure and electrical properties in undoped or light n- or p-type doped materials[83]. Lightly phosphorous-doped n-type Si <111> was used throughout these studies - Texas Instruments 6-20 Ω, Wacker 5-9 Ω and Monsanto 4-7 Ω 75 mm diameter wafers, as available (E.M. Wittam, Harwell laboratory). SiO_2 was thermally grown to a thickness of ~1.2 μm on the same material.

2.4.2 Aluminised Wafers

Aluminised wafers were prepared either by evaporation of aluminium onto silicon wafers (E.M. Wittam, Harwell Laboratory), or by sputter deposition of Al/1% Si onto a thin oxide layer on silicon wafers (Fraunhofer Institut, Berlin). In both cases the aluminium was ~2 μm thick.

2.4.3 Electrode Cover-Plates

The 170 mm diameter, lower, driven electrode of the Plasma Technology RIE80 plasma etcher was made of anodised aluminium. In order to study the influence of electrode material on etch performance cover-plates were made from a wide range of materials in sheet form. These are described in table 8 below. Sodium and potassium

"doped" quartz covers were prepared by immersing quartz discs in a 2M solution of the respective nitrate, followed by drying and then calcining in air at 700 °C.

Table 8. Electrode cover-plate materials.

Material	Thickness (mm)	Description
Al	1.98	99% purity
Ag	0.10	99.9% purity
Cu	0.61	99.9% minimum purity
Fe	0.53	99.5% purity
Ni	1.02	99% minimum purity
Pb	0.99	99.99% minimum purity
Quartz	3.5	95 mm diameter silica disc
Soda glass	3.02	"Window glass"
Polythene	5.99	Grade "Z", natural
PTFE	2.44	Grade "A" (BS.6564)

2.4.4 Gases

The process gases used were all BOC Electra ll grade with the exception of:-

Ar 99.998% purity

CO_2 Liquid (unspecified)

N_2O Medical grade, >99% purity.

CHAPTER 3 - RESULTS: PLASMA ETCHING

This chapter describes the results of experiments designed to study the chemistry of three aspects of the plasma etching of silicon and silicon dioxide in fluorine containing discharges: plasma parameters, oxygen additions, electrode material.

3.1 Plasma Parameters

3.1.1 Introduction

The aim of this series of experiments was to study, for a given etchant, the influence of three process parameters - gas flow rate, chamber pressure and applied RF power - on the etch rates of silicon and silicon dioxide over a wide range of values of the process parameters, and to study the corresponding gas-phase chemistry using optical emission spectroscopy with argon actinometry. Two etchants - CF_4 and SF_6- commonly used in plasma etch processes, were chosen for investigation. Response surface methodology was employed both to maximise the amount of useful data generated from the minimum necessary number of experiments in the parameter space, and to assist in a comparison of the results from the etchants through modelling.

A limited number of experiments was also performed, under conditions of fixed flow, pressure and power, using CF_4/SF_6 gas mixtures in order to both further study differences in plasma chemistry, and to look for synergistic effects. The influence of d.c. bias on SiO_2 etch rates, highlighted by these experiments, was investigated using SF_6 systems.

3.1.2 Response Surface Methodology: Experimental Design

Many process parameters, e.g. choice of gases, flow, pressure power, electrode temperature, d.c. bias, electrode spacing, determine the performance, e.g. etch rate, selectivity, anisotropy, of a plasma etcher. As the process parameters may also be interactive, the one-parameter-at-a-time approach to process optimisation can require very many experiments, as well as giving potentially misleading results.

Response surface methodology is a statistical experimental design technique developed in the 1950's that has only recently become popular for the study of plasma processes[83-86]. In this approach the factors (parameters) of interest are represented as orthogonal axes in space. The limits of the axes are the physical maximum and minimum possible parameter settings. Responses (experimental results) are then systematically measured within the defined space. These, in turn, are fitted to a polynomial equation which models all of the defined space, but not beyond.

The number of levels (settings) used for each factor determines the complexity of the model which can be produced. A three-level design is needed in order to include quadratic terms for curvature as well as linear, two-factor interactions. For example, a three-factor, three-level design gives a model of the form:

$$Y = c_o + c_1X_1 + c_2X_2 + c_3X_3 + c_4X_1X_2 + c_5X_1X_3 + c_6X_2X_3 + c_7X_1^2 + c_8X_2^2 + c_9X_3^2 \quad (3.1)$$

where Y is a response, e.g. etch rate; X_1, X_2 and X_3 are factors, e.g. flow, pressure and RF power; and c_0 - c_9 are coefficients to be determined.

In this work, a Box-Behnken experimental design was used[88]. It consists of replicated centre points and the set of points lying at the midpoints of each edge of the multidimensional cube that defines the region of interest. The three-factor design requires fifteen experiments - the midpoint of each of the 12 edges of a cube, and replicates of the centre point in order to assess the experimental error. The chosen values of the factor were scaled by normalisation about their respective means. Thus high, middle and low settings were represented by 1, 0 and -1. Comparison of the magnitude of the coefficients obtained from modelling then provided an estimate of the relative importance of each parameter in the model. The 15 experiments needed covered the ranges in table 9, and were carried out in a randomised order.

Table 9. *Parameter settings.*

Setting	**-1**	**0**	**1**
Parameter			
Flow (sccm)	20	30	40
Pressure (mtorr)	65	130	195
RF power (W)	50	150	250

The data generated was analysed using least squares regression analysis, with the aid of a commercially available software package - Statgraphics[89] - run on a personal computer. The software also provided statistical information on the model produced. The statistical significance of each term in the model is given by its F-ratio. The F-ratio is the ratio of the variation in the response accounted for by the model term to the residual

error (the variation between the model and the data). A larger F-ratio value indicates a greater statistical significance of that term. Critical values have been tabulated for the F-ratio, with 1 and n-p-1 degrees of freedom (n = number of data points; p = number of model terms), above which the model term is statistically significant for a given confidence level - typically 95%. The software used here allows the stepwise inclusion of significant terms into a model.

The success of the final model can be assessed in a number of ways. The correlation coefficient, R^2, gives a measure of how well the model fits the experimental data. It is defined as the ratio of the sum of squares due to regression to the total sum of squares:

$$R^2 = \Sigma_i (\hat{y}_i - \bar{y})^2 / \Sigma_i (y_i - \bar{y})^2 \qquad (3.2)$$

where y_i are observed values, $\hat{y}_i$ predicted values and $\bar{y}$ mean values.
The values of R^2 vary between 0 and 1, a value of 1 indicating a perfect fit.

The standard error, s, is given by:

$$s = (R_i (y_i - \bar{y})^2 / (n-p))^{\frac{1}{2}} \qquad (3.3)$$

The requirement here is for the standard error to be significantly smaller than the magnitude of the response.

As with the individual terms, the statistical significance of the model may be tested by determining the F-ratio (the ratio of regression mean square to the residual mean square). However, it is also important to know whether any inadequacies in the fit of the model are due to experimental error or are inherent in the model itself. As the experimental design included repeated points, the experimental error and lack-of-fit can be compared. This is termed analysis of variance (ANOVA). An F-ratio, the ratio of

replicate error to lack-of-fit mean square, is calculated and compared with critical values as before.

3.1.3 CF_4

The results of the experiments to determine the silicon and silicon dioxide etch rates are given in table 10. The randomised experimental order was: 6, 5, 2, 14, 11, 3, 12, 9, 4, 10, 1, 13, 15, 8, 7. Table 11 shows the corresponding optical emission spectroscopy results. In this case the experimental order was: 15, 10, 3, 8, 6, 2, 11, 12, 7, 14, 1, 9, 13, 4, 5. Here, the Ar (750.4 nm) emission intensity and Ar^+(480.6 nm):Ar(470.2 nm) emission intensity ratio were measured, together with changes in atomic-F and CF_2 relative concentration using the technique of argon actinometry described in chapter 2, section 2.2.2.

Table 10. Silicon and silicon dioxide etch rates in CF_4.

Experiment	Setting			Etch rate ($nm.min^{-1}$)		Selectivity	Bias
#	Flow	Press.	Power	Si	SiO_2	Si:SiO_2	(V)
1	1	1	0	115	76	1.51	340
2	1	-1	0	100	76	1.32	420
3	-1	1	0	166	66	1.52	330
4	-1	-1	0	126	74	1.70	420
5	1	0	1	168	120	1.40	470
6	1	0	-1	26	22	1.18	190
7	-1	0	1	200	140	1.43	470
8	-1	0	-1	30	38	0.79	190
9	0	1	1	214	132	1.62	430
10	0	1	-1	80	5	16.0	140
11	0	-1	1	200	108	1.85	560
12	0	-1	-1	40	28	1.43	230
13	0	0	0	130	76	1.71	370
14	0	0	0	118	70	1.69	370
15	0	0	0	108	78	1.38	370

Table 11. Optical emission spectroscopy results for CF_4.

Experiment #	Setting Flow	Press.	Power	Ar	Ar^+:Ar	[F]	[CF_2]	Bias (V)
1	1	1	0	680	0.69	42	36	320
2	1	-1	0	310	0.78	17	10	420
3	-1	1	0	450	1.0	102	37	340
4	-1	-1	0	310	0.95	27	10	440
5	1	0	1	520	1.0	51	33	490
6	1	0	-1	475	0.20	14	20	175
7	-1	0	1	445	1.3	85	4	500
8	-1	0	-1	435	0.39	25	18	200
9	0	1	1	540	1.5	56	61	450
10	0	1	-1	630	0.22	23	34	140
11	0	-1	1	360	1.0	34	13	560
12	0	-1	-1	250	0.48	8	7	220
13	0	0	0	510	0.85	35	23	380
14	0	0	0	465	0.82	42	23	370
15	0	0	0	500	0.82	37	13	380

The regression coefficients for the models developed from the two CF_4-plasma sets of experiments are shown in table 12. Least squares regression analysis with stepwise inclusion of statistically significant terms was used to limit the complexity of the models. No model was found for $Si:SiO_2$ selectivity, perhaps due to the relatively small variation in selectivity seen for the majority of the fifteen experiments.

Table 12. Regression coefficients for CF_4-plasma models.

Model term	Etch Rate		Selectivity	Bias	[F]	$[CF_2]$	$Ar^+:Ar$
	Si	SiO_2	$Si:SiO_2$	(V)			
Constant	111	73.9		376	33.8	22.8	0.844
Flow	-14.1				-14.4		-0.121
Pressure	13.6			-48.8	17.1	16.0	
Power	75.8	50.9		153	19.5		0.439
$Flow^2$					11.8		
$Pressure^2$	18.7						
$Power^2$				-37.7			-0.083
(Flow)(Pressure)					-12.5		
(Flow)(Power)							
(Power)(Pressure)		11.8					0.19

Before considering the models further, it is necessary to check their validity. Table 13 summarises the results of statistical analysis of the models. The adjusted R^2 term shows that the data is reasonably to well represented, e.g. 96% of the variation in the Si etch rate is accounted for by the model. The adjusted R^2 value of 0.61 for the $[CF_2]$ model is therefore disappointing. Nonetheless, the regression F-ratios all show statistical significance of all the models at a 95% confidence level. The higher relative standard errors, s, and errors attached to the replicate mean values for [F] and $[CF_2]$ are consistent with their lower adjusted R^2 and regression F-ratio values. However, the lack-of-fit F-ratios all indicate that a greater error lies in the modelling than the experimentation. This suggests that additional terms, such as third-order interactions, need to be included in the models.

Table 13. Evaluation of CF_4-plasma models.

Model	R^2_{adj}	F-ratio (Regression)	s	Replicate (mean value)	F-ratio (lack of fit)
Si etch rate	0.96	91.0	12	119 ± 11	0.85
SiO_2 etch rate	0.96	177	8	75 ± 5	0.24
Bias	0.99	847	9	375 ± 5	0.07
[F]	0.82	14.0	14	38 ± 4	0.09
$[CF_2]$	0.61	22.7	9	19 ± 6	0.33
Ar^+:Ar	0.97	122	0.06	0.83 ± 0.02	0.76

As the machine parameters were standardised to a common range of values (-1, 0, 1), a number of features of the models may be identified by examination of the relative size of the coefficients in table 12. In all cases, other than [CF_2] (where modelling was least successful), a positive, linear power-term was dominant. Interestingly, the Si etch rate and F-atom concentration both increased with pressure and both decreased with flow. The dc bias is shown to decrease with increasing pressure, consistent with experimental observation. A number of interactive terms can be seen. Here the relative influence of one parameter on a response varies according to the setting of another parameter.

The models are more readily visualised through contour plots. In this technique the axes of a graph are assigned to two of the factors, whilst the other factor(s) are held constant. The curves then appearing on the graph are lines of equal response. For example, figure 12 shows silicon etch rate, and figure 13 shows relative F-atom concentration as a function of pressure and RF power for a fixed flow (setting 0). It can be seen that at low pressures the silicon etch rate is, to a first approximation, dependent only on power level, whereas at high pressures the etch rate increases with both pressure and power. In contrast, the the F-atom concentration is linearly, and almost equally dependent on power and pressure for the full pressure range studied.

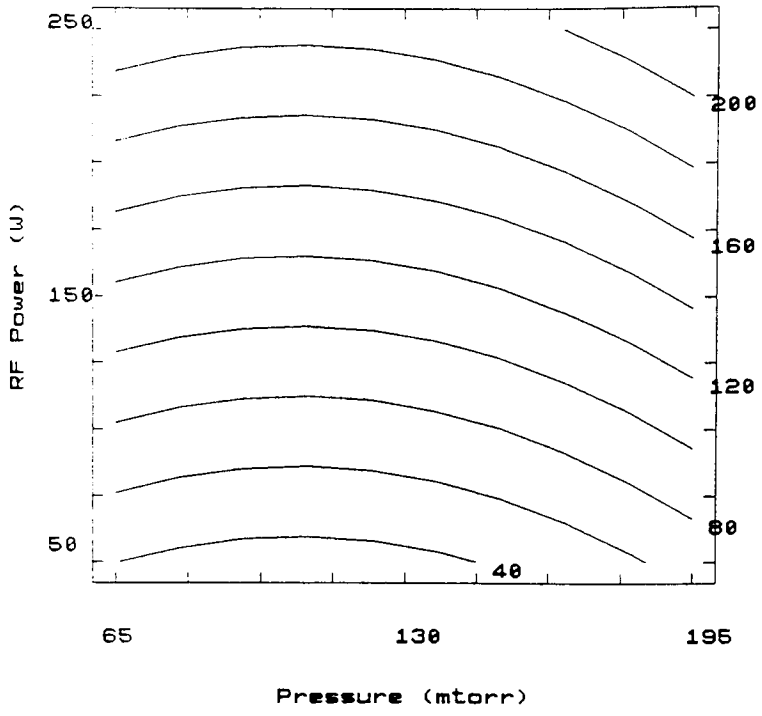

Figure 12. *Silicon etch rate ($nm.min^{-1}$) in a CF_4 plasma as function of pressure and RF power. 30 sccm flow.*

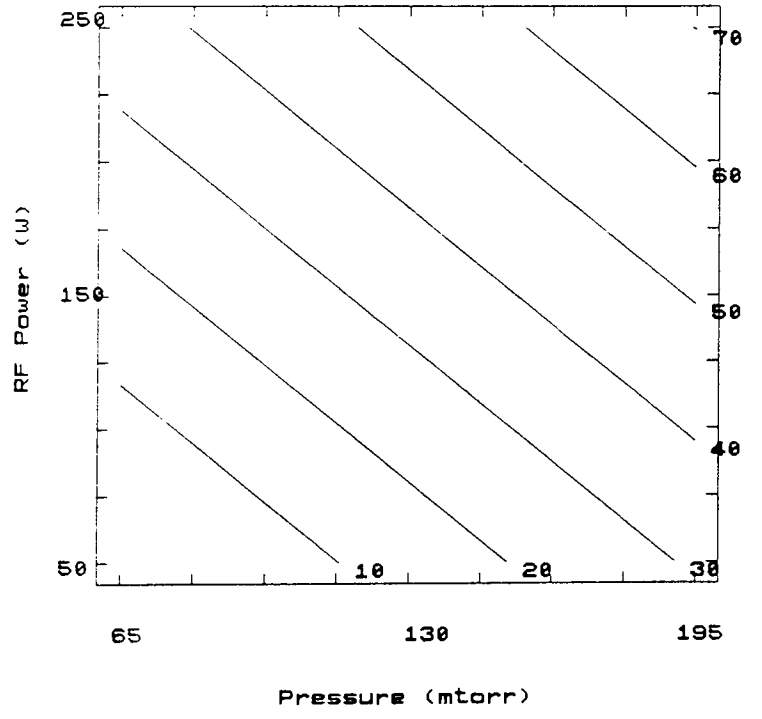

Figure 13. *Relative F-atom concentration in a CF_4 plasma as a function of pressure and power. 30 sccm flow.*

3.1.4 SF_6

The results of the experiments to determine the silicon and silicon dioxide etch rates in SF_6 are given in table 14. The randomised experimental order was: 6, 5, 2, 14, 11, 3, 12, 9, 4, 10, 1, 13, 15, 8, 7. Table 15 shows the corresponding optical emission spectroscopy results. In this case the experimental order was: 15, 10, 3, 8, 6, 2, 11, 12, 7, 14, 1, 9, 13, 4, 5.

Table 14. Silicon and silicon dioxide etch rates in SF_6.

Experiment #	Setting			Etch rate ($nm.min^{-1}$)		Selectivity	Bias
	Flow	Press.	Power	Si	SiO_2	Si:SiO_2	(V)
1	1	1	0	2400	40	60	20
2	1	-1	0	1560	40	39	150
3	-1	1	0	2220	32	69	20
4	-1	-1	0	1640	45	32	160
5	1	0	1	2740	80	34	120
6	1	0	-1	960	9	107	15
7	-1	0	1	2800	94	30	120
8	-1	0	-1	1040	7	149	20
9	0	1	1	3600	75	48	40
10	0	1	-1	840	7	120	10
11	0	-1	1	2100	90	23	290
12	0	-1	-1	900	14	64	40
13	0	0	0	2280	46	50	50
14	0	0	0	2300	44	52	50
15	0	0	0	2360	48	49	50

Table 15. Optical emission spectroscopy results for SF_6.

Experiment #	Setting Flow	Press.	Power	Ar	Ar^+:Ar	[F]	Bias (V)
1	1	1	0	1560	0.56	177	20
2	1	-1	0	680	0.46	79	180
3	-1	1	0	1570	0.57	179	340
4	-1	-1	0	710	0.45	120	180
5	1	0	1	1480	0.33	183	120
6	1	0	-1	690	0.31	66	20
7	-1	0	1	1490	0.35	183	120
8	-1	0	-1	700	0.34	65	20
9	0	1	1	2000	0.57	140	50
10	0	1	-1	690	0.60	64	10
11	0	-1	1	730	0.45	92	310
12	0	-1	-1	455	0.22	42	50
13	0	0	0	1290	0.34	144	60
14	0	0	0	1280	0.37	147	60
15	0	0	0	1240	0.31	146	60

Prior to modelling of the SF_6 data, it is immediately apparent from comparison of the SF_6-plasma results with those from CF_4-plasma that there are considerable differences between the two systems. Most dramatic is the high $Si:SiO_2$ selectivity obtained with SF_6 - the result of a ca. twenty-fold increase in Si etch rates and ca. halving of SiO_2 etch rates. It can be seen that this was accompanied by a ~400% increase in F-atom concentration, and a general reduction in d.c. bias. The relationship between the Ar^+:Ar ratios - representing changes in the proportion of electrons with energy >35 eV:electrons with energy >15 eV - for the two systems is clearly more complex.

All the responses measured were successfully modelled. The SF_6 models (table 16) were of a generally higher quality (table 17) than those for CF_4, as evidenced by the adjusted R^2 and F-ratio values. Consideration of the standard errors and the replicate errors shows that this was due to an improved set of experimental results. Thus the lack-of-fit F-ratio values are even smaller than those for CF_4. Again, although the models are statistically significant, their residual error is due to lack-of-fit rather than experimental error.

Figures 14 and 15 show respectively contour plots of the silicon etch rate and F-atom concentration as a function of RF power and pressure. It can immediately be seen that, unlike the CF_4 case, they both take a similar form. This indicates a direct correlation between etchant concentration and etch rate over a wide parameter space for SF_6, whereas with CF_4 other factors are also of importance. Although of differing values, the SiO_2 etch rate and d.c. bias showed similar dependencies on the process parameters to those found with CF_4. Contour plots are shown in figures 16 and 17 respectively. It can be seen that the oxide etch rate is directly proportional to RF power and that the bias increases with power and decreases with pressure. These results are considered again in the next section.

Table 16. Regression coefficients for SF_6-plasma models.

Model term	Etch Rate Si	Etch Rate SiO_2	Selectivity Si:SiO_2	Bias (V)	[F]	Ar^+:Ar
Constant	2313	44.7	50.1	63.6	142	0.336
Flow						
Pressure	358	-4.38	17.4	-71.9	45.0	0.09
Power	938	37.75	-38.1	61.3	61.8	
$Flow^2$	-167					
$Pressure^2$	-192			34.6		0.149
$Power^2$	-262		21.7		-20.7	
(Flow)(Pressure)						
(Flow)(Power)						
(Power)(Pressure)	390			-55.0	39.8	-0.065

Table 17. Evaluation of SF_6-plasma models.

Model	R^2_{adj}	F-ratio (Regression)	s	Replicate (mean value)	F-ratio (lack of fit)
Si etch rate	0.99	243	79	2310 ± 50	0.08
SiO_2 etch rate	0.97	187	6	46 ± 2	0.11
Selectivity (Si:SiO_2)	0.82	22.5	15	50 ± 2	0.01
Bias	0.98	147	12	55 ± 5	0.21
[F]	0.97	101	12	146 ± 2	0.01
Ar^+:Ar	0.86	21.9	0.05	0.34 ± 0.03	8.35

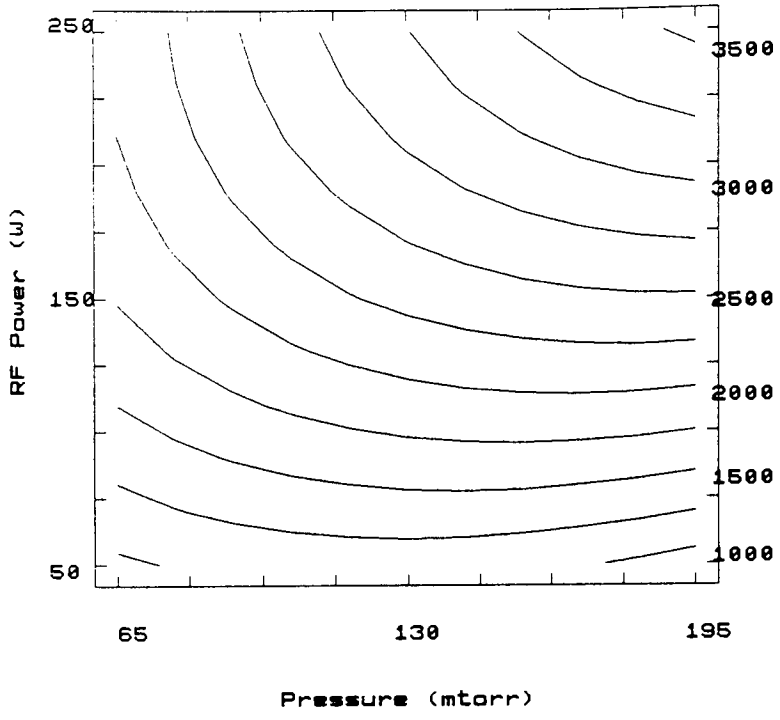

Figure 14. *Si etch rate ($nm.min^{-1}$) in a SF_6 plasma as a function of RF power and*

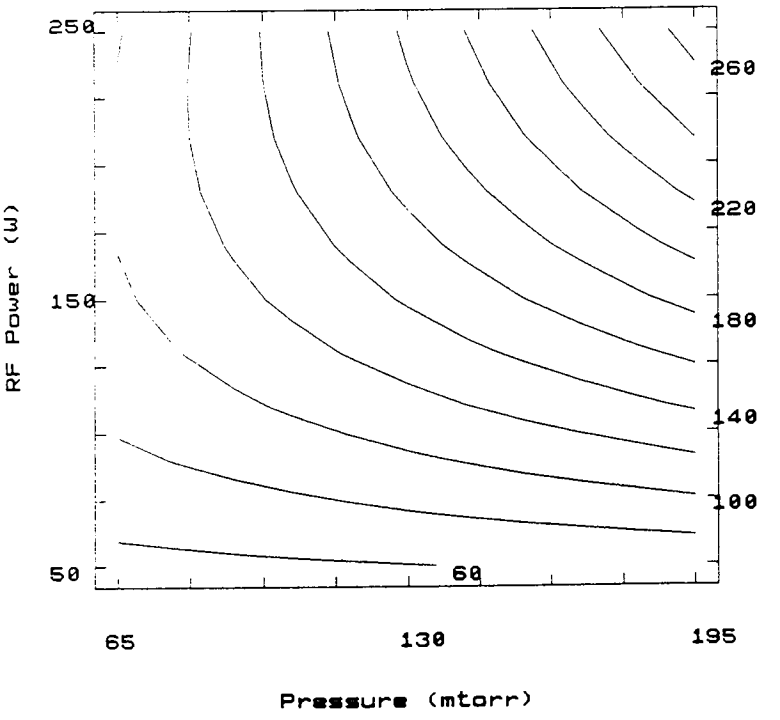

Figure 15. *Relative F-atom concentration in a SF_6 plasma as a function of RF power and pressure.*

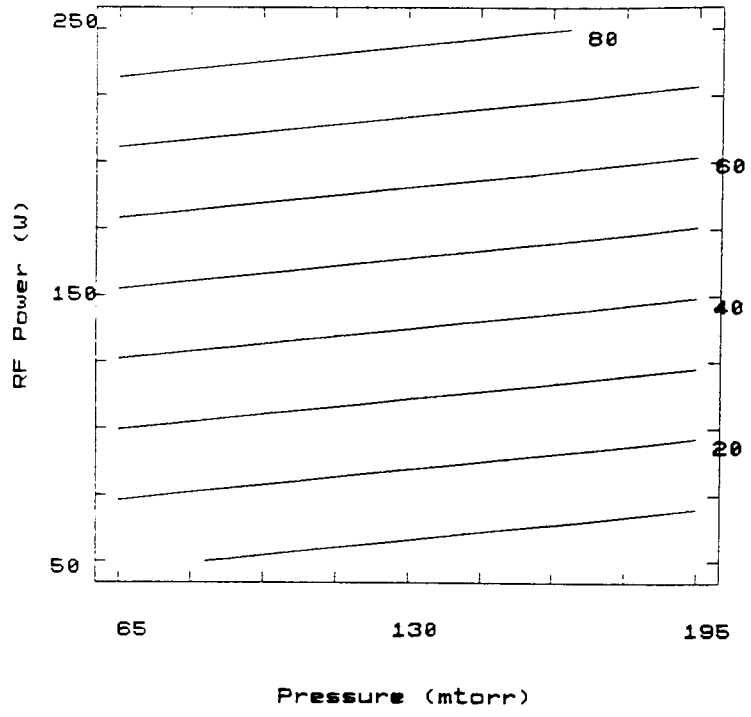

Figure 16. *SiO_2 etch rate ($nm.min^{-1}$) in a SF_6 plasma as a function of RF power and pressure.*

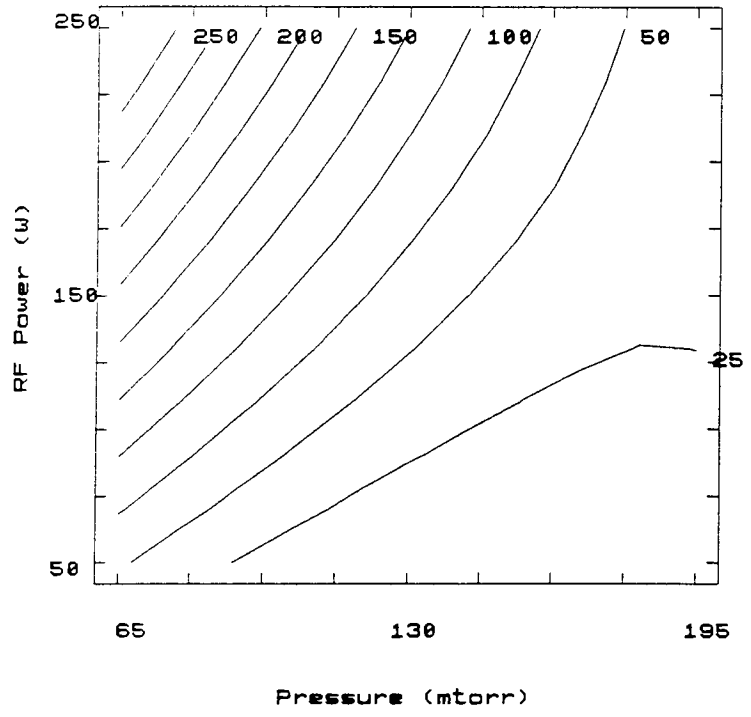

Figure 17. *d.c. bias (V) produced by a SF_6 plasma as a function of RF power and pressure.*

3.1.5 CF_4/SF_6 Mixtures

In order to further investigate the differences between the two systems, and to study any possible synergistic effects CF_4/SF_6 mixtures were studied under conditions of fixed flow, pressure and RF power (20 sccm, 60 mtorr and 100 W respectively).

Consistent with the previous results the silicon etch rate and F-atom concentration both fell with increasing percentage additions of CF_4 to SF_6, as shown in figure 18. Under these conditions, the change in silicon etch rate was an order of magnitude and the change in F-atom concentration a factor of four on going from pure SF_6 to pure CF_4. However, whereas the F-atom concentration varied linearly with $\%CF_4$, with SF_6/75% CF_4 the silicon etch rate was almost double that which would have been predicted by linear extrapolation between the pure gas results, indicating a degree of synergism. Similarly, the silicon dioxide etch rate and d.c. bias both rose with increasing percentage additions of CF_4 to SF_6. In this case an excellent, though non-linear, correlation was found between etch rate and d.c. bias (figure 19).

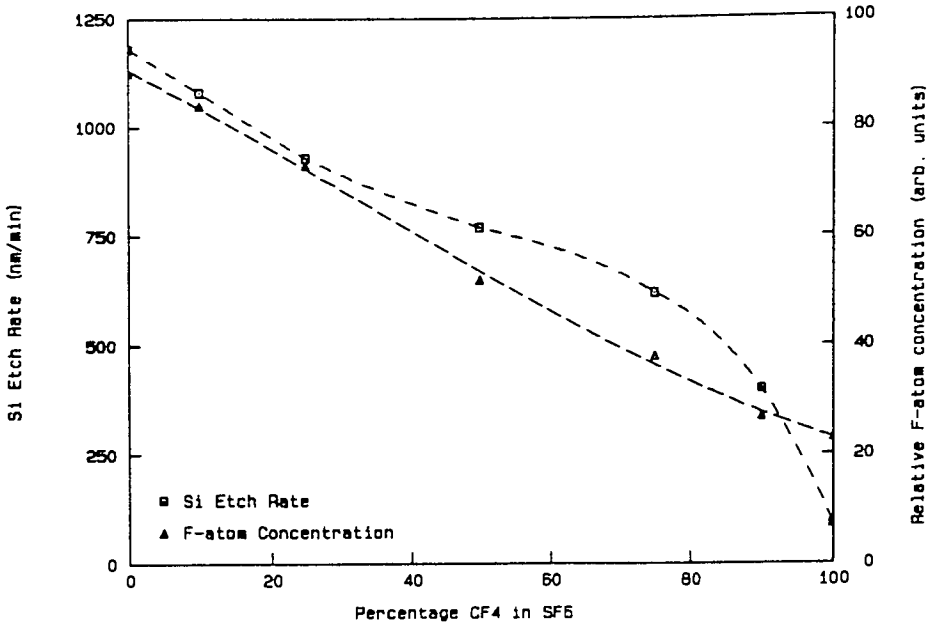

Figure 18. *Si etch rate and relative F-atom concentration as a function of percentage CF_4 in SF_6.*

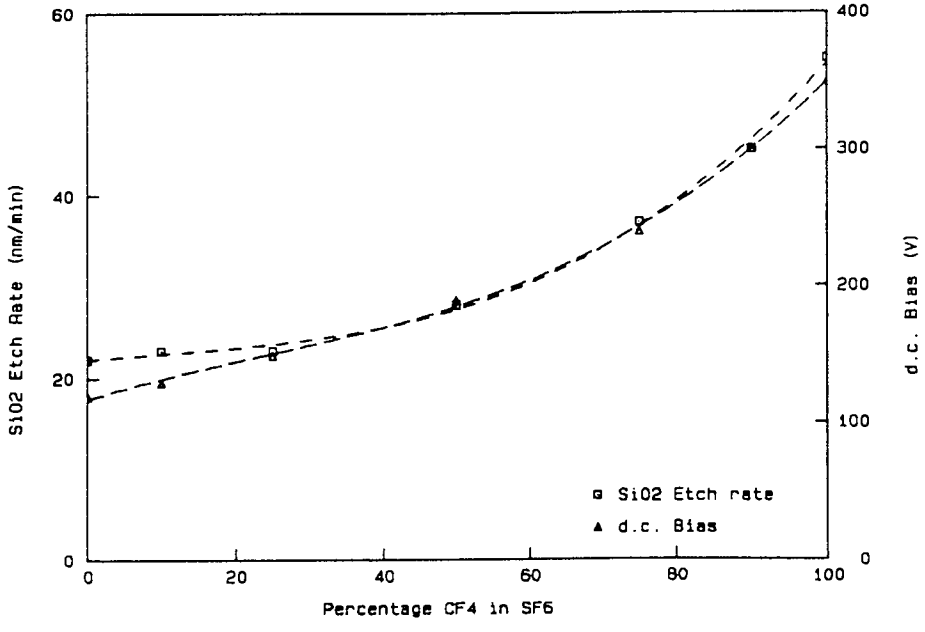

Figure 19. *SiO_2 etch rate and d.c. bias as a function of percentage CF_4 in SF_6.*

3.1.6 Influence of d.c. Bias on Silicon Dioxide Etch Rates

The previous sections showed that SiO_2 etch rates in fluorine containing discharges are, for a given etchant, dependent on RF power level, and at fixed power and pressure dependent on d.c. bias. However, the bias dependency was demonstrated by the addition of CF_4 to SF_6. CF_4 is an established oxide etchant; CF_x radicals and CF_3^+ ions produced from it have both been considered active oxide etchants. Thus the increase in SiO_2 etch rate with additions of CF_4 to SF_6 could be entirely due to an increase in etchant concentration, the rise in d.c. bias being entirely coincidental. (N.B. the d.c. bias is a self bias measured with respect to ground; no independent control of bias was available with the RIE 80 configuration used.)

In order to test this hypothesis, alternative SF_6 additives - Ar, O_2, CO_2, H_2 and CH_4 -, none of which are oxide etchants, were used. CO_2 and CH_4 were included in the experiments to establish whether the addition of carbon-containing species had a beneficial effect on the oxide etch rate. The results, at two RF power levels (100 and 200 W), together with measurements for pure SF_6 and Ar, are shown in table 18. All experiments were at 60 mtorr pressure and 20 sccm flow. Relative F-atom concentrations were also measured. It can be seen that all the additives, even when present in small percentages, significantly increased the d.c. self bias. O_2 and CO_2 additions served to increase, and H_2 and CH_4 additions to decrease the F-atom concentration, as expected. No correlation between F-atom concentration and oxide etch rate was found.

Table 18. Si and SiO_2 etch rates in SF_6/additive plasmas.

RF Power (W)	Additive	Etch Rate ($nm.min^{-1}$) Si	SiO_2	[F]	d.c. bias (V)
50	-	830	12		50
100	-	1260	22	103	115
"	50% Ar	1000	30		215
"	20% O_2	1730	25	400	175
"	20% CO_2	1820	23	157	150
"	10% H_2	1220	25	54	155
"	20% H_2	830	30	41	170
"	10% CH_4	700	27	37	165
200	-	1730	53	132	235
"	50% Ar	1450	100		405
"	20% O_2	2540	78	449	325
"	20% CO_2	2260	56	179	290
"	10% H_2	1740	73	81	290
"	20% H_2	1380	80	59	315
"	10% CH_4	1240	72	56	315
100	100% Ar	1	5		340

Figure 20 shows that, within experimental error, the SiO_2 etch rate is indeed proportional to d.c bias. Also included in the figure is the result for pure Ar, and the previous results for SF_6/CF_4 mixtures. The former demonstrates that the oxide sputter rate is more than an order of magnitude lower than the etch rate in the presence of fluorine/fluorinated species at the same d.c. bias. Taken with the spectroscopic results, this implies that although attack by fluorine is not the rate determining step in oxide etching it is nonetheless essential. It is interesting to note that the results of the SF_6/CF_4 experiments, which were performed at 100 W, lie on the same etch rate vs. bias curve as the present SF_6/additive 100W results. For a given d.c. bias the 200 W experiments gave significantly higher etch rates.

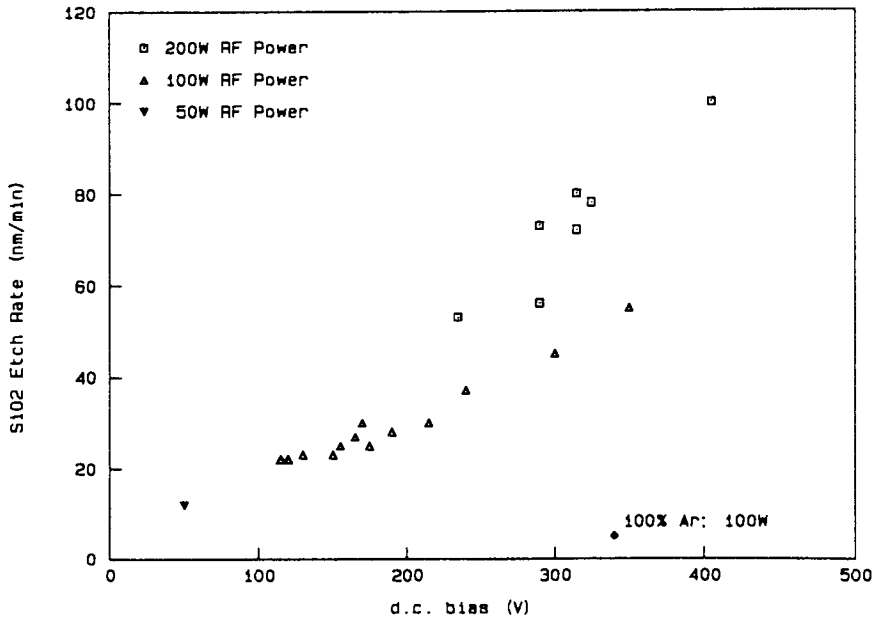

Figure 20. SiO_2 etch rates as a function of d.c. bias in SF_6 plasmas.

3.2 Addition of Oxygen-containing Additives to Fluorocarbon and SF_6 Plasmas

This section reports results of studies of the influence of the source of oxygen additions- O_2, N_2O or CO_2 - on the etch rates of silicon and silicon dioxide in CF_4, C_2F_6, CHF_3 and SF_6 plasmas. The corresponding gas phase chemistry was studied by optical emission spectroscopy with argon actinometry. All experiments were carried out at 100 W RF power, 60 mtorr pressure and 20 sccm flow rate. Experiments were then performed with increasing percentages of a given additive. The etch time was 10 mins.

3.2.1 CF_4

Figure 21 shows Si etch rates in a CF_4 discharge as a function of the addition of each of O_2, N_2O and CO_2. Maxima in the etch rates are seen for ~10% O_2 (250 $nm.min^{-1}$.) and ~20% N_2O (220 $nm.min^{-1}$.). It can be seen from the OES results that, though at 25% additive the fluorine intensities are in the order $O_2>N_2O>CO_2$ (figure 22), the atomic-O signal from N_2O is much lower than that from O_2 (figure 23). Reduced competition from atomic-O for silicon surface sites might therefore account for the observed CF_4/N_2O etch rates. Oxide etch rates (~55 $nm.min^{-1}$) were largely insensitive to gas chemistry.

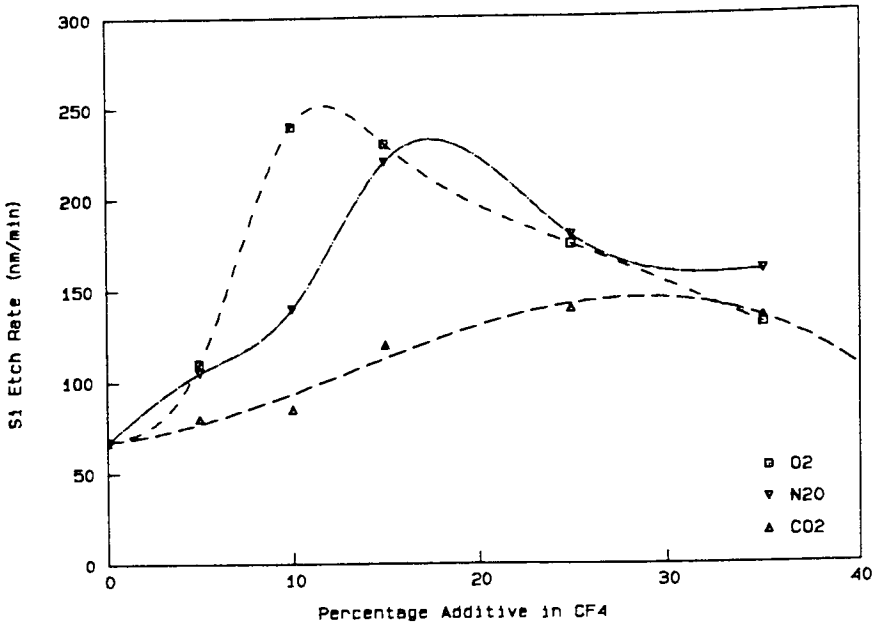

Figure 21. *Si etch rates in a CF_4 plasma as a function of the addition of O_2, CO_2 and N_2O.*

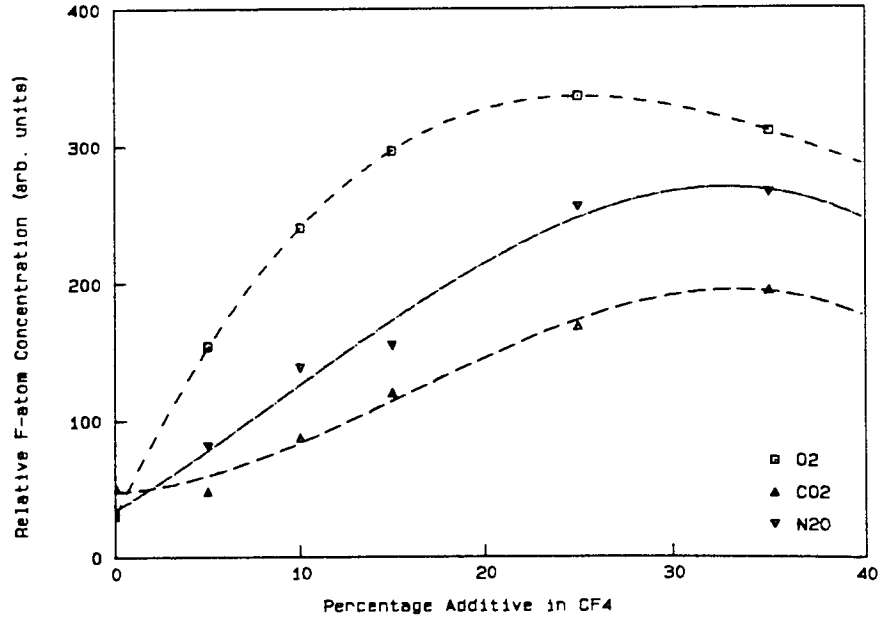

Figure 22. *Actinometered F (703.7 nm) emission from a CF_4 plasma as a function of the addition of O_2, CO_2 and N_2O.*

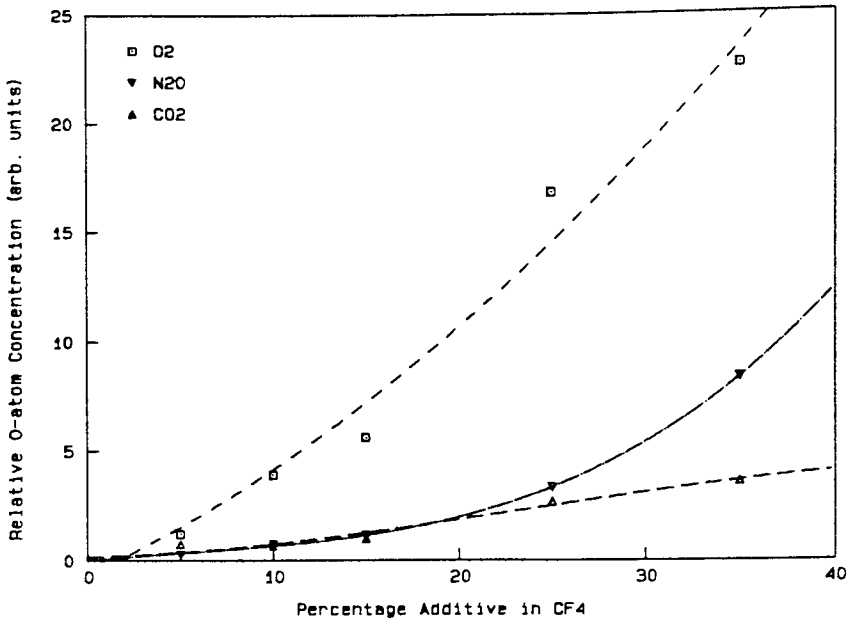

Figure 23. Actinometered O (844.6 nm) emission from a CF_4 plasma as a function of the addition of O_2, CO_2 and N_2O.

3.2.2 C_2F_6

The higher C:F ratio of the system was reflected in a five-fold increase in CF_2 intensity w.r.t. CF_4, and a higher % additive required to produce a maximum in the F-intensity . As with CF_4, the maximum silicon etch rate occurred for a higher % addition of N_2O (55%) than O_2 (40%). The maximum etch rates which were generally lower than with CF_4, reflecting the lower F:O and F:CF_2 ratios, were in this case higher with O_2 (~250 nm.min^{-1}.) than N_2O (~150 nm.min^{-1}). Again, silicon etch rates with the addition of CO_2 were relatively low.

In contrast to the CF_4 system, oxide etch rates (figure 24) showed some dependence on % additive. They approximately doubled in the region 0-40% additive to reach a value similar to that found with CF_4. The etch rates at 40% additive were in the order O_2>CO_2>N_2O.

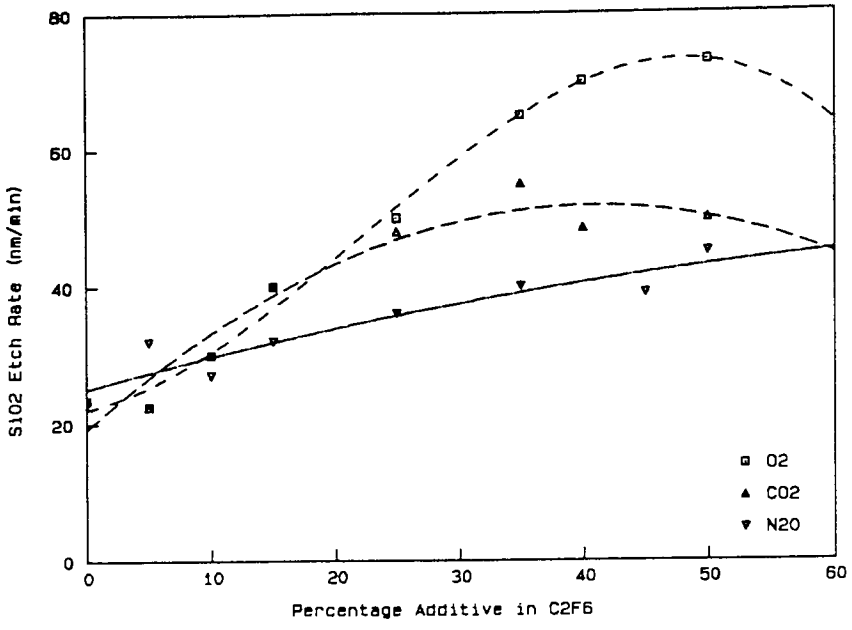

Figure 24. *SiO_2 etch rates in C_2F_6 plasmas as a function of the addition of O_2, CO_2 and N_2O.*

3.2.3 CHF_3

The low silicon etch rates found with CHF_3 (~12nm.min^{-1}) were consistent with the observed low F-atom concentrations and high CF_2 radical concentrations. As expected, selective (3:1) oxide etching was obtained at low additive concentrations. The oxide etch rate was largely in variant with the plasma chemistry. Silicon etch rates were in the order N_2O>O_2>CO_2.

3.2.4 SF_6

Silicon etch rates in a SF_6 discharge are shown in figure 25 as a function of the addition of O_2 and N_2O. The corresponding oxide etch rates, not shown, remained fairly constant at ~20 $nm.min^{-1}$. As with CF_4 and C_2F_6, a maximum in the Si etch rate was observed with the addition of a higher % N_2O than % O_2. In this case the % additives and etch rates were: O_2 (15-20%, 2100 $nm.min^{-1}$.) and N_2O (40-45%, 1400 $nm.min^{-1}$.). These represent considerably higher etch rates than the CF_4 system, consistent with the earlier results in this chapter.

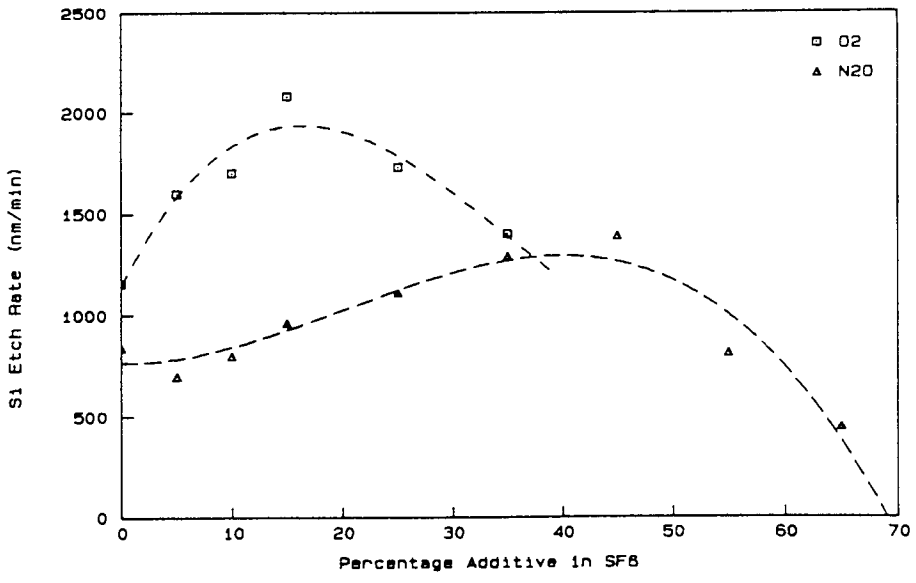

Figure 25. Si etch rates in SF_6 plasmas as a function of the addition of O_2 and N_2O.

3.3 Influence of Electrode Materials

In this section the influence of another parameter, choice of electrode material, on the etch rate of silicon and thermally grown oxide in CF_4 and CF_4/O_2 plasmas is studied. The etch rate results have been related to the corresponding relative atomic fluorine concentration, as determined by optical emission spectroscopy with argon actinometry. The extent of contamination of silicon surfaces by the electrode materials, the chemical state of the transferred materials, and their influence on the silicon surface chemistry have been assessed by X-ray photoelectron spectroscopy. Experiments were also performed to study the influence of certain electrode materials on fluorocarbon polymer deposition and stripping rates.

3.3.1 Silicon and Silicon Dioxide Etch Rates

Silicon etch rates are shown in figure 26 as a function of electrode material for both a CF_4 and a CF_4/10% O_2 plasma. It is clear from this that the silicon etch rates were, as expected, generally higher for a CF_4/10% O_2 discharge than for pure CF_4; and that compared with an uncovered (anodised aluminium) electrode the silicon etch rate was not significantly influenced by the use of an aluminium or quartz cover-plate. However, a soda-glass electrode was found to confer an unexpectedly large increase in the silicon etch, particularly in the presence of oxygen. The absence of a similar effect on etch rate when a quartz plate was used suggested that the insulating properties of the glass were not responsible for the enhanced etching. As the most likely explanation would therefore involve the participation of sodium from the glass, etch rates were also measured with quartz plates coated with sodium and potassium salts. As figure 26 shows, both these cover-plates produced a significant enhancement in etch rate.

In contrast to these observations, figure 27 demonstrates that the same range of electrode materials had little effect on the relative etch rates of SiO_2. If anything, the alkali-metal doped electrodes had a negative effect.

Silicon etch rates were also measured under identical conditions in SF_6 with a bare electrode and a soda glass cover-plate. In this case only a slight (20%) etch rate enhancement in the presence of soda glass was found compared to the 250% enhancement observed for CF_4 and the 400% enhancement for CF_4/10% O_2. However, it should be noted that the silicon etch rate in SF_6 on a bare electrode (825 $nm.min^{-1}$) was already even higher than that in CF_4/10% O_2 on a soda glass electrode (390 $nm.min^{-1}$).

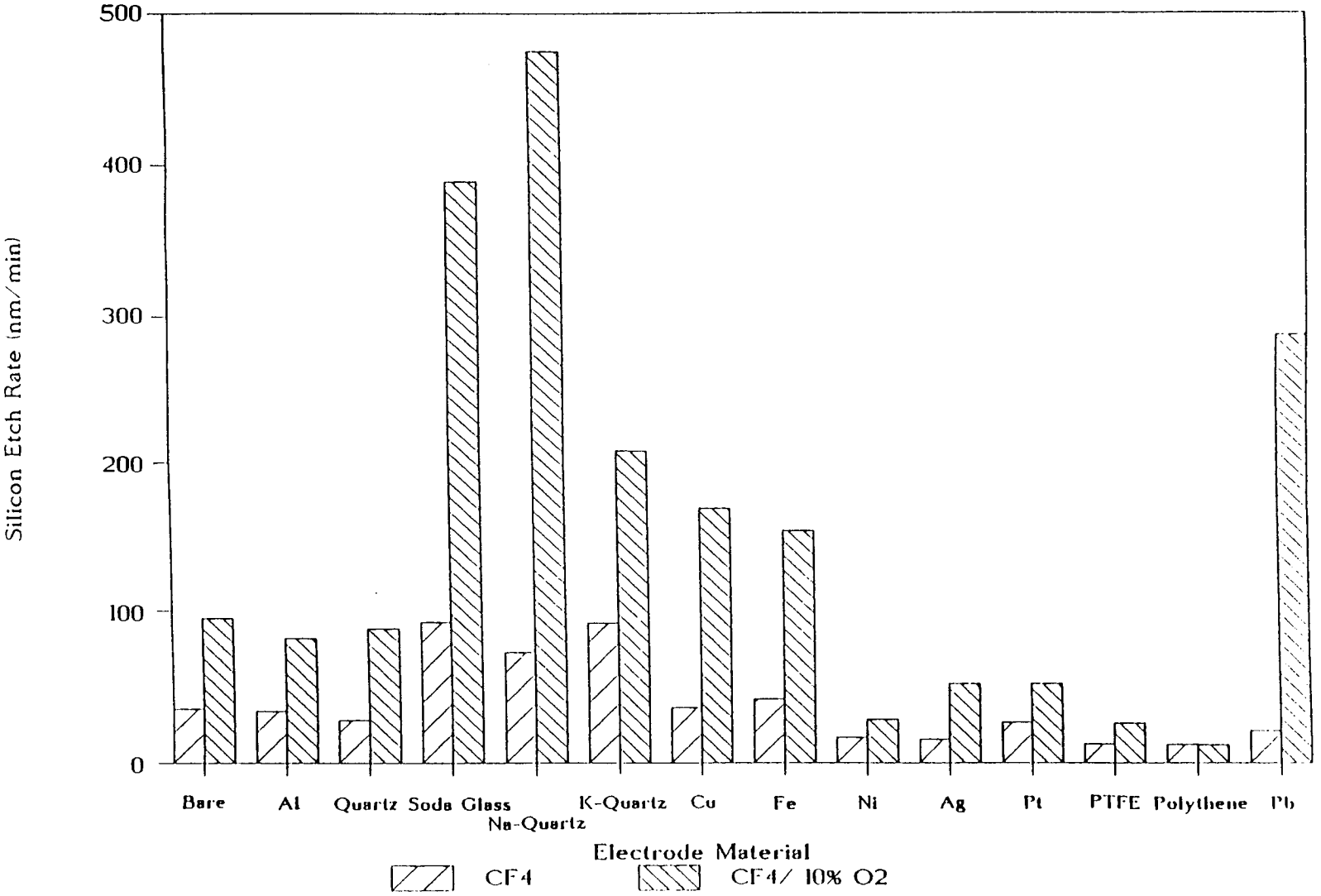

Figure 26. Si etch rates as a function of electrode cover-plate material.

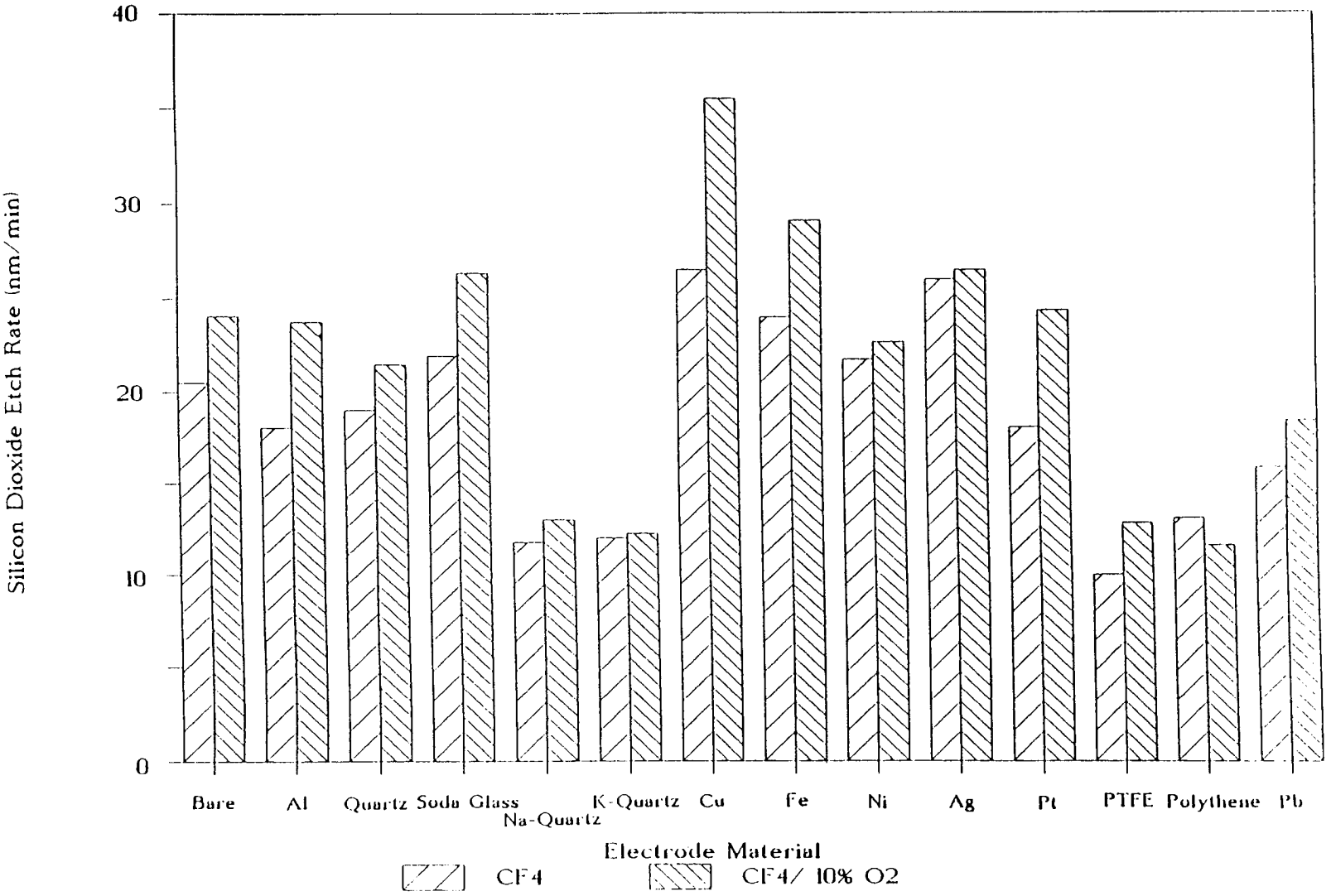

Figure 27. *SiO_2 etch rates as a function of electrode cover-plate material.*

3.3.2 Optical Emission Spectroscopy

It is instructive to consider first the Ar (750.4 nm) emission to which the F (703.7 nm) emission is ratioed in order to obtain relative F-atom concentrations. Figure 28 shows that for the CF_4/5% Ar discharge the variations in the Ar emission can largely be accounted for by physical changes in the optical path due to electrode thickness - with the exception of silver. This implies that the various electrode materials do not substantially alter the electrical characteristics of the plasma.

OES results are presented in figures 29 and 30 in the form of corrected atomic fluorine intensity versus silicon etch rate for CF_4 and CF_4/10% O_2 plasmas respectively. Some correlation between silicon etch rate and relative atomic fluorine concentration would be expected for the reactive ion etching of silicon in these plasmas. Figures 29 and 30 show that, although there is a much wider range of relative atomic fluorine concentrations than silicon etch rates, to a first approximation this is indeed the case. However, it is clear that the high etch rates associated with the presence of alkali metal cannot be accounted for by a corresponding increase in available atomic fluorine. This suggests that the alkali metal influences surface chemistry rather than gas-phase processes.

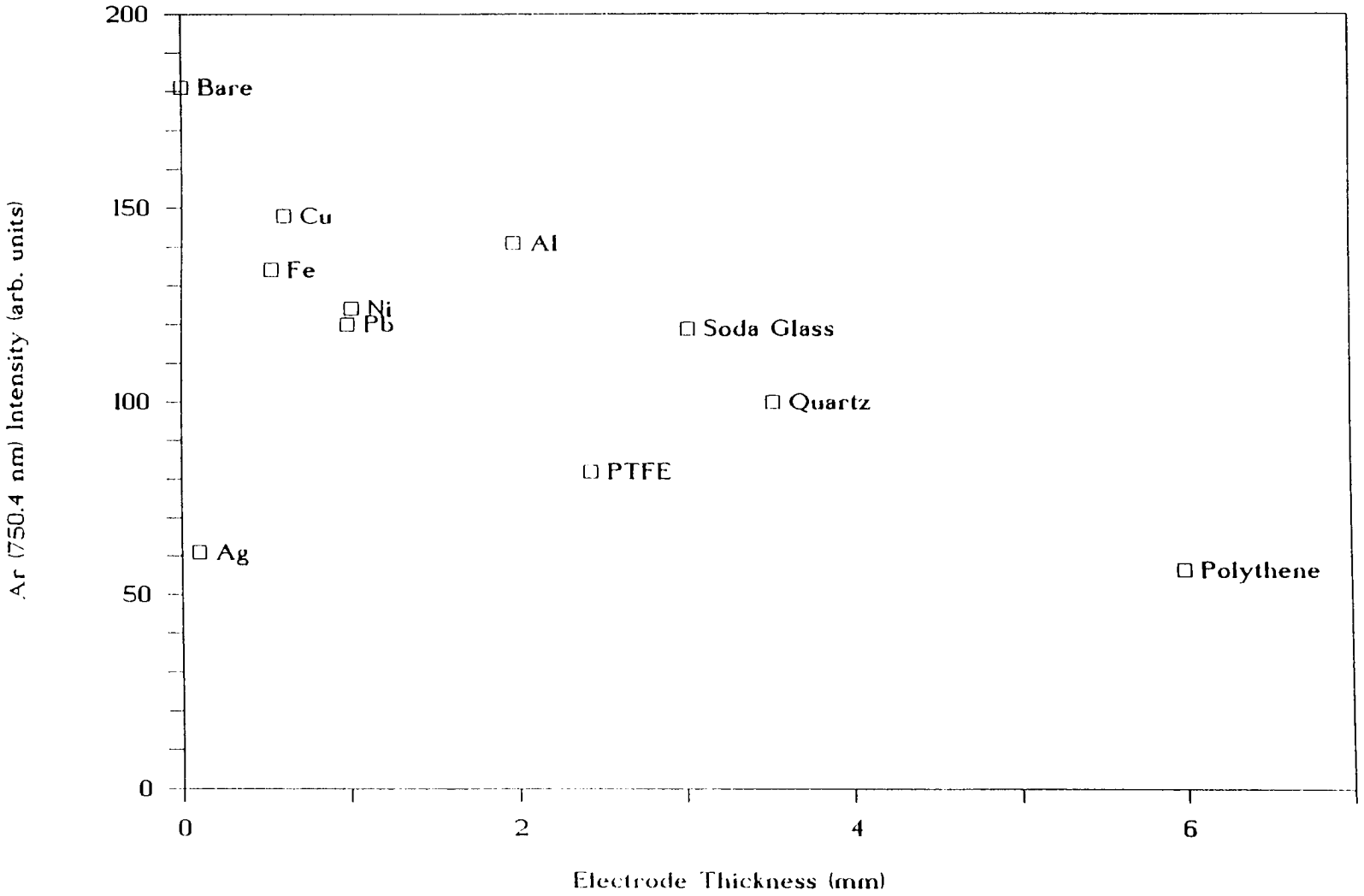

Figure 28. *Ar (750.4 nm) emission intensity vs. electrode cover-plate thickness; CF_4/5% Ar plasma.*

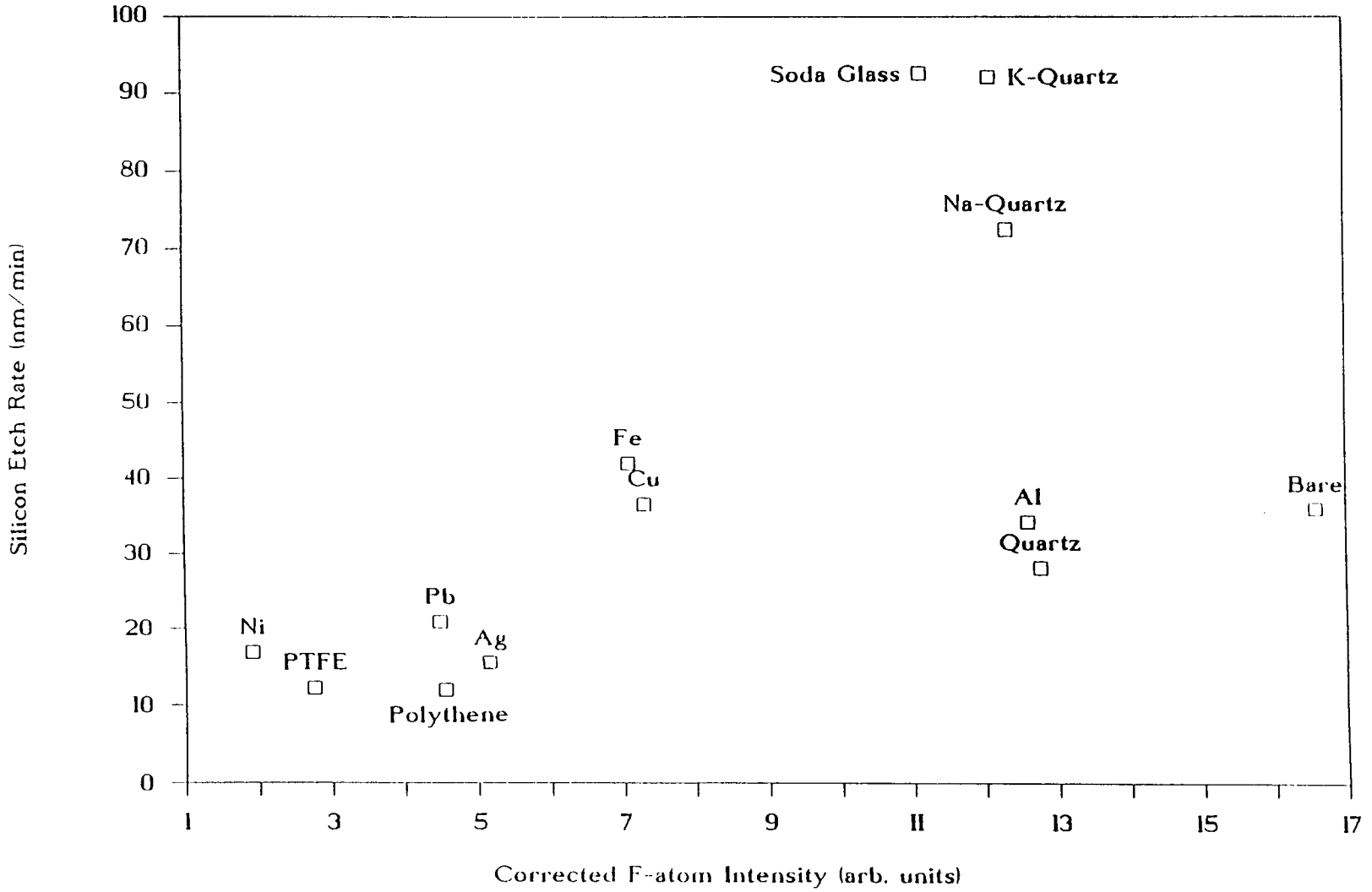

Figure 29. Si etch rate vs. actinometered F (703.7 nm) emission; CF_4 plasma.

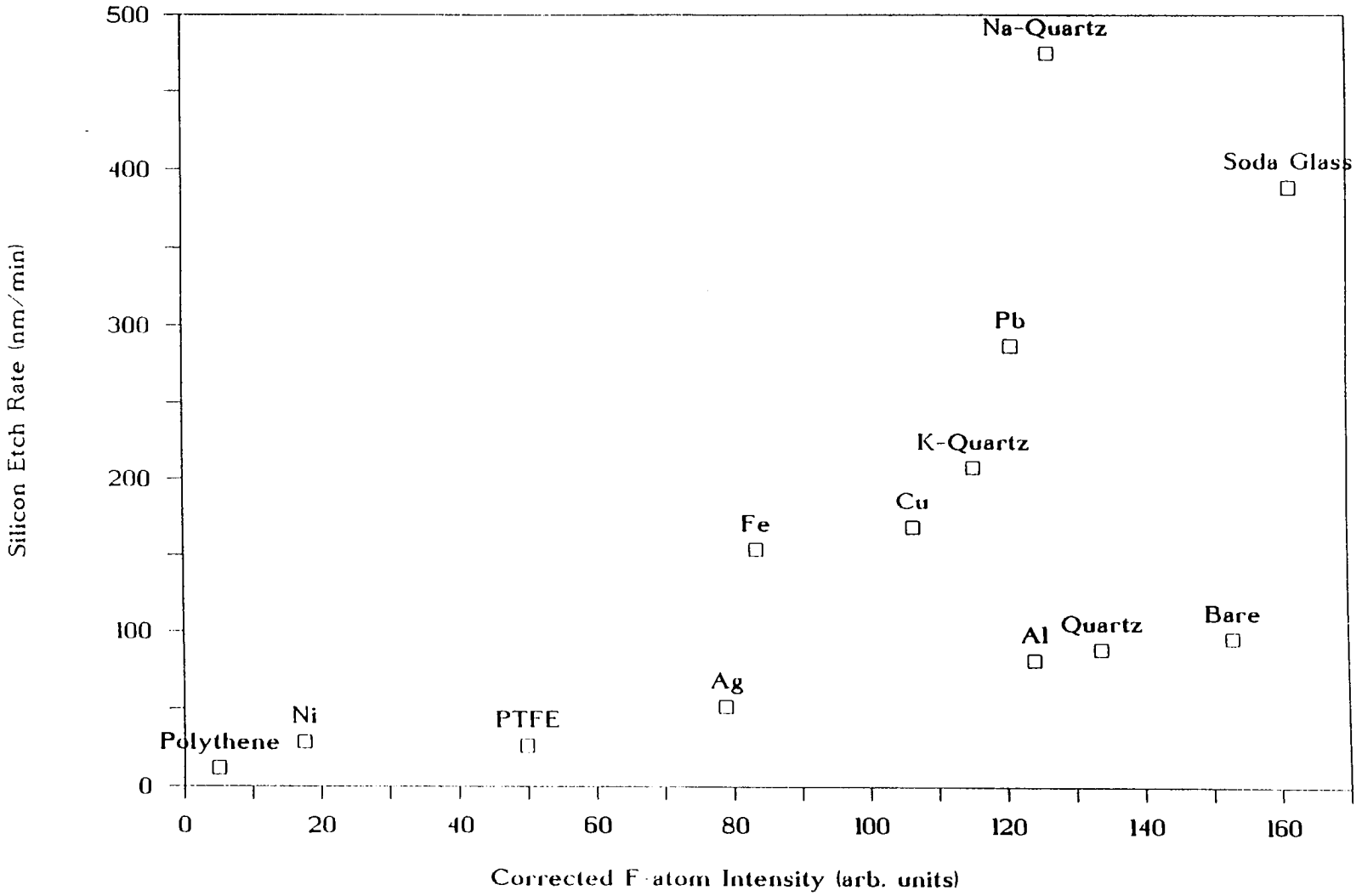

Figure 30. Si etch rate vs. actinometered F (703.7 nm) emission; CF_4/10% O_2 plasma.

3.3.3 X-ray Photoelectron Spectroscopy

XPS surface elemental analyses of silicon etched in CF_4/10% O_2 on a variety of electrode cover-plates are shown in table 19, together with the corresponding etch rates. Results are also given, for comparison, for unetched silicon and silicon etched in SF_6. The corresponding binding energies and Auger parameters are given in table 20. Table 19 confirms that sodium had been transferred on to the silicon wafer from the soda glass cover-plate. Similarly, nickel, copper and lead were detected on the surface of silicon samples after etching on the respective cover-plates. No material was found to have been transferred onto a silicon sample from an uncovered (anodised aluminium) electrode or an aluminium electrode.

Table 19. XPS surface elemental analysis of silicon samples as a function of etchant and electrode material.

Etchant	Electrode Material	Etch Rate (nm/min)	Atomic Concentration (%) Si(total)	Si(IV)	Metal	F	O	C
Unetched			40.4	3.7			34.8	24.8
CF_4/10% O_2	Ni	30	15.1	5.5	6.1	15.4	31.9	31.5
"	Bare	95	25.2	5.5	0.0	16.0	28.7	30.1
"	Al	82	18.2	1.4	0.0	15.4	19.9	46.5
"	Quartz	88	21.7	3.1	0.0	6.3	27.6	46.5
"	Cu	170	18.4	10.4	3.8	9.3	41.4	27.1
"	Pb	290	23.3	7.7	3.1	2.0	37.3	34.3
"	Soda Glass	390	31.8	4.8	3.9	5.7	34.6	24.0
SF_6	Bare	825	33.9	4.7	0.0	1.7	32.9	31.5

The split in the Si2p binding energy (table 20) shows that the silicon is present in both an unoxidised, Si(0), and an oxidised, Si(IV), form. It can be seen from table 19 that the relative proportion of Si(IV) is increased in the presence of nickel, copper and lead. This is consistent with an increase in the thickness of an oxidised silicon layer on a single crystal silicon substrate. However, there is no correlation with etch rate.

The binding energies and Auger parameters given in table 20 provide information on the likely chemical environment of the transferred metals. It is difficult, though, to assign a chemical environment to the sodium levels, but the sodium is certainly in a highly oxidised state.

The $Ni2p_{3/2}$ binding energies at 860.2 and 853.6 eV show the presence of nickel in two oxidation states. These correspond to a Ni-F species, possibly NiF_6^{2-} at 860.2 eV, and most likely Ni(II) at 853.6 eV.

Data from the silicon etched on a copper electrode are interesting in that the $Cu2p_{3/2}$ level at 933.7 eV is due to Cu(II) oxide, not fluoride, although a tail on the $Cu2p_{3/2}$ level at approximately 937 eV could correspond to the fluoride. The presence of a Cu-F species is shown by a CuLMM Auger level at 915 eV, but no FKLL Auger level for CuF_2 was detected. Thus, the bulk of the copper is CuO with a trace of CuF_2 only.

The F1s level at 684.5 eV and the FKLL Auger parameter at 657.7 eV for the silicon on the lead electrode are indicative of a Pb-F species, possibly $>PbF_2$. The $Pb4f_{7/2}$ level at 139.6 eV shows the lead to be present in a highly electropositive state.

Table 20. *XPS binding energies of silicon samples as a function of etchant and electrode material.*

Etchant	Electrode Material	Binding Energy (eV) C1s	Si2p	O1s	F1s	FKLL(k.e.)	Metal	
Unetched		285.6 289.9	99.3 103.3	533.3				
CF_4/10% O_2	Ni	285.2 287.4 288.9	99.1 102.8	533.0	688.5 686.6	652.7	$Ni2p_{3/2}$	860.2 853.6
"	Bare	285.5 287.5 289.2	99.3 102.9	532.9	688.3	652.0		
"	Al	285.4 286.5 287.9	99.2 102.7	533.0	688.8	651.2		
"	Quartz	285.3 287.0 289.2	99.3 102.8	533.1	687.8	651.8		
"	Cu	285.3 287.0 289.1	99.3 103.2	533.3	687.2	653.2	$Cu2p_{3/2}$ CuLMM	933.7 915
"	Pb	285.9 287.5 289.9	99.7 103.7	533.3	684.5 687.2	657.7	$Pb4f_{7/2}$	139.6
"	Soda glass	285.8 287.5 289.6	99.4 103.6	533.6	688.2	651.4	Na1s	1073.2
SF_6	Bare	285.5 286.7 289.2	99.5 103.5	533.1	687.6	654		

3.3.4 Polymer Deposition and Stripping Rates

It was shown in chapter 1 that the etching of silicon in fluorocarbon plasmas proceeds by a competition between silicon etching, polymer deposition and polymer etching. In order to ascertain **the influence of electrode materials** on polymer formation and removal processes (and hence, potentially, net silicon etch rates), the deposition rates and etch rates of polymers analogous to those expected from a CF_4 plasma were measured as a function of electrode material. (N.B. studies of fluorocarbon polymer formation per se is the subject of the next chapter.) C_3F_8 and CHF_3, and a higher chamber pressure, were used to achieve measurable deposition rates and thick polymer films for the stripping rate studies.

C_3F_8 and CHF_3 plasma polymer deposition rates are shown in tables 21(a) and 21(b) respectively for silicon and silicon dioxide samples on an uncovered (anodised aluminium), a soda glass and a quartz electrode. It can be seen that for the lower deposition rates found with C_3F_8: (i) the silicon and silicon dioxide have similar polymer deposition rates; and (ii) the presence of quartz and soda glass electrodes approximately halves the deposition rate. With CHF_3, however, where deposition rates are more rapid, no differences are observed when glass and quartz electrodes are used. These results are consistent with oxygen from the quartz and soda glass electrodes inhibiting polymer formation and being available for a longer period with C_3F_8 than CHF_3. It seems therefore that sputtered alkali metal atoms have no influence on fluorocarbon polymer deposition rates from these gases, although it is possible that polymer deposited on the electrodes inhibits sputtering of alkali metals.

Stripping rates of polymer films on silicon (from both C_3F_8 and CHF_3 plasmas) were studied with bare and soda glass electrodes: see tables 22(a) and 22(b). The

stripping rates were identical within experimental error for both electrode materials in CF_4, CF_4/10% O_2 and O_2 plasmas. Alkali metals from the glass electrode clearly have no significant influence on these polymer etch rates.

Table 21(a). Deposition rate of C_3F_8 plasma polymer onto Si and SiO_2 samples as a function of electrode material.

Electrode Material	**Deposition Rate (nm/min)**	
	Si	**SiO_2**
Bare	10.0	8.8
Quartz	4.7	4.7
Soda Glass	3.7	5.3

Table 21(b). Deposition rate of CHF_3 plasma polymer onto Si and SiO_2 samples as a function of electrode material.

Electrode Material	**Deposition Rate (nm/min)**	
	Si	**SiO_2**
Bare	40.0	45.5
Quartz	36.2	38.7
Soda Glass	42.0	43.3

Table 22(a). Etch rate of C_3F_8 plasma polymer as function of electrode material.

Etchant	Etch Rate (nm/min)	
	Bare Electrode	Soda Glass Electrode
CF_4/10% O_2	230	170

Table 22(b). Etch rate of CHF_3 plasma polymer as function of electrode material and etchant.

Etchant	Etch Rate (nm/min)	
	Bare Electrode	Soda Glass Electrode
CF_4	110	100
CF_4/10% O_2	175	200
O_2	270	275

CHAPTER 4 - RESULTS: PLASMA POLYMERISATION

4.1 Introduction

It was shown in chapter 1 that fluorocarbon polymers often play an essential role in controlling both etch anisotropy and etch selectivity. Further, these polymers offer significant commercial potential in their own right.

This chapter reports the results of studies of the influence of plasma chemistry on polymer deposition rate, polymer chemistry and polymer properties for a wide range of plasma chemistries - each of CF_4, C_2F_6 and C_3F_8 with additions of hydrogen, and CHF_3.

All polymer depositions were onto aluminised silicon wafers. This offered two major benefits:

(i) aluminium is stable in fluorine-containing discharges - the fluoride is involatile;

(ii) the aluminised wafers had a highly reflective, mirror-like surface ideal for reflection infrared studies. Further, aluminium has no absorption bands in the spectral region of interest.

In order to minimise the number of variables under consideration, the depositions were all carried out at a fixed chamber pressure and gas flow rate. Whereas all the fluorocarbons studied are net etchants at 60 mtorr, both C_3F_8 and CHF_3 deposit polymeric material at 200 mtorr (the upper limit of the RIE 80 pressure gauge). This higher chamber pressure was therefore used in order to maximise the range of gas chemistries that could be studied. The flow rate was 20 sccm.

A study of the influence of chamber history and deposition time on deposition rate is described first. Then the deposition rates and gas chemistries of C_3F_8 and CHF_3 are compared as a function of applied RF power. Finally, the influence of hydrogen additions on the plasma polymerisation of each of CF_4, C_2F_6 and C_3F_8 is assessed.

The chemical structures of a number of the polymers thus produced were characterised by infrared and X-ray photoelectron spectroscopy, and their physico-chemical properties examined by thermal analysis. The electrical properties (resistivity and dielectric constant) of two of the polymers - those derived from C_3F_8 and CHF_3 - were measured also.

4.2 Chamber History

This first set of experiments was designed to study the influence of chamber history on the polymerisation process. Starting with a "clean" plasma chamber, aluminium, anodised aluminium and pyrex surfaces are all available for interaction with the plasma species. As well as having a potential, direct chemical influence on the deposition process they will also be sources of trace adsorbed moisture etc. (After venting with dry nitrogen the chamber was opened to atmosphere for sample changing.) During polymerisation all surfaces are coated with polymer, and, after a certain time, the chamber could be considered fully lined with polymeric material of a steady-state composition.

CHF_3 was the chosen monomer for this work. All depositions were carried out at 50 W applied RF power. Initially, three samples were loaded into the previously cleaned chamber. The sequence of experiments is best described by the bar chart below:-

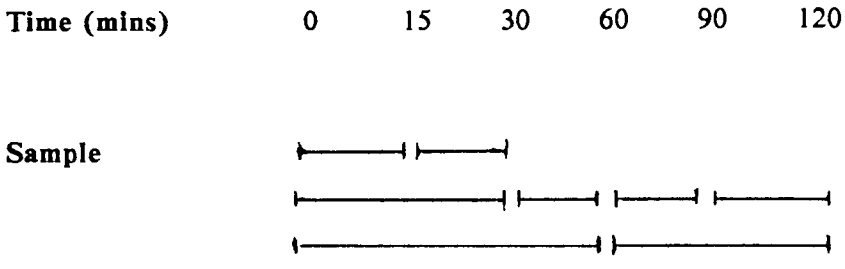

Thus eight samples were produced over a 2 hr. period (deposition time), and no sample was in the chamber for more than one hour. The 0-60 min. sample, for example, was twice exposed to atmosphere (at 15 and 30 min.) during the course of its preparation. The measured deposition rates are shown in table 23.

Table 23. *CHF_3 plasma polymer deposition rates as a function of time.*

Sample (times (min.))	**Deposition rate (nm. min^{-1})**
0 - 15	33
15 - 30	36
0 - 30	35
30 - 60	37.5
0 - 60	35
60 - 90	37
90 - 120	37
60 - 120	40

These results provide evidence that a clean chamber reduces the observed deposition rate (0-15, 0-30 and 0-60 min. samples) over the first 15 minutes, perhaps due to loss of depositing species to the chamber surfaces. In all subsequent experiments the plasma chamber was therefore conditioned, under the appropriate operating conditions, for a minimum of 15 min. prior to use.

4.3 Influence of RF Power

The effect of RF power on the deposition rate of polymer onto aluminium substrates was studied for both C_3F_8 and CHF_3.

For C_3F_8, RF powers in the range 5-100 W were employed, and deposition times of 1 hr. No net polymer deposition was observed at 5 W, and this experiment was subsequently repeated for a 3 hr. period. Again, no net deposition was detected implying that the deposition rate was less than 5×10^{-3} nm.min^{-1} (the detection limit of the Dektak profilometer is 9 nm). The corresponding optical emission spectra were recorded also. The actinometered CF_2 (polymer precursor) and atomic-F (etchant) signals both increased with increasing power.

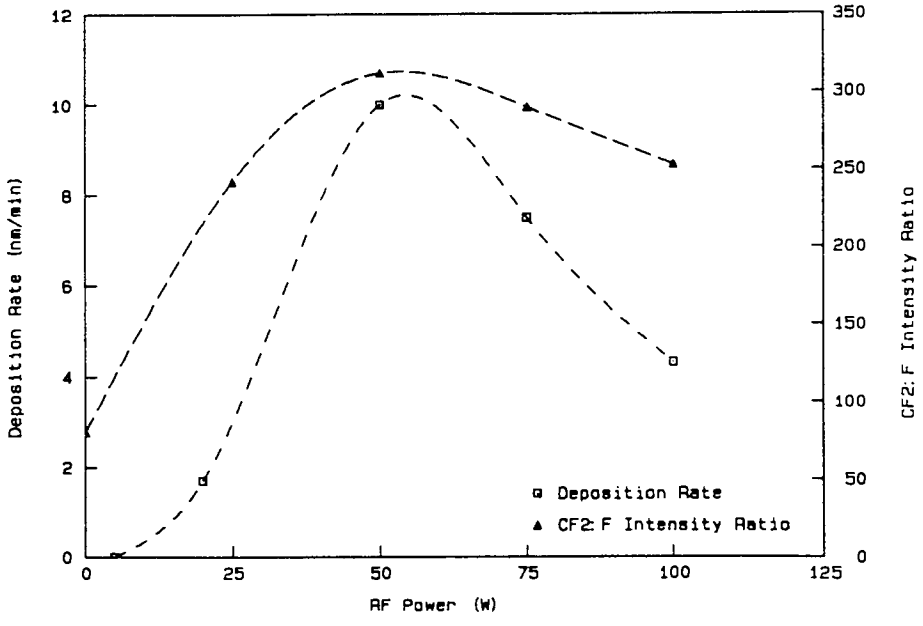

Figure 31. *C_3F_8 plasma-polymer deposition rate and CF_2(251.9 nm):F(703.7 nm) emission intensity ratio as a function of RF power.*

Figure 31 shows both the measured deposition rate and the CF_2:F emission intensity ratio as a function of applied RF power. The curves take similar forms, each going through a maximum at ~50 W. Thus, as expected, there is some correlation between deposition rate and CF_2:F relative concentration ratio. It is likely that the CF_2:F ratio was below a critical value for deposition to occur at 5 W.

A similar series of depositions was performed with CHF_3 over the RF power range 5-200 W. The results are shown in figure 32. Again, a maximum in the deposition rate was observed at 50 W. However, this deposition rate was four times that found with C_3F_8. Further, deposition also occured at 5 W. Raising the RF power level as high as 200 W resulted in net etching/sputtering of the aluminium substrate.

Turning to the optical emission results, it can be seen from figure 32 that not only does the CF_2:F ratio take on a much wider range of values than in the case of C_3F_8, but that it decreases with increasing power, and, indeed, has a lower value at 50 W than C_3F_8. The major difference between the two systems is clearly the presence with CHF_3 of hydrogen. The actinometered atomic-H signal increased monotonically with power. Studies of the influence of hydrogen on the deposition rate, chemical structure, and physical properties of fluorocarbon plasma polymers are the subject of much of the rest of this chapter.

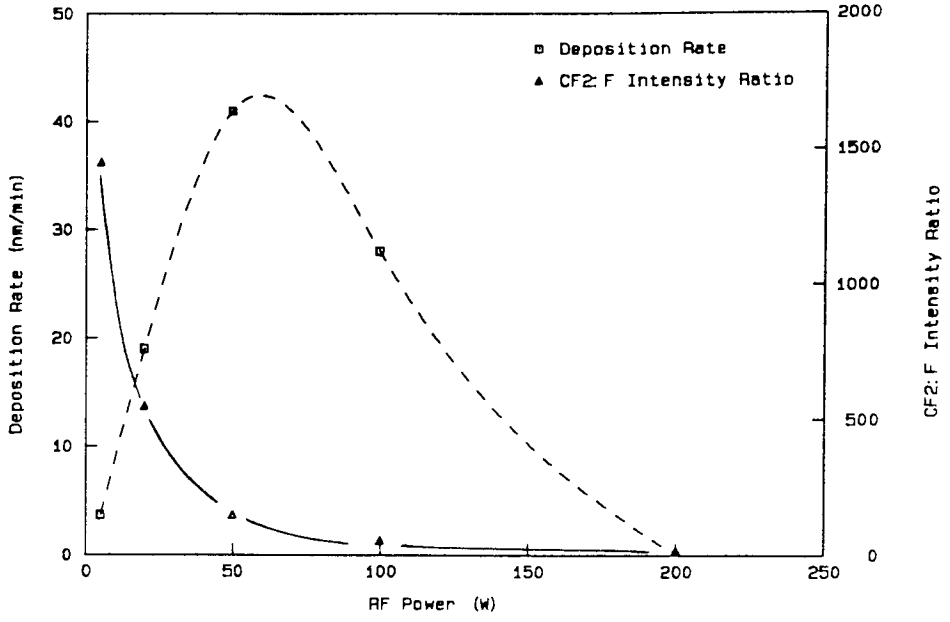

Figure 32. CHF_3 plasma-polymer deposition rate and CF_2(251.9 nm):F(703.7 nm) emission intensity ratio as a function of RF power.

4.4 Hydrogen Additions

This section reports the results of experiments to study the influence of hydrogen on the polymer deposition rates of each of CF_4, C_2F_6 and C_3F_8, and the associated gas phase chemistry. On the basis of the previous results (section 4.3), two RF power levels - 50 and 100 W - were chosen to yield close to the maximum likely polymer deposition rates. Hydrogen additions were varied from 0-50% in increments of 10%. All depositions were 30 min. in duration.

a) $\underline{CF_4}$.

At both RF power levels net polymer deposition occured for a minimum addition of 30% hydrogen. The colour of the deposits varied from golden (30% H_2), through brown (40% H_2) to dark brown (50% H_2), cf. PTFE: white, consistent with increased unsaturation in the polymer structure. Table 24 summarises the deposition rates. At 100 W the deposit was too thin for measurement with 30% H_2 and too poorly adherent with 50% H_2. Note that the onset of deposition (30% H_2) coincided with the maximum deposition rate at 50 W.

Table 24. *CF_4/H_2 plasma polymer deposition rates.*

% Hydrogen	Deposition Rate ($nm.min^{-1}$)	
	50 W	100 W
30	190	>0
40	180	220
50	140	>0

The corresponding changes in F- and H-atom, and CF_2 radical relative concentrations, at 50 W RF power, are shown in figure 33. The results at 100 W were of a similar form. The atomic-H concentration rose steadily with percentage H_2 in CF_4. The atomic-F concentration dropped by more than an order of a magnitude to a minimum value with 20% H_2 and then rose again slightly with increasing percentage H_2. However, the CF_2 results are of greatest interest. The CF_2 radical (polymer precursor)

concentration reached a maximum with the addition of only 20% hydrogen, and then declined with further additions of hydrogen. Thus, at first sight it is not obvious why deposition did not occur at 20% H_2 (or below). This simplistic view is reinforced when one considers the CF_2:F ratio, which peaks even more strongly at 20% H_2. The subsequent decline in deposition rate is more than adequately accounted for - indeed, it could reasonably be expected to be more rapid.

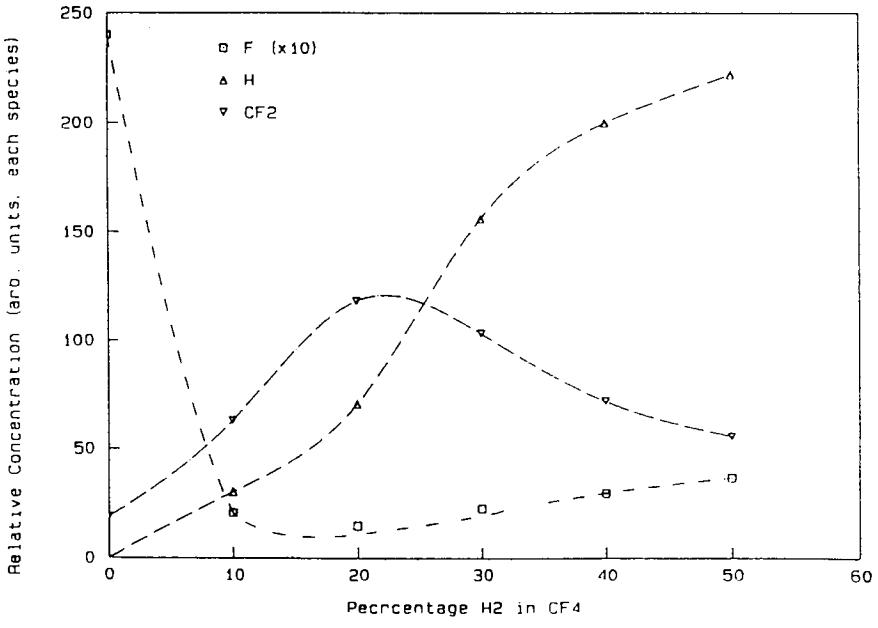

Figure 33. Relative concentrations of F and H atoms, and CF_2 radicals in a CF_4 plasma as a function of the addition of H_2. (50 W RF power).

b) $\underline{C_2F_6}$

The results, shown in table 25, of measurements of C_2F_6 plasma polymer deposition rates as a function of added hydrogen show a number of major differences from those from CF_4:

(i) the onset of a measurable deposition rate occured with 10% less hydrogen than previously for both the 50 and 100 W cases;

(ii) where there are data points in common, the deposition rate with C_2F_6 was roughly double that for CF_4;

(iii) the deposition rate increased with increasing percentage hydrogen.

The first two points are consistent with the use of a fluorocarbon with a higher C:F ratio. The third requires consideration of the relevant optical emission data.

Table 25. *C_2F_6/H_2 plasma polymer deposition rates.*

% Hydrogen	Deposition Rate ($nm.min^{-1}$)	
	50 W	100 W
20	130	0
30	290	95
40	470	470
50	490	520

It is clear from figure 34 that the relative CF_2 concentration in a C_2F_6 discharge is considerably higher over the entire range of hydrogen additions studied than with CF_4 - ranging from an order of magnitude for the pure gases, to a factor of ca. three with the addition of hydrogen. Further, with the exception of the pure monomers, there is little difference between the relative F-atom concentrations produced by the two plasma systems. Thus at 20% hydrogen addition the CF_2:F ratio for C_2F_6 is 4.5 times that for CF_4. Note also both that the maximum CF_2 concentration occurs at a higher percentage addition H_2 (30%) than with CF_4 (20%), and that this maximum is ill-defined being part of a plateau covering a wide range of additions (20-40%). These factors account, in part, for the observed differences in deposition rate between CF_4 and C_2F_6 as a function of hydrogen addition .

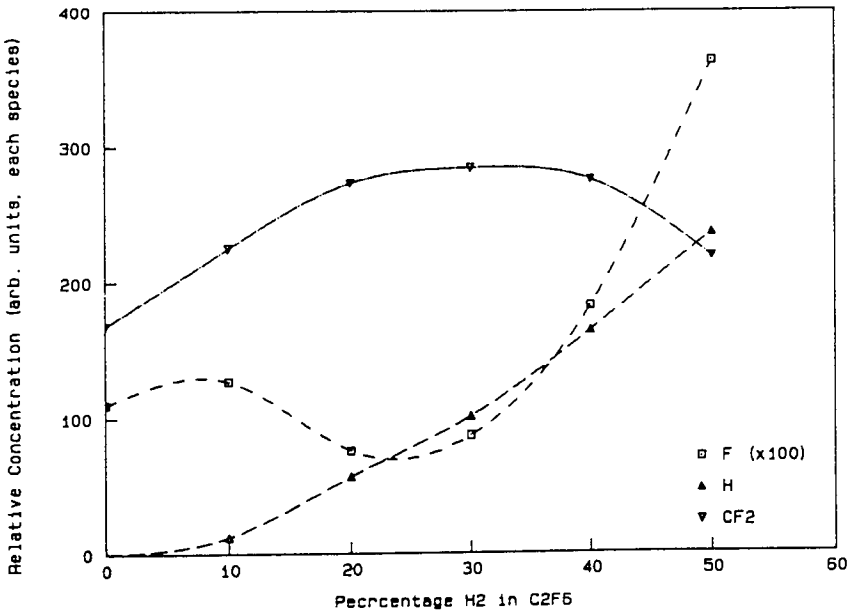

Figure 34. Relative concentrations of F and H atoms, and CF_2 radicals in a C_2F_6 plasma as a function of the addition of H_2. (50 W RF power).

(c) $\underline{C_3F_8}$

The C_3F_8/H_2 system was only studied at 50 W RF power. The previously observed (section 4.3) plasma polymerisation of the pure monomer was confirmed. As with C_2F_6, the deposition rate increased with additions of hydrogen (table 26). Indeed, surprisingly similar results were obtained for additions of $\geq$30% H_2, where higher deposition rates might reasonably have been expected.

Table 26. *C_3F_8/H_2 plasma polymer deposition rates.*

% Hydrogen	Deposition Rate ($nm.min^{-1}$)
0	65
10	155
20	255
30	385
40	430
50	500

Two unexpected results were obtained from the optical emission studies of this system (figure 35):

(i) the relative CF_2 radical concentration was invariant (within experimental error) with the addition of up to 50% H_2;

(ii) the F-atom concentration increased with all H_2 additions.

Thus the observed order of magnitude increase in deposition rate can most readily be accounted for by correlation with the corresponding changes in H-atom concentration. A major positive influence on polymer deposition rate by hydrogen is consistent with the results of the comparison of deposition from C_3F_8 and CHF_3 as a function of RF power (section 4.3), and is helpful in interpreting the results for the CF_4/H_2 and C_2F_6/H_2 systems in this section.

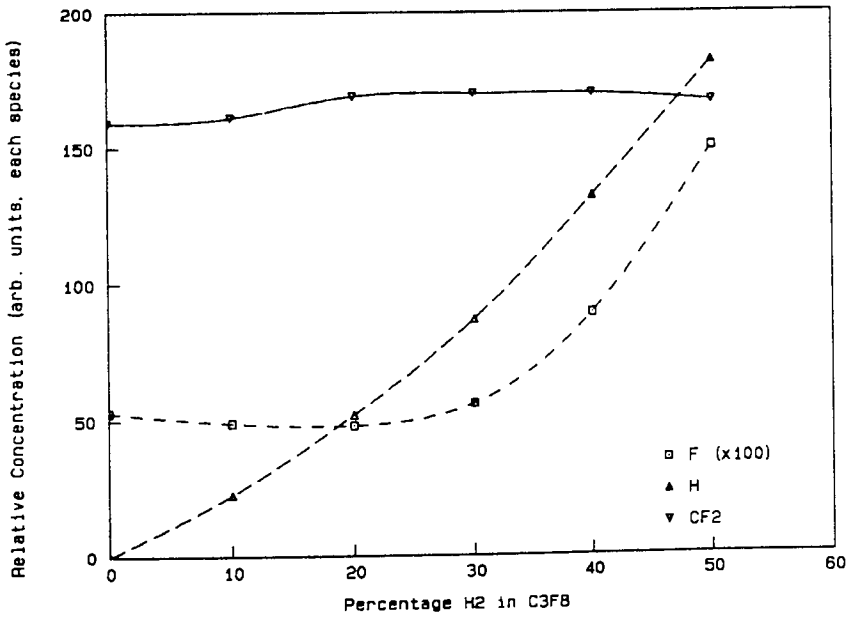

Figure 35. Relative concentrations of F and H atoms, and CF_2 radicals in a C_3F_8 plasma as a function of the addition of H_2. (50 W RF power).

4.5 Infrared analysis of Polymers

The detection of halogen by infrared spectroscopy has been described as "totally unreliable"[77]. Nonetheless infrared spectra for both fluorocarbon gases and fluorocarbon plasma polymers are well established[90]. The polymers show two distinctive absorption bands: 1000-1400 cm^{-1}, assigned to C-F stretch and consisting, in part, of CF stretch at 1100 cm^{-1} and CF_2 stretch at 1170 and 1210 cm^{-1}; 1600-1800 cm^{-1} assigned to C=C stretch.

Reflection infrared spectra were recorded for all the CHF_3, C_3F_8 and C_3F_8/H_2 polymers described. These were initially recorded as a linear function of percentage transmission over the range 4000 - 180 cm^{-1}. Typical spectra, those for plasma-polymerised C_3F_8 and C_3F_8/50% H_2 are shown in figures 36 and 37 respectively. Despite the differing gas chemistries they clearly have a similar overall form, with the expected C=C and C-F bands prominent. For comparison, the reflection spectrum of a sample of PTFE was recorded also. Only a sharp absorption at 1280 cm^{-1} was noted. The band at 3250 cm^{-1} was present even with an uncoated (aluminised silicon) substrate and is ascribed to atmospheric CO_2.

Comparing the two plasma polymer spectra in more detail, it can be seen that the presence of hydrogen in the plasma caused a broadening of the C-F band and an increase in the relative intensity of the C=C band of the resultant polymer. The absence of bands at 3000 cm^{-1} (C-H stretch) indicates both that no significant quantity of hydrogen was incorporated into the polymer structure, and that the C-F band broadening was not due to C-H deformation bands (1400 cm^{-1}). Qualitative examination of the other spectra revealed an apparently inconsistent variety of C-F band widths, and no marked change in the C=C band width.

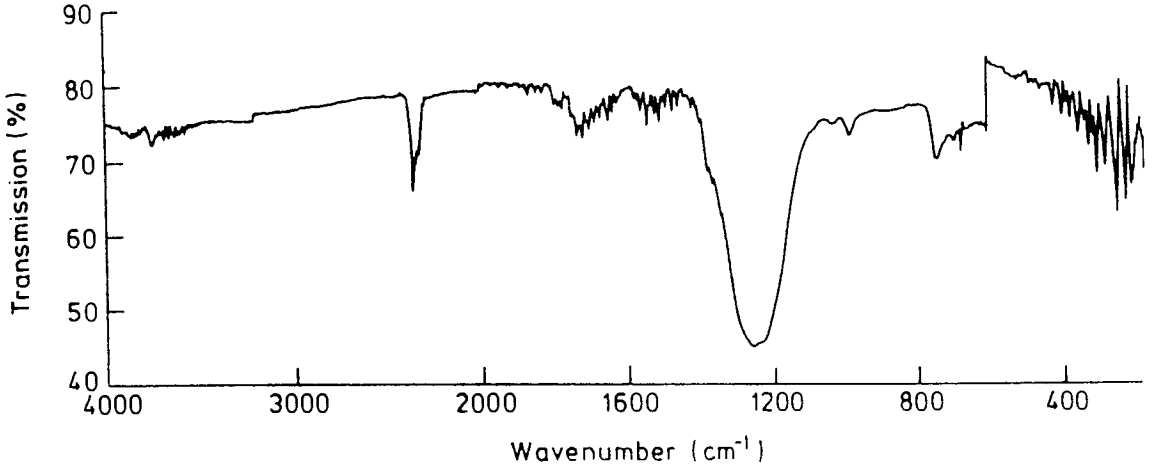

Figure 36. *Reflection infrared spectrum of plasma polymerised C_3F_8 on aluminium.*

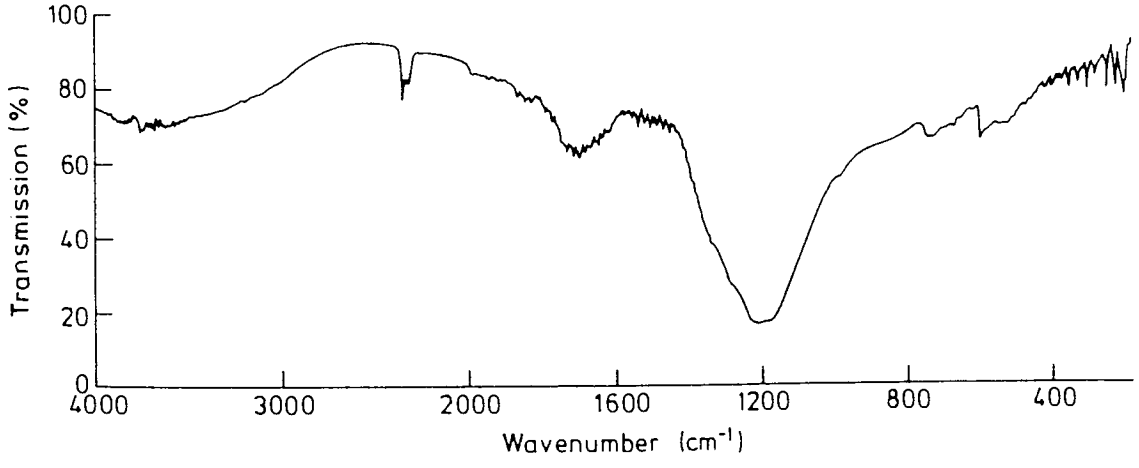

Figure 37. *Reflection infrared spectrum of plasma polymerised C_3F_8/50% H_2 on aluminium.*

The composition of the fluoropolymers, and therefore the width C-F band (which is made up of contributions from many C-F moieties), would be expected to be sensitive to:

(i) changes in deposition gas chemistry due to choice of monomer, presence of an additive, i.e. hydrogen, or variation of RF power,

(ii) similar changes in etchant gas chemistry, and

(iii) degree and type of ion bombardment during polymer growth.

In order to quantify the observed C-F band-broadening effect, all the spectra were rerecorded as a linear function of absorption, over the range 2000 - 800 cm^{-1}, and the C-F band width at half maximum peak height was measured. It was noted that the band width was a function of fluorocarbon film thickness, independent of monomer, RF power or deposition time (figure 38). This, surprisingly, dimisses all the offered chemical explanations of the broadening. If the polymers were highly thermally insulating then surface temperature might play a role in controlling structure as a function of film thickness, but it is unlikely that this would be dominant over the considerable changes in process parameters. The broadening is, at best, ascribed to an instrumental effect.

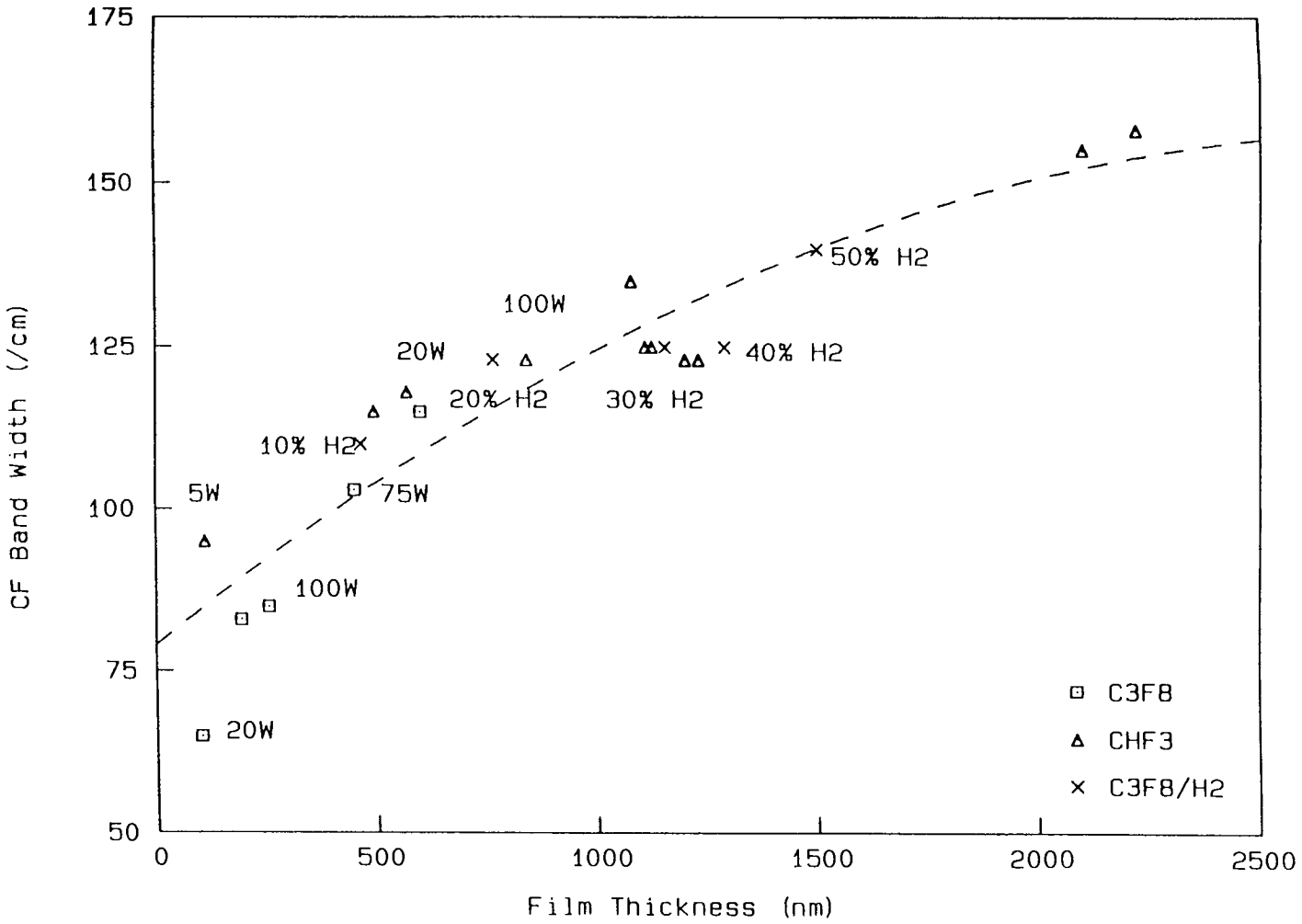

Figure 38. C-F infrared band width (at half maximum height) as a function of fluorocarbon plasma polymer film thickness.

In order to assess the degree of unsaturation in the fluoropolymers the C=C : C-F peak area ratios were measured by the "cut and weigh" technique, and the ratios plotted against film thickness (figure 39).

It can be seen that for the pure gases:

(i) the C=C : C-F ratio decreases with increasing film thickness, consistent with the broadening of the C-F band, and

(ii) the points for C_3F_8 all lie below those for CHF_3, indicating that the C_3F_8 plasma polymers have less unsaturation than those derived from CHF_3

In contrast, hydrogen additions to C_3F_8 caused an increase in C=C : C-F ratio with increasing film thickness. (N.B. it should be remembered that the polymer deposition rate increased with additions of up to 50% hydrogen.) This result, taken together with the comparison of the pure gases, clearly demonstrates that hydrogen, whether as an additive or contained within a monomer, increases the degree of unsaturation in plasma fluoropolymers.

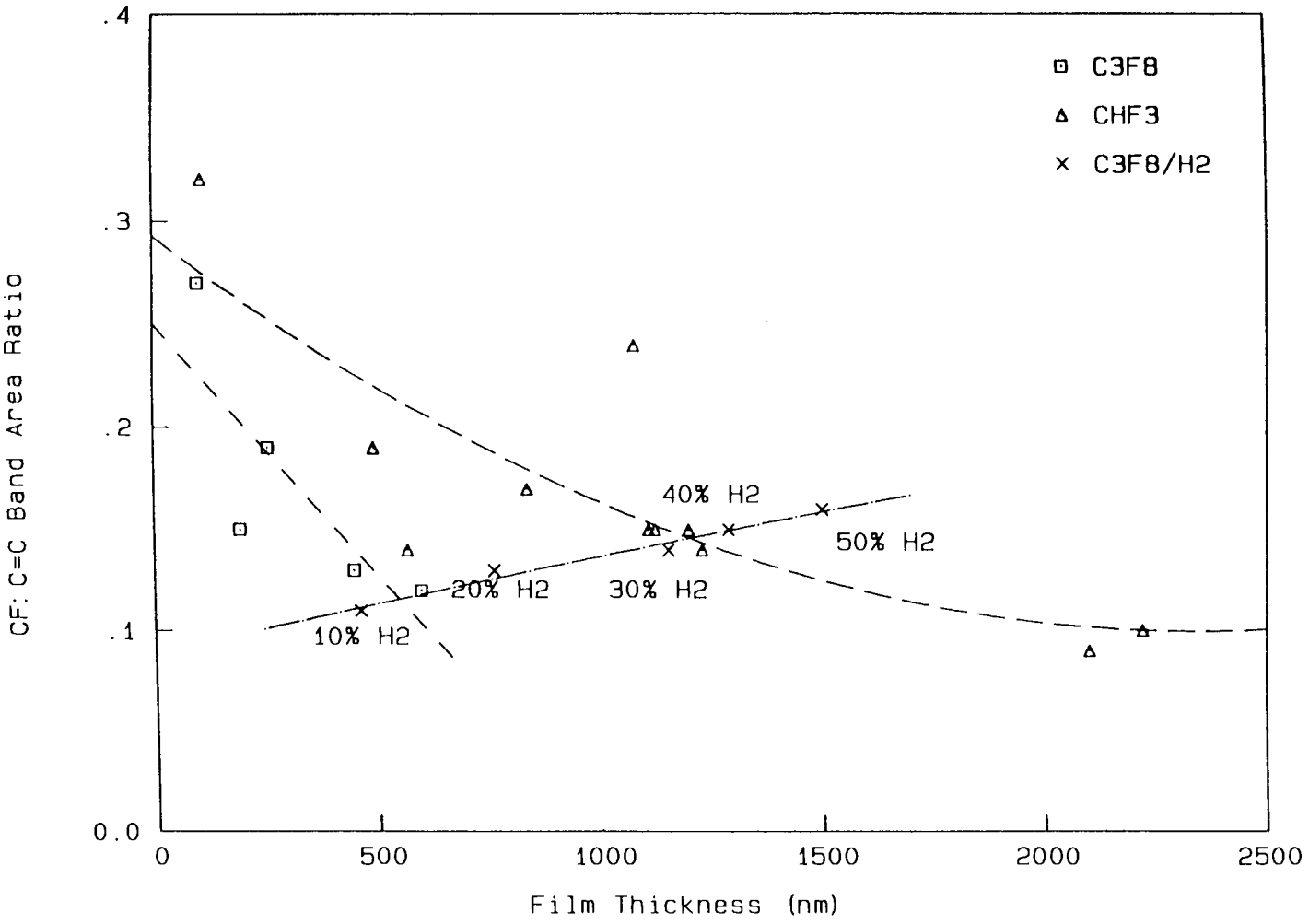

Figure 39. *C=C : C-F infrared band area ratio as a function of fluorocarbon plasma polymer film thickness.*

4.6 X-ray Photoelectron Spectroscopy (XPS) Analysis of Polymers

Fluorocarbon plasma polymers produced at 50 W RF power were analysed by XPS. A general wide scan was obtained from each sample to provide an elemental analysis and to identify species requiring detailed chemical scans. The samples were all sufficiently thick to mask the underlying aluminium substrate. Thus only carbon, fluorine and oxygen were identified in the wide scans. The oxygen was ascribed to adventitious material as the analyses were carried out ex situ after exposure of the samples to the atmosphere. The C1s peak showed broadening. Detailed C1s spectra were obtained and stripped into their component parts according to the degree of fluorination, i.e. C (bridgehead carbon), C-CF, CF, CF_2 and CF_3. A typical fluorocarbon polymer C1s spectrum is shown in figure 40.

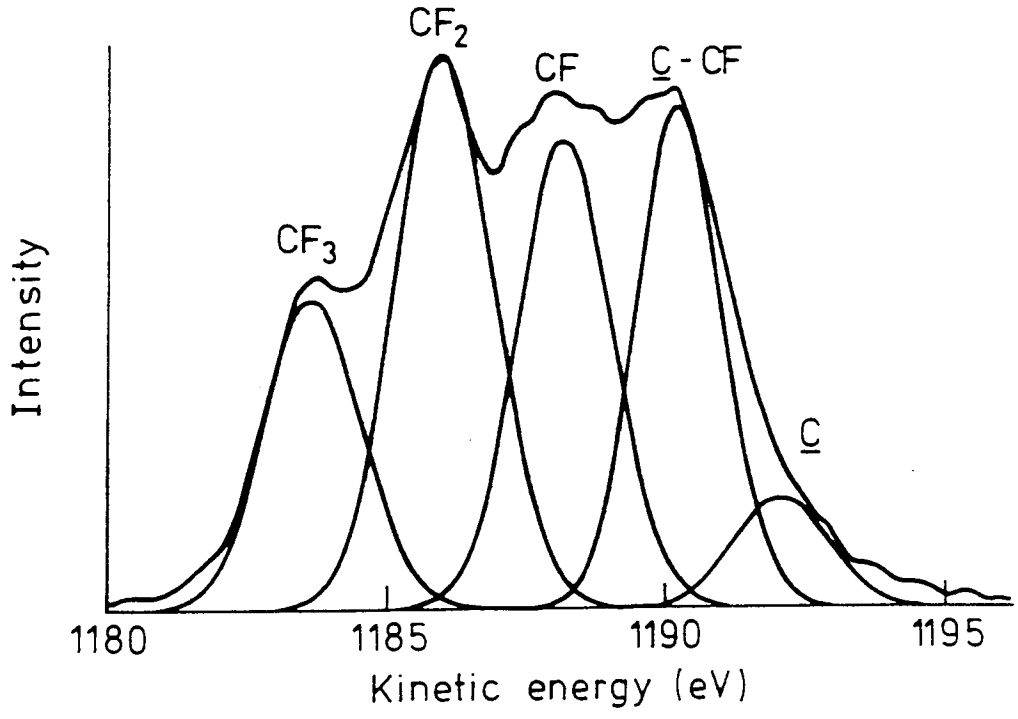

Figure 40. A typical C1s fluorocarbon (CHF_3) plasma polymer spectrum obtained by X-ray photoelectron spectroscopy.

Tables 27 and 28 summarise the results of the wide scan elemental analysis and the stripping of the detailed C(1s) spectra of the fluorocarbon plasma polymers.

Considering the elemental analyses first, it can be seen that the majority of the polymers are fluorine rich. The C:F ratio varies from 1:1.8 (C_3F_8) to ~1:1 (C_2F_6/50% H_2 and C_3F_8/50% H_2). Thus all of the polymers studied here were fluorine deficient with respect to PTFE (C:F, 1:2). For a given monomer, the C:F ratio of the resultant polymer decreased with increasing percentage hydrogen in the plasma. Interestingly, the C_2F_6 and C_3F_8 plasma polymers had very similar compositions for the same percentage addition of hydrogen. Finally, the atomic percentage of oxygen associated with each sample, although low in every case, is clearly dependent on the C:F ratio of that sample - a higher C:F favouring a higher percentage of oxygen. This could equally be attributed to partial oxidation of an increasingly carbonaceous surface, or increased atmospheric adsorption onto a potentially less hydrophobic material.

Analysis of each of the C(1s) spectra shows carbon present in five chemical environments according to the degree of fluorination - from bridgehead carbon through to CF_3. With the exception of the bridgehead carbon - carbon atoms bound to other unfluorinated carbon atoms - these components are, in most instances, present in roughly equal proportion, whereas PTFE consists entirely of the CF_2 component. Indeed, only in a few cases is CF_2 the major component of the plasma polymer, and even then it accounts for little more than 30% of the total structure. The change in the structure of the C_2F_6 and C_3F_8 polymers with the addition of hydrogen reflects the change in C:F ratio of the materials seen in the elemental analysis. In both cases hydrogen additions cause a decrease in the CF_3 and CF_2 components, with a corresponding increase in all the other components. Ultimately the CF component would be expected to decline also. These results are consistent with the increased unsaturation detected by infrared.

Table 27. Elemental analysis of fluorocarbon plasma polymers.

Plasma polymer	Atomic %		
	C	F	O
CF_4/30% H_2	47.8	49.6	2.5
C_2F_6/20% H_2	36.2	63.3	0.4
C_2F_6/30% H_2	39.3	59.9	0.6
C_2F_6/40% H_2	41.7	56.1	2.0
C_2F_6/50% H_2	48.7	46.7	4.4
C_3F_8	35.8	63.5	0.6
C_3F_8/10% H_2	36.5	62.9	0.4
C_3F_8/20% H_2	38.3	59.8	1.7
C_3F_8/30% H_2	39.6	58.9	1.4
C_3F_8/40% H_2	41.8	55.9	2.1
C_3F_8/50% H_2	48.9	47.4	3.5
CHF_3	42.3	56.3	1.2

Table 28. Carbon(1s) components of fluorocarbon plasma polymers.

Plasma polymer	Carbon(1s) component (%)				
	C	C-CF	CF	CF_2	CF_3
CF_4/30% H_2	10	34	29	20	7
C_2F_6/20% H_2	5	21	23	32	19
C_2F_6/30% H_2	7	24	22	28	19
C_2F_6/40% H_2	7	28	27	24	14
C_2F_6/50% H_2	6	40	29	18	7
C_3F_8	3	21	21	31	24
C_3F_8/10% H_2	5	22	20	30	23
C_3F_8/20% H_2	6	24	22	27	21
C_3F_8/30% H_2	7	26	24	24	19
C_3F_8/40% H_2	10	29	23	21	17
C_3F_8/50% H_2	15	32	25	17	11
CHF_3	8	25	25	26	16

4.7 Thermal Analysis of Polymers

A number of thick polymer films were grown on a previously cleaned quartz disc which covered the whole of the RIE 80 driven electrode. After deposition, the films were scraped from the disc, and the resultant powders subjected to thermal analysis. All the depositions were carried out at 50 W RF power.

4.7.1 Thermogravimetric Analysis

Thermogravimetric analysis was used to study polymer weight loss in flowing air as a function of temperature. The trace obtained for the C_3F_8/50% H_2 polymer is shown in figure 41. The peak of the derivative of the weight vs. temperature curve indicated the temperature at which the maximum rate of weight loss occured. All of the five plasma polymers studied in this way had a peak in the range 294-361 °C ("low temperature", table 29). The position of this peak was approximately proportional to the polymer C:F ratio as determined by XPS. In the cases of CHF_3 and C_2F_6/30% H_2 the peak had a low temperature shoulder. The C_3F_8 polymer also showed a minor (~5%) weight loss at 125 °C, and the two polymers produced from plasmas containing 50% hydrogen a "high temperature" weight loss (~50% of the sample weight) in the region 453-489 °C.

The low temperature results are consistent with gains in polymer thermal stability due to increased cross-linking accompanying the increase in C:F ratio. The presence of a high temperature component in the polymers produced from plasmas containing 50% hydrogen is perhaps indicative of both fluorocarbon and carbonaceous constituents within the polymer structure. In contrast, the high thermal stability of PTFE should be noted.

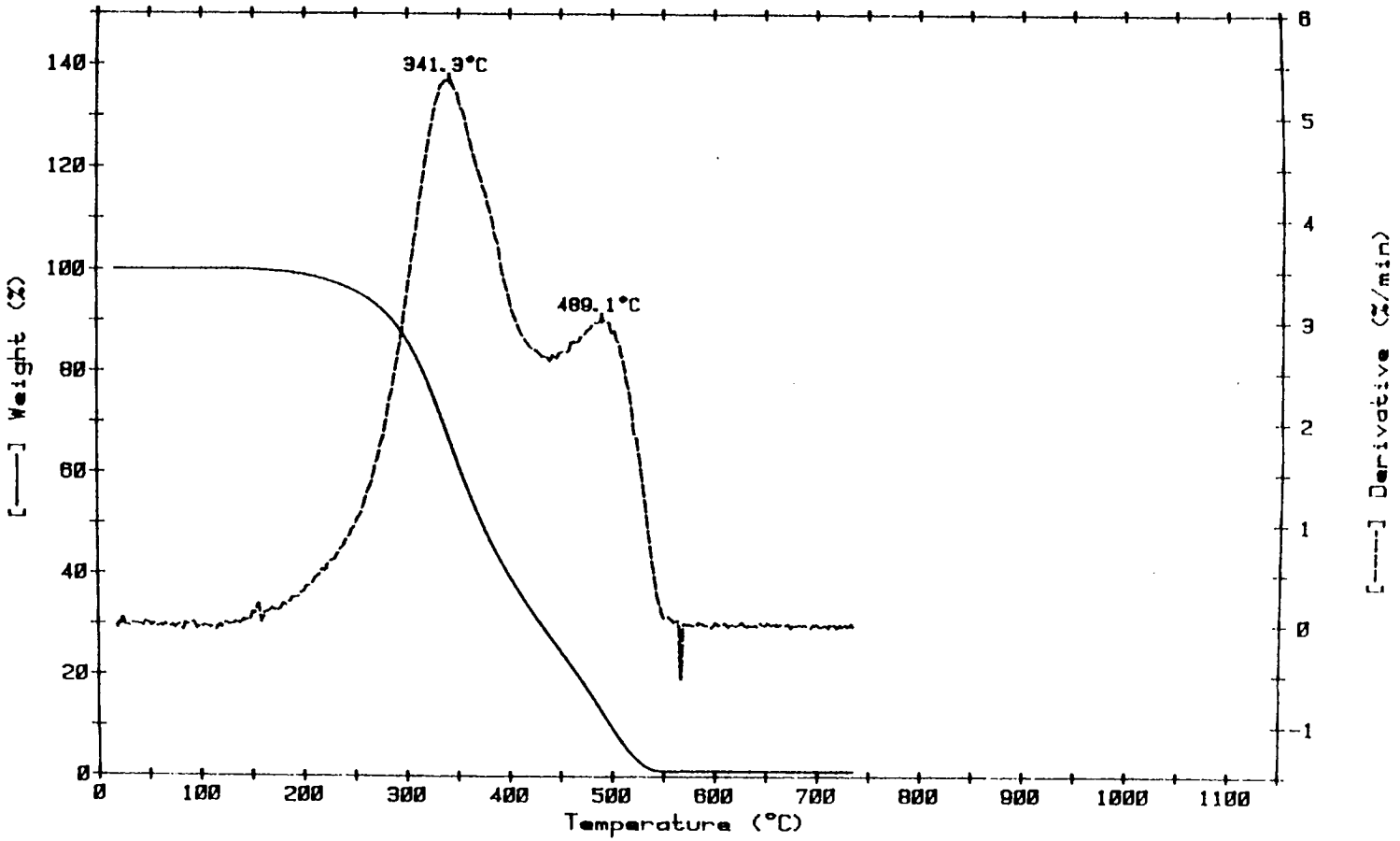

Figure 41. Thermogravimetric analysis of plasma polymerised C_3F_8/50% H_2.

Table 29. Results of thermogravimetric analysis of plasma polymers..

Plasma polymer	Low temperature weight loss maximum (°C)	High temperature weight loss maximum (°C)
C_2F_6/30% H_2	263(s), 327	
C_2F_6/50% H_2	361	453
C_3F_8	125, 294	
C_3F_8/50% H_2	341	489
CHF_3	280(s), 326	
(PTFE	662)	

(s) : shoulder

4.7.2 Differential Scanning Calorimetry

Differential scanning calorimetry (DSC) was used to study heat flow due to polymer decomposition in air as a function of temperature. It was carried out in an essentially similar manner to the thermogravimetric analysis (TGA), and may be considered a complementary analytical technique. It should be noted, however, that whereas the polymer sample was placed in an open platinum boat for TGA, a closed aluminium container with air access via a pinhole was used for DSC.

Initial runs were performed with a ramp rate of 10 °C.min^{-1} as previously used for TGA. Under these conditions all the polymers, except the two derived from C_2F_6/50% H_2 and C_3F_8/50% H_2, showed exotherms with maxima at broadly coincident temperatures to those found for weight loss by TGA. The results are summarised in table 30.

The DSC traces of the two polymers derived from the feeds containing 50% H_2 showed signs of an exotherm maximum above the maximum operating temperature (600 °C). Further, polymer residues were found after these experiments even though TGA analysis had shown 100% weight loss by 500 °C. The experiments were therefore repeated at half the ramp rate, which lowered the temperature of the exotherm. These results are shown in table 30. Although there are considerable differences between the DSC exotherm temperatures and TGA weight loss temperatures for these two polymers, it follows that this is most probably due to an inadequate air supply.

Table 30. Results of differential scanning calorimetry analysis of plasma polymers.

Plasma polymer	Low temperature weight loss maximum (°C)	High temperature weight loss maximum (°C)
C_2F_6/30% H_2	288, 330	
C_2F_6/50% H_2	439	536
C_3F_8	150, 298	
C_3F_8/50% H_2	361	567
CHF_3	308, 344	

4.8 Electrical Properties of Polymers

The electrical characteristics of thin films of plasma-polymerised C_3F_8 and CHF_3 were studied using a Gen Rad Digibridge operated in parallel configuration. For this study ~2 μm thick polymer films were deposited onto 75 mm diameter aluminised silicon wafers. A small area at the edge of each wafer was masked with a microscope slide. A thin layer of gold in the form of a circle (diameter 35.6 mm) surrounded by a ring (inside diameter 37mm; outside diameter 51.5 mm) was sputter deposited onto the polymer. Wires, for connection to the Digibridge, were bonded to the exposed aluminium, gold circle and gold ring with silver "dag". The arrangement is shown schematically in figure 42.

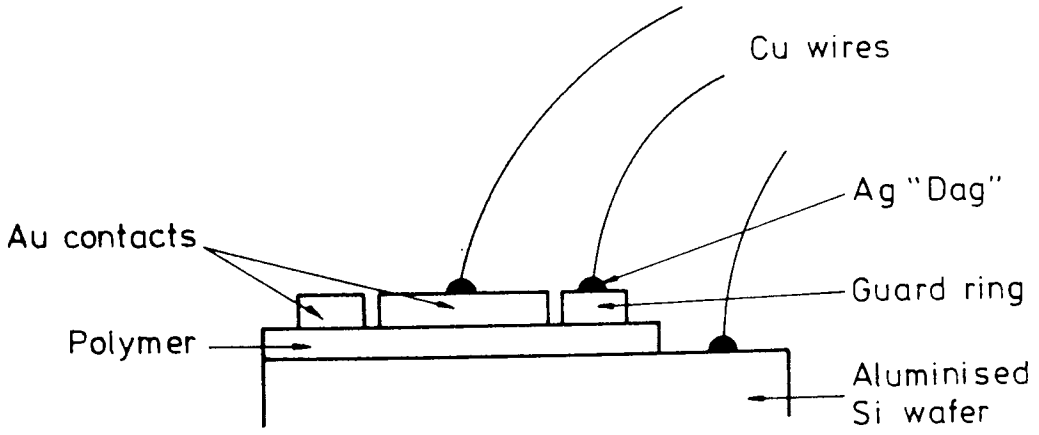

Figure 42. Schematic of experimental arrangement for electrical characterisation of plasma polymers.

Preliminary measurements established both that the polymer was free of pinholes, and that the surface conductivity was below the detection limit, i.e. the outer gold ring was not required as a guard ring. All subsequent electrical measurements were made between the aluminium and both areas of gold. Resistance and capacitance were recorded as a function of frequency for an applied voltage of 0.1 V (5.5×10^{4} $V.m^{-1}$). An average of three measurements was taken. Tables 31 and 32 summarise the results obtained for C_3F_8 and CHF_3 plasma polymers respectively, and show the calculated equivalent volume resistivity, reactance, impedance, dielectric constant and dissipation factors as a function of frequency.

The resistivity of both polymers at 100 Hz was greater than 10^{10} Ωm (10^{12} Ωcm). (the upper measurement limit for this configuration). However, the resistivities fell rapidly with increasing frequency to 2×10^{6} Ωm for plasma polymerised CHF_3 and to 3.5×10^{6} Ωm for plasma polymerised C_3F_8 at 100 kHz. Note that the resistivity of the C_3F_8 polymer was ~70% higher than that of the CHF_3 polymer over the entire frequency range studied.

The capacitance measurements, however, remained essentially constant over the entire frequency range studied. Taking into account the film thicknesses (accurate to ±5-10%) and areas, these figures represent dielectric constants of 2.2 and 2.0 respectively, cf. PTFE 2.2.

Frequency (kHz)	Resistance (Ω)	Capacitance (nF)	Resistivity (Ωm)	Reactance (Ω)	Impedance (Ω)	Dielectric Constant	Dissipation Factor
1	3.181×10^{6}	20.10	3.54×10^{9}	7920	7900	2.04	0.00249
2	1.484×10^{6}	20.10	1.65×10^{9}	3960	3950	2.04	0.00267
5	4.724×10^{5}	20.06	5.26×10^{8}	1590	1580	2.04	0.00336
10	1.725×10^{5}	20.04	1.92×10^{8}	794	790	2.03	0.00460
20	5.701×10^{4}	20.02	6.35×10^{7}	397	395	2.03	0.00697
50	1.154×10^{4}	19.99	1.28×10^{7}	159	157	2.03	0.0138
100	3.130×10^{3}	19.96	3.48×10^{6}	80	78	2.03	0.0255

Table 31. Electrical characteristics of C_3F_8 plasma polymer.

Frequency (kHz)	Resistance (Ω)	Capacitance (nF)	Resistivity (Ωm)	Reactance (Ω)	Impedance (Ω)	Dielectric Constant	Dissipation Factor
1	2.027×10^{6}	21.76	2.26×10^{9}	7310	7290	2.21	0.00361
2	9.020×10^{5}	21.73	1.00×10^{9}	3660	3650	2.21	0.00406
5	2.757×10^{5}	21.69	3.07×10^{8}	1470	1460	2.20	0.00532
10	1.013×10^{5}	21.65	1.13×10^{8}	735	730	2.20	0.00726
20	3.354×10^{4}	21.61	3.73×10^{7}	368	364	2.19	0.0110
50	6.820×10^{3}	21.55	7.59×10^{6}	148	145	2.19	0.0217
100	1.871×10^{3}	21.50	2.08×10^{6}	74	71	2.18	0.0396

Table 32. Electrical characteristics of CHF_3 plasma polymer.

CHAPTER 5 - DISCUSSION: PLASMA ETCHING

The results of studies of the plasma etching of silicon and silicon dioxide in fluorine-containing discharges were presented in chapter 3. This chapter considers, in turn, the etching of silicon, the etching of silcon dioxide, and the influence of electrode materials on etch processes.

The results of statistically designed experiments are used to examine and model the etching of silicon in both SF_6 and CF_4. The former, a "clean" etchant is contrasted with the latter, which is a potential source of etch inhibiting fluorocarbon polymer. Under conditions of fixed flow, pressure and power, silicon etch rates in a range of fluorocarbons (CF_4, C_3F_8 and CHF_3) as a function of the addition oxygen-containing additives (O_2, N_2O and CO_2) are all accounted for in terms of relative concentrations of gas phase species.

Several chemical species have been considered silicon dioxide etchants. Here, evidence is presented that, for the conditions used, etching proceeds by an ion-assisted mechanism. The presence of fluorine in the discharge is necessary for etching to proceed, but the etch rate is independent of relative F-atom concentration. No enhancement was found in the presence of carbonaceous or CF_x species.

It was found that the silicon etch rate in a CF_4 plasma was considerably enhanced, relative to an anodised aluminium electrode, in the presence of soda glass or sodium or potassium "doped" quartz. The effect was even more pronounced in a CF_4/O_2 discharge. In the latter system lead and copper electrodes also enhanced the silicon etch rate. These results could not be accounted for by a corresponding rise in atomic fluorine concentration. The results presented clearly require the participation of

transferred alkali metals in surface processes during etching. Three ways in which etching might be assisted by the presence of alkali metals are considered:

(i) effects of transferred metals on fluorocarbon films which inhibit etching.

(ii) direct enhancement of silicon etching by the formation of favourable intermediates;

(iii) modification of the electronic properties of the silicon ("band bending") which may enhance silicon etching.

5.1 Plasma Etching of Silicon

It was established in chapter 1 that in fluorine-containing discharges atomic fluorine is the principal silicon etchant, and that silicon etch rates are enhanced by simultaneous ion bombardment, with synergism occuring between purely chemical etching and physical sputtering. Ion bombardment of the substrate is considerably enhanced when the reactive ion etching configuration is used. Optical emission spectroscopy with argon actinometry (chapter 2.2) is readily used to measure changes in relative atomic-fluorine concentration, as well as those in other species, and direct measurement of the d.c. self-bias to ascertain the degree of ion bombardment. The formation of residues, such as fluorocarbon polymers, may hinder etching.

The parametric studies of the plasma etching of silicon and silicon dioxide in CF_4 and SF_6 revealed considerable differences between the two gas systems. The former gave an average $Si:SiO_2$ selectivity of ~1.5:1 whereas the latter gave ~50:1 (tables 10 and 12). This was caused by a ca. twenty-fold increase in Si etch rate and a ca. halving of the SiO_2 etch rate. Modelling showed that although RF power was the dominant process parameter in each case, there were considerable differences in the dependencies of the Si

and SiO_2 etch rates on the process parameters in the two plasma etch gases (tables 13 and 17). Optical emission spectroscopy showed that the relative F-atom concentrations in the SF_6 plasmas were only ~four times higher than with CF_4 (tables 11 and 15). It is therefore not immediately apparent why the silicon etch rates were so much more greatly enhanced. The problem is compounded by the fact that considerably higher d.c. self-biases, which are expected to enhance etch rates, were produced by CF_4 than SF_6. Table 33 (data drawn from tables 10, 12, 14 and 15) shows that for similar F-atom concentrations Si etch rates were almost an order of magnitude higher with SF_6 than CF_4 despite the lower SF_6 biases. Much of this section is devoted to considering the differences between the two systems.

Table 33. Comparison of Si etching with CF_4 and SF_6.

Etchant	[F] (arb. units)	Bias (V)	Etch Rate $nm.min^{-1}$
CF_4	42	320	115
CF_4	85	500	200
SF_6	42	50	900
SF_6	79	180	1560

The role of sulphur atoms in the plasma etching of silicon was investigated by Ninomiya et al.[91] employing a microwave system. In a comparison of Si etching by F_2 and SF_6 plasmas using a quartz discharge tube they found by XPS that the Si surface was considerably oxidised after exposure to the F_2 plasma but not the SF_6 plasma. The

source of oxygen was attributed to the quartz tube (etched in fluorine-containing discharges), and this was confirmed by substitution for an alumina tube (note both that a pyrex chamber is used in the present work, and that there is a small but potentially significant atmospheric leak rate). The deliberate addition of O_2 to a F_2 discharge caused a reduction in the silicon rate, and a corresponding rise in silicon-surface oxidation was detected by XPS. For a fixed percentage oxygen, the presence of a sulphur plate outside the discharge caused an increase in silicon etch rate and a reduction in surface oxidation. This was attributed to the consumption of atomic oxygen, which would otherwise compete with fluorine for silicon surface sites, by sulphur and SF_n species. Sulphur atoms in SF_6 are expected to have a similar role.

Brault et al.[92] also analysed silicon surfaces by XPS after etching SF_6 and F_2 plasmas. For this work an alumina RF discharge tube was used. The etchants were buffered with He to give similar F-atom concentrations (as detected by actinometry). In this case a thinner overlayer was detected on the SF_6-etched than F_2 etched silicon, indicating a more efficient etch, but both layers had similar compositions, including O:F ratio, in disagreement with Ninomiya's findings[91]. No sulphur was detected on the SF_6-etched surface.

Ryan and Plumb[93] have developed a model for the etching of silicon in SF_6/O_2 plasmas which accounts well for earlier experimental observations by d'Agostino and Flamm using an RF discharge. They suggest that the main SF_6 dissociation reaction is:

$$SF_6 + e^- \rightarrow SF_2 + 4F + e^-$$

SF_x (x = 2 - 5) species then rapidly recombine with F in order to maintain a low percentage conversion of SF_6. Si etching is exclusively by F, and terms for ion-assisted etching are not included for the tubular reactor modelled. It should be noted that the

experimental results were all obtained at fixed flow pressure and power, and were primarily aimed at studying the influence of oxygen on discharge chemistry.

In contrast, two other theoretical models describing the RF plasma etching of silicon in SF_6[94] and SF_6/O_2[95] respectively include terms for adsorption of SF_x species. (Tang and Hess[96] in a study of tungsten etching in CF_4 and SF_6 discharges noted that the free radicals SF_3 and SF_5 may be a source of fluorine through dissociative chemisorption). In one model[95], the adsorption probabilities of F, SF_3 and SF_5 are equal. Whilst modelling a reactive ion etcher, Lii et al.[94] note that the etching of silicon in SF_6 is predominately chemical and summarise the main reactions occuring in the chamber as:

Gas Phase	$e^- + SF_x \rightarrow SF_{x-1} + F + e^-$	(x = 3 - 6)
Wafer Surface	$F(g) + \frac{1}{4}Si \rightarrow \frac{1}{4}SiF_4(g)$	
	$SF_x(g) + Si \rightarrow \frac{1}{4}SiF_4(g) + SF_{x-1}(g)$	(x = 3, 5)
	$F(g) + \text{Photoresist} \rightarrow C_xF_yH_zO_w(g)$	
Electrode Surface	$SF_x(g) \rightarrow SF_x(s)$	
	$F(g) + SF_x(g) \rightarrow SF_{x+1}(g)$	(x = 2 - 5)

The contour plots shown in chapter 3 for silicon etch rate (figure 14) and F-atom concentration (figure 13) as a function of RF power and pressure in a SF_6 plasma were of a similar form, indicating a strong correlation. Mathematically, the data (tables 14 and 15) best fits an equation of the form:

$$\text{Si etch rate} = 45[F]^{0.78} \qquad (5.1)$$

A plot of the etch rate predicted by this expression versus the actual etch rate is shown in figure 43.

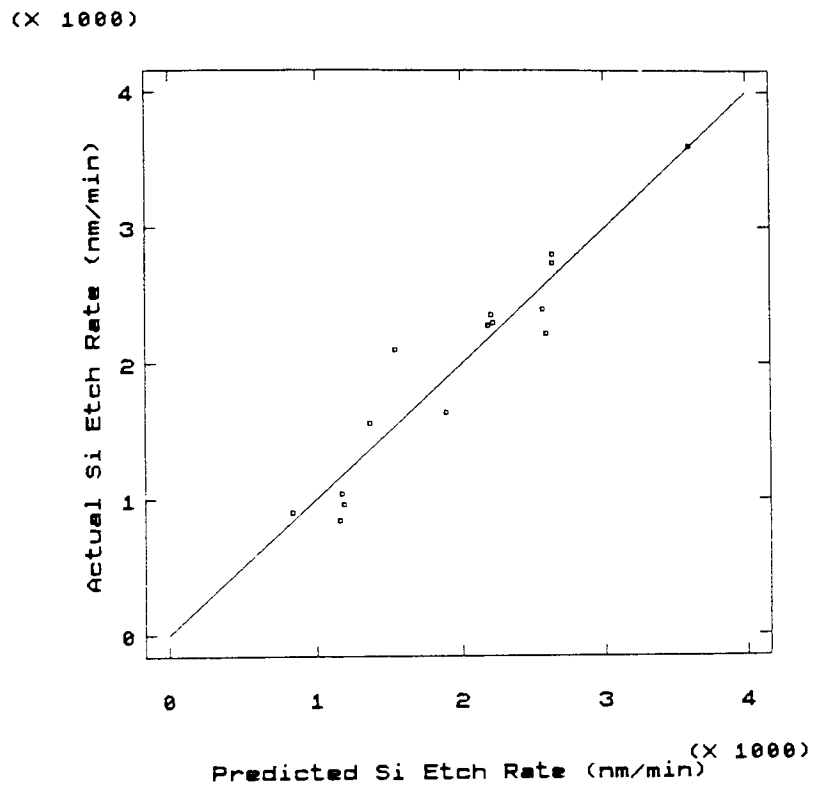

Figure 43. Predicted versus actual silicon etch rate in SF_6 plasmas.

In the absence of mass spectrometric data, the extent of etch rate enhancement due to the presence of SF_x radicals in these studies is unknown. However, it is reasonable to assume that, under these operating conditions, the radical concentration is proportional to the F-atom concentration, and that deviations from this simplistic view may account for the slight errors in the model presented. In summary, SF_6 is a "clean" (residue free) etchant which may enhance Si etch rates relative to F_2 by the prevention of surface oxidation. SF_6 etch rates may be higher than those predicted from plasma F-atom concentrations alone, due to the possibility of dissociative chemisorption of SF_x radicals on Si.

The situation with CF_4 is more complex for two main reasons:

(i) although the positive ion density is likely to be similar in SF_6 and CF_4, SF_6 is electronegative (the discharge may contain more negative ions than electrons[97]) - this is reflected in the higher d.c. self-biases obtained with CF_4;

(ii) there is the possibility of competition between fluorocarbon polymer deposition and etching.

Certainly, for this work, comparison of figures 12 and 13 shows that there is no direct correlation between silicon etch rate and etchant (atomic fluorine) concentration as a function of chamber pressure and RF power.

Thomson and Helms[98] studied the ion beam sputtering of Si by CF_3^+ (the principal ion in CF_4 plasmas) and SF_5^+ for ion energies in the range 0.5 - 3.0 keV. The etch yields with SF_5^+ were close to the maximum predicted for physical sputtering alone, whereas those for CF_3^+ were at or below the minimum. Results for Xe^+ lay between the two. Auger analysis of the etched surfaces showed the formation of Si-C bonds in the case of CF_3^+, and a low concentration of S, not bound to Si, with SF_5^+. Thus the retardation in Si etch rates with CF_3^+ was attributed to the formation of involatile surface layers.

In order to study the influence of d.c. bias on the etching of silicon in CF_4, Lejeune et al.[99] used a d.c.-excited plasma and independent d.c. substrate biasing. This arrangement allowed the energy dependence of ion-assisted chemistry to be studied whilst the composition of ions and neutrals remained unchanged. It was found that for a given set of plasma conditions there existed a threshold bias above which an etch-retarding C-F overlayer was formed, the steady state thickness of which increased with increasing ion energy.

Oehrlein and Williams[100] measured the influence of fluorocarbon film thickness on silicon etch rates in CF_4/H_2 plasmas. They found both that the film thickness increased with increasing percentage H_2 in the discharge, and that the silicon etch rate was inversely related to the film thickness for films greater than 1 nm. They found that the silicon etch rate was invariant with fluorocarbon film thickness in the range ~0.3 - 1 nm (1 - 4 monolayers). When reactive ion etching with pure CF_4 the film was only ~ 0.3 nm (~1 monolayer) thick, and thus had no apparent influence on the Si etch rate. The influence of RF power density on the film thickness was studied for CF_4/40% H_2 plasmas. Under RIE conditions the film thickness increased with increasing power to a plateau, then dropped substantially at higher powers. It should be noted that the highest power densities used by Oehrlein and Williams (0.2 Wcm^{-2}) correspond to the lowest power densities used for this work. However, Oehrlein and Williams worked exclusively at 25 mtorr whereas pressures of up to 200 mtorr were used in this work.

A number of pertinent points arise from these three papers:

(i) the very ion, CF_3^+, most likely to assist Si etch processes in CF_4 plasmas, through sputtering of SiF_x and fluoropolymer, can itself inhibit etching through the formation of an involatile Si-C layer[98];

(ii) contrary to expectation, increased Si ion bombardment during etching in CF_4-containing discharges can give rise to an increased steady-state thickness of etch-inhibiting fluoropolymer[99];

(iii) the thickness of fluoropolymer formed on Si by reactive ion etching in pure CF_4 at high RF powers is likely to be of the order of a monolayer or less, and would be expected to have little influence on etch rates[100].

Only ex-situ XPS was available for the present work, and it was not possible to distinguish between polymer and adventitious carbon (atmospheric contaminants) on an etched silicon surface. This result demonstrates that the fluoropolymer film, if present, was very thin. However, it should be remembered that:

(i) in pure CF_4, CF_x radicals (mainly CF_2) are present at roughly half the F-atom concentration[101];

(ii) CF_x radicals are readily adsorbed on silicon surfaces, as demonstrated by XPS[100].

Clearly, no data can be available for silicon etching in pure CF_4 in the absence of competition between F and CF_x for silicon surface sites. This author believes that even under reactive ion etch conditions hindrance of silicon etching, either by the adsorption of CF_x or at high powers by the formation of Si-C bonds, should not be dismissed lightly. The potential role of fluorocarbon polymers in inhibiting silicon etching during reactive ion etching in CF_4 and CF_4/10% O_2 is discussed again in section 3 of this chapter, *Influence of Electrode Materials*, and the mechanisms of fluorocarbon polymer formation are discussed in detail in the next chapter.

It follows both from this discussion, and from the silicon etch mechanisms described in chapter 1, that both F-atom concentration and ion bombardment, as represented by d.c. self-bias[31], are likely to play a significant role during the reactive ion etching of silicon in CF_4. This is indeed the case for the data presented in table 10, which fits an equation of the form

$$\text{Silicon etch rate} = 0.061[F]^{0.46} \times \text{d.c. self-bias} \qquad (5.2)$$

as demonstrated in figure 44.

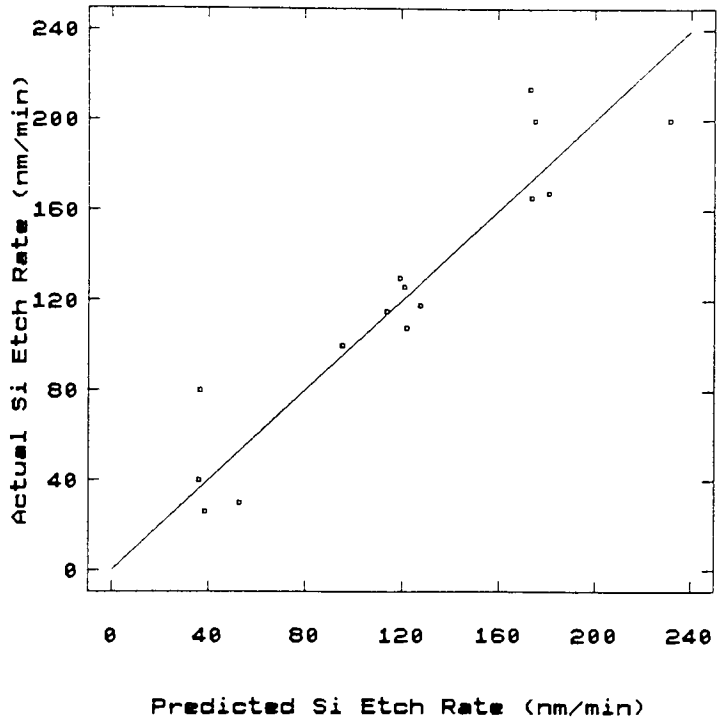

Figure 44. Predicted versus actual silicon etch rate in CF_4 plasmas.

In conclusion, the apparent involvement of ion bombardment in CF_4 etching of Si might be expected to make it a more efficient etchant for a given F-atom concentration than SF_6. Clearly, this is not the case. It cannot be ascertained from the present results to what extent fluoropolymers, or adsorbed precursors, may hinder etching with CF_4 or SF_x radicals promote etching with SF_6.

In order to further investigate the differences between the two systems, and to study any possible synergistic effects CF_4/SF_6 mixtures were examined. Consistent with the previous results the silicon etch rate and F-atom concentration both fell with increasing percentage additions of CF_4 to SF_6 (figure 18). The change in silicon etch rate was an order of magnitude and the change in F-atom concentration a factor of four on going from pure SF_6 to pure CF_4. However, whereas the F-atom concentration varied linearly with $\%CF_4$, with SF_6/75% CF_4 the silicon etch rate was almost double that

which would have been predicted by linear extrapolation between the pure gas results, at first sight indicating a degree of synergism.

However, if it is assumed that in all the discharges containing SF_6 the F-atom concentration arises solely from the dissociation of SF_6 - the S-F bond dissociation energy (326 $kJ.mol^{-1}$) is considerably lower than that for C-F (448 $kJ.mol^{-1}$)[102] - then the models described above can be used to predict the etch rates shown in figure 45. Thus, equation 5.1 (SF_6) is used to predict the silicon etch rates in both pure SF_6 and the SF_6/CF_4 mixtures, and equation 5.2 (CF_4) the silicon etch rate in pure CF_4. Excellent agreement is seen between predicted and measured etch rates.

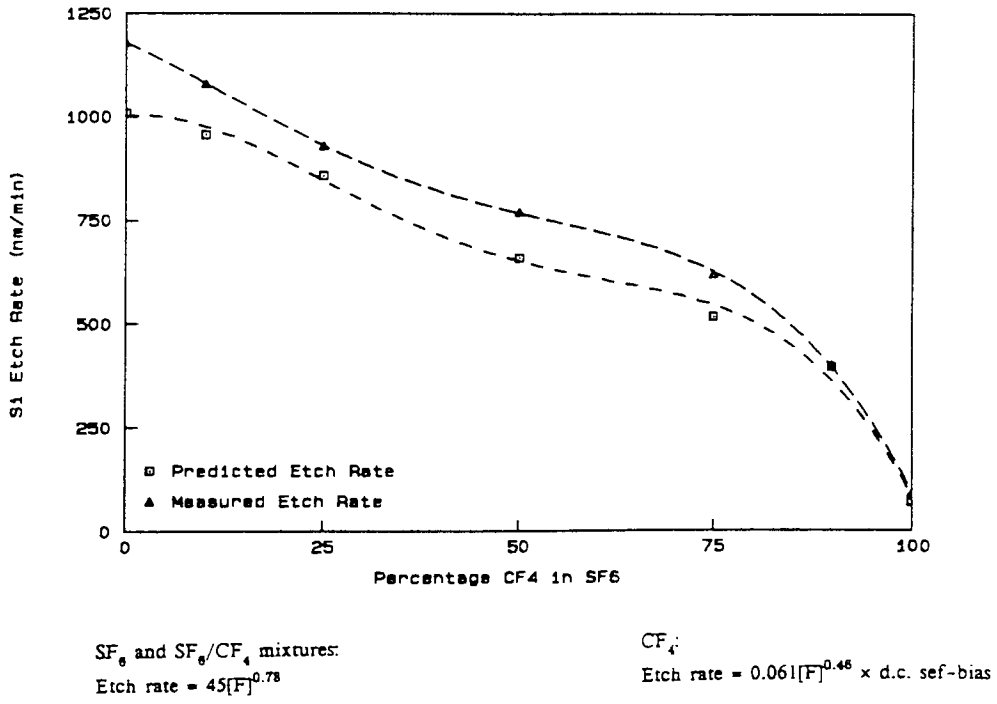

Figure 45. Measured and predicted Si etch rates as a function of percentage CF_4 in SF_6.

The silicon etch rate results presented in table 18 for SF_6/additive mixtures show that, to a first approximation, there is a correlation between relative F-atom concentration and silicon etch rate. However, looking at the SF_6/O_2 and SF_6/CO_2 results in more detail it is evident that although at both power levels the F-atom concentration with the O_2 addition is more than double that with CO_2, there is little difference between the silicon etch rates. It is apparent that both F and O are playing a crucial role in determining silicon etch rates. In order to study this effect further, silicon etch rates in CF_4, C_2F_6, CHF_3 and SF_6 were measured as a function of the addition of each of O_2, CO_2 and N_2O. The experiments were conducted at constant flow, pressure and RF power which resulted in a near-invariant d.c. bias for all the fluorocarbon/additive mixtures. This allowed the effects of changes in the neutral species (F, O and CF_2) concentrations on Si etch rates to be more readily followed.

Consistent with the etch mechanisms presented in chapter 1, it was found that:

(i) the addition of low percentages of all three additives to a fluorocarbon resulted in an increase in F-atom and a decrease in CF_2 radical concentration;

(ii) for a given fluorocarbon/additive mixture there was an optimum percentage additive for maximum F-atom concentration;

(iii) for a given additive, the percentage additive required to achieve a maximum in F-atom concentration increased with the effective C:F ratio of the fluorocarbon;

(iv) for a given percentage additive in a particular fluorocarbon, the F-atom and O-atom concentrations were in the order $O_2>N_2O>CO_2$;

(v) maxima in Si etch rates occured for a lower percentage additive than that which gave the maximum F-atom (etchant) concentration.

Item (iv) is worthy of particular mention. It is clear from table 34 that the dissociation energy of N_2O is considerably lower than those for O_2 and CO_2[17]. It is thus surprising that, in agreement with others[35], the O-atom concentrations found with N_2O are lower than those with O_2. It can only be assumed that in the plasma environment dissociation mechanisms other than those implied by thermodynamics may occur.

Table 34. Bond dissociation energies.

Bond	D°_{298} (kJ mol^{-1})
$O-N_2$	167
O-O	498
O=CO	532

Silicon etching in CF_4/O_2 is often represented as a competition between F and O for Si surface sites, but this may be an over simplification for reactive ion etching where additional etch mechanisms are likely to occur[32]. In the present work, the use of C_2F_6 and CHF_3 as etchants, with higher C:F ratios than CF_4, makes more likely the need for an additional etch retardation term due to polymer formation (particularly in the absence of oxygen). Silicon etching may therefore be represented by:

$$\text{Silicon etch rate} = a + b[F] + c[O] + d[CF_2] \qquad (5.3)$$

where a-d are constants.

A best fit of the experimental data to the model is found with a=45, b=0.64 c=-4.6 and d=-0.10. Figure 46, a plot of predicted vs actual etch rates, shows that this model

provides a reasonable description of silicon etching for the wide range of gas chemistries studied.

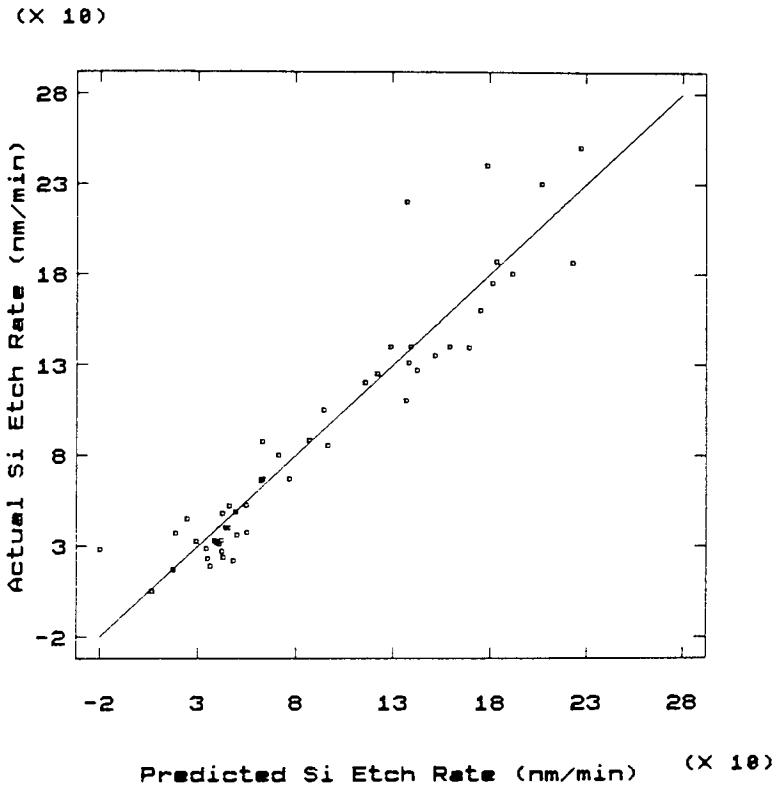

Figure 46. Plot of predicted vs. actual Si etch rate.

Although the d.c. bias remained near constant for all the fluorocarbon/additive experiments, a considerable reduction in the Ar (750.4 nm) actinometer signal was seen with increasing percentage additions of additive, indicating changes in the electron energy distribution function of the plasma. This signal has been used to approximate changes in the ion flux to the substrate[103]. Assuming that the three competing processes at the silicon surface are ion assisted, a revised model can be developed:

$$\text{Silicon etch rate} = e + I_{Ar} \times (f[F] + g[O] + h[CF_2]) \qquad (5.4)$$

where I_{Ar} is the Ar (750.4 nm) intensity; e-h are constants - e=38, f=0.0043, g=-0.026 and h=-0.00054.

The improvement in the model is shown by figure 47. It is interesting to note that for pure CF_4 the model predicts only a ~4% reduction in etch rate due to the presence of CF_2, whereas the predicted etch rate for CHF_3 is reduced by ~80% reflecting its the higher propensity for polymer formation. In the case of CF_4/10% O_2 there is a ~9% reduction in etch rate due to oxygen. Although, for reasons discussed, Si etch rates with SF_6 gas mixtures were very much higher than with CF_4 variations in etch rate could again be rationalised in terms of competition between etchant and oxygen for Si surface sites.

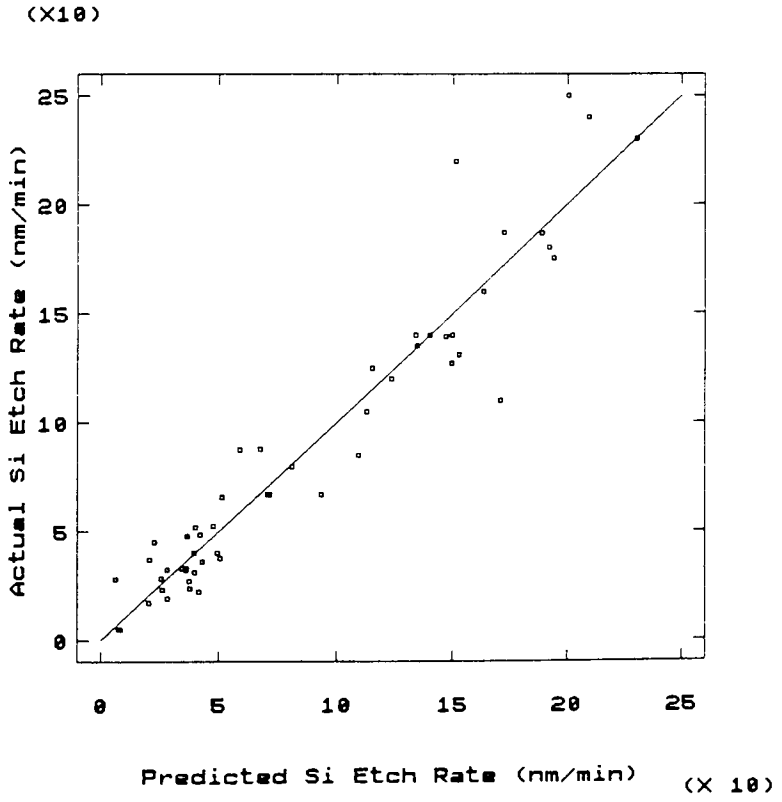

Figure 47. Predicted vs. actual Si etch rates; improved model.

5.2 Plasma Etching of Silicon Dioxide

The precise mechanism of oxide etching is still unclear; in fluorocarbon discharges F-atoms[41, 42], CF_2 radicals[43, 44], CF_3^+ ions[45] and even anhydrous HF[37, 46] have variously been considered active oxide etchants. Measurements of oxide etch rate as a function of RF power density demonstrated that etching occurs by an ion assisted process[48], and is dependent only on the measured ion density[45]. Further, a comparison of plasma and reactive ion beam etching showed that, at a fixed ion energy, the estimated etch yields per ion were independent of the radical flux to the substrate, leading the authors to the conclusion that the ions themselves were the etchants[45].

In the present work, modelling of the SiO_2 etch rates in CF_4 as a function of flow, pressure and RF power showed that they were dependent on RF power, and, to a lesser extent, on an interactive power-pressure term (table 12). These dependencies were mirrored in the measured Ar^+:Ar emission intensity ratio.

The glow region of a plasma discharge may be fully characterised by the electron energy distribution function (eedf) which may, in principle, be uniquely determined by Langmuir probes. However, this technique is fraught with experimental difficulties. Cox et al.[104] have shown that for an argon plasma some corroborative information on the shape of the eedf may be obtained by considering the relative emission intensity of an Ar atom (470.2 nm, emission threshold 15 eV) and an Ar^+ ion (480.6 nm, emission threshold 35 eV), i.e. two species with widely differing and relatively high threshold energies for emission. The Ar^+:Ar intensity ratio may be used to estimate the electron temperature.

The ion flux to the substrate is given by the Bohm equation:

$$\text{Ion Flux} = 0.6n_e(kT_e/m_i)^{0.5}$$

where n_e is the electron density, T_e is the electron temperature, and m_i is the mass of the ion.

Thus, if the Ar atom emission intensity is considered proportional to the electron density, and the Ar^+:Ar intensity ratio proportional to electron temperature then an estimate of relative ion flux can be made.

Little correlation was found between SiO_2 etch rate and the relative ion flux estimated in this way. However, as shown in figure 48 a good correlation was found between SiO_2 etch rate and the product of ion flux and d.c. bias. This is in agreement with results discussed later in this section.

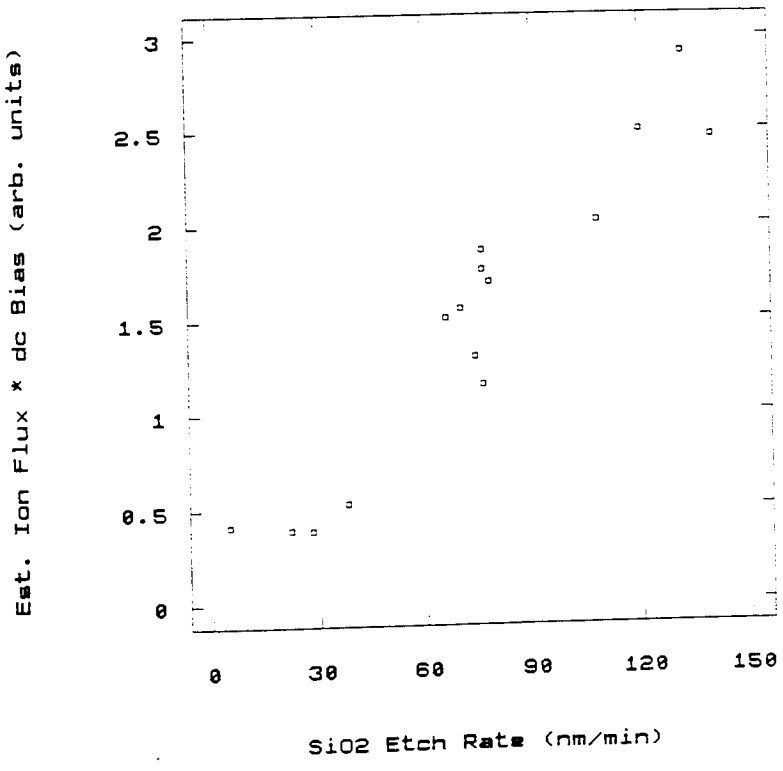

Figure 48. *SiO_2 etch rate vs. ion flux (estimated from OES results) × d.c. bias; CF_4 plasma.*

In the case of SF_6 the oxide etch rates were almost directly proportional to RF power alone (table 16), whereas the Ar^+:Ar intensity ratio was largely pressure dependent. A degree of correlation was found between etch rate and the product of F-atom concentration and d.c. bias (figure 49). This result, taken with that for CF_4, is in agreement with the views of Steinbruchel and Curtis[49] that at low F-atom concentrations (CF_4) direct reactive ion etching dominates, whereas at high F-atom concentrations (SF_6) the etching is ion enhanced with F-atoms as the main neutral reactants.

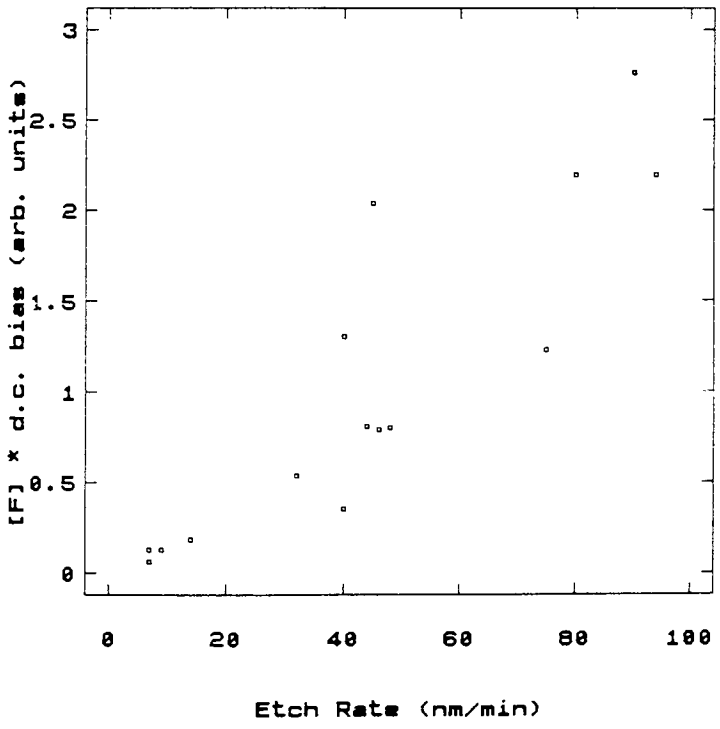

Figure 49. *SiO_2 etch rate vs. $[F]$ × d.c. bias; SF_6 plasma.*

However, in a study of SF_6/CF_4 mixtures at constant, flow, pressure and power, the silicon dioxide etch rate and d.c. bias both rose with increasing percentage additions of CF_4 to SF_6 (figure 19), whereas the F-atom concentration declined. Taken together with the results from the pure gases a number of points can be made regarding oxide etching:

(i) over the parameter space studied the oxide etch rate is, to a first approximation, directly proportional to RF power level and independent of chamber pressure;

(ii) the d.c. bias and the F-atom concentration are dependent on both RF power and pressure - with both pure gas systems the bias decreased and the F-atom concentration increased with increasing pressure;

(iii) the presence of CF_x species is not essential for the reactive ion etching of oxides to proceed;

(iv) under conditions of fixed pressure and power, in a fluorine-containing discharge, the oxide etch rate is proportional to d.c. bias and shows no direct dependence on F-atom concentration.

The bias dependency demonstrated by the addition of CF_4 to SF_6 could have been entirely due to an increase in etchant concentration, e.g. CF_3^+, and the rise in d.c. bias entirely coincidental. In order to test this hypothesis, alternative SF_6 additives (O_2, CO_2, H_2, CH_4 and Ar) were used (table 18). All the additives, even when present in small percentages, significantly increased the d.c. self bias. O_2 and CO_2 additions served to increase, and H_2 and CH_4 additions to decrease the F-atom concentration. No correlation between F-atom concentration and oxide etch rate was found. The etch rate was, however, proportional to d.c. bias (figure 20).

The presence of carbon, or carbonaceous species, has been considered beneficial to oxide etching due to the thermodynamic gain from breaking Si-O bonds and the

formation of C-O bonds. For example, Nakamura et al. studying Si/SiO_2 selectivity during reactive ion etching with HBr found that the oxide etch rate was reduced by the use of an ultraclean (carbon free) system[105]. Conversely, the addition of carbon-containing gases such as CO_2 or CH_4 enhanced oxide etching. Similarly, the thermal etching of SiO_2 by HF vapour is enhanced when carbon is present on the surface being etched[106]. No such effects were noted in the present work with the addition of CO_2 or CH_4 to SF_6. However, the chamber used for these studies could in no way be described as "clean". Considerable trace carbon was undoubtedly present due to rubber seals, back-diffusion of oil, air leaks etc.

Figure 20 showed that the SiO_2 etch rates vs. d.c. self bias with SF_6/CF_4 mixtures lay on the same line as the SF_6/additive results described. Enhanced etching by CF_x species can therefore be dismissed for the experimental conditions used. Two other points should be remembered, though:

(i) for a given d.c. bias the 200 W experiments gave significantly higher etch rates than those experiments performed at 100W;

(ii) the oxide sputter rate (pure Ar) was more than an order of magnitude lower than the etch rate in the presence of fluorine/fluorinated species at the same d.c. bias.

These results indicate, for the range of process parameters studied, that:

(i) RF power (ion density) has a dominant influence on oxide etch rates;

(ii) for a given RF power level, d.c. bias (ion energy) has a secondary influence on oxide etch rates;

(iii) fluorine/fluorinated species are required for etching to proceed, but their attack on the oxide is not the rate determining step.

(iv) the presence of CF_x/carbonaceous species has no chemical influence on oxide etch rates.

5.3 Influence of Electrode Materials

Chapter 3 (section 3.3) decribes the results of studies of the influence of a wide range of electrode materials on the etch rate of silicon and thermally grown silicon oxide in CF_4 and CF_4/O_2 plasmas. Optical emission spectroscopy with argon actinometry was used to determine the corresponding relative gas-phase concentration of atomic fluorine. X-ray photoelectron spectroscopy (XPS) was used to examine selected silicon surfaces after etching.

It was found that the silicon etch rate in a CF_4 plasma was considerably enhanced, relative to an anodised aluminium electrode, in the presence of soda glass or sodium or potassium "doped" quartz. The effect was even more pronounced in a CF_4/O_2 discharge. In the latter system lead and copper electrodes also enhanced the silicon etch rate. These results could not be accounted for by a corresponding rise in atomic fluorine concentration. Variations in the Ar (750.4 nm) actinometer emission were largely accounted for by physical changes in the optical path due to electrode thickness implying that the various electrode materials did not substantially alter the electrical characteristics of the plasma. Also, for the CF_4/5% Ar system the Ar^+:Ar intensity ratio remained essentially constant at 0.50 $\pm$0.10 for all the electrode materials (except PTFE, 0.33) providing further evidence that the eedf is little altered by the choice of electrode material. Thus the observed variations in silicon etch rate do not arise from changes in the physical characteristics of the plasma, but must be predominantly due to chemical effects. XPS confirmed the presence of transferred electrode material on the silicon surface. The same range of electrode materials had little effect on the relative etch rates of SiO_2.

The results presented clearly require the participation of transferred alkali metals in surface processes during etching. Three ways in which etching might be assisted by the presence of alkali metals are considered:

(i) effects of transferred metals on fluorocarbon films which inhibit etching;

(ii) direct enhancement of silicon etching by the formation of favourable intermediates;

(iii) modification of the electronic properties of the silicon ("band bending") which may enhance silicon etching.

(i) Effects of transferred metals on fluorocarbon films which inhibit etching.

The first mechanism involves polymer films which may form during etching with fluorocarbon gases and significantly modify etching behaviour. The formation and role of these films was described in an earlier section of this chapter. It should be remembered that silicon etch rates in fluorocarbon discharges are increased by both increasing the F atom concentration and decreasing the concentration of CF_x radicals in the plasma. Figures 29 and 30 show that a 10% addition of O_2 to a CF_4 plasma results in a ca. tenfold increase in the F-atom concentration. However, a laser-induced fluorescence study of this plasma under similar conditions showed only a halving of the CF_2 concentration[30]. Thus, if fluoropolymers, derived from CF_2, do limit silicon etch rates in pure CF_4, it is possible that a similar effect occurs with CF_4/10% O_2.

The enhanced silicon etching could therefore be explained by the action of specific metals in limiting the formation of polymer films on a silicon surface[107]. There are some interesting parallels with the known effects of alkali metals, lead, and copper as carbon combustion catalysts[108]. Consistent with this, the relative etch rate

enhancement is greater in the presence of added oxygen (N.B. trace oxygen will always be present due to chamber leaks, and from the chamber and electrode materials). Indeed, in the case of lead or copper no enhancement is seen in the absence of oxygen. This suggests that where such metals enhance the plasma etching of silicon, the most significant role of the metals might lie in removal of the polymer films.

In an attempt to clarify the role of polymer films in silicon etching, the effects of soda glass and quartz electrodes on the deposition rates and etch rates of C_3F_8- and CHF_3-derived fluorocarbon polymers were studied (tables 21 and 22). It was found that for the lower deposition rates found with C_3F_8 the presence of quartz and soda glass electrodes approximately halves the deposition rate relative to an uncovered electrode. With CHF_3, however, where deposition rates are more rapid, no differences are observed when glass and quartz electrodes are used. These results are consistent with oxygen from the quartz and soda glass electrodes inhibiting polymer formation and being available for a longer period with C_3F_8 than CHF_3. Thus alkali metal had no apparent influence on the deposition rates of either plasma polymer. It should be noted, though, that in contrast to the studies with CF_4 and CF_4/10% O_2 where net etching of Si and SiO_2 occurred, such heavy polymer deposition might mask any alkali metal effect.

Etch rates in CF_4 and CF_4/O_2 plasmas of polymer deposited from both CHF_3 and C_3F_8 plasmas were unaffected by the presence of quartz or soda glass electrodes. Alkali metals from the glass electrode clearly had no apparent influence on the etch rates of these fluoropolymers. However, these polymer films might be expected to have significant differences in structure and properties from those polymers now known to be produced from CF_4 during silicon reactive ion etching.

In summary, it has been shown that:

(i) fluorocarbon polymer has been detected on the surface of silicon after reactive ion etching in CF_4[109];

(ii) the addition of 10% O_2 to CF_4 only halves the gas phase concentration of CF_2 radicals (polymer precursors)[30];

(iii) alkali metals, copper and lead are well known combustion catalysts[108].

Thus, although the results on C_3F_8- and CHF_3-derived polymer film deposition and stripping in plasmas provide no support for transferred metals having any beneficial effect on fluorocarbon films which inhibit silicon etching, this mechanism may still have a significant role in the etch enhancements observed. It is fully consistent with the considerably higher silicon etch rates found with SF_6, a "clean" etchant, than CF_4 described earlier in this chapter. Further, it also accounts for the lack of etch rate enhancement found with SF_6 in the presence of a soda glass electrode (chapter 3, section 3.3.1).

(ii) Direct enhancement of silicon etching by the formation of favourable intermediates.

The potential influence of metals on the etch rates of silicon is well documented in the literature - the effects of alkali metal contamination were noted as early as 1981[110] - and a variety of direct etch rate enhancement mechanisms have been considered. These are now briefly examined in the light of the present work.

White and Maa[111] have reported an increase in the etch rate of amorphous silicon in a CF_4/O_2 plasma after implantation of the silicon with sodium ions or wet

chemical contamination of the surface with sodium or potassium salts. Boron-doped Si<100> previously treated with NaOH also showed an enhanced etch rate, but phosphorous-doped polysilicon and n-type Si<100> did not (lightly phosphorus-doped n-type Si <111> was used in these studies). In their tentative explanation, the increased rate resulted from the formation of an alkali metal fluorosilicate (or oxyfluoro-silicate) which helps provide more reactive fluorine bonding sites, summarised by:

$$Na_2SiF_6 \rightarrow 2NaF + SiF_4$$

$$2NaF + Si + 4F \rightarrow Na_2SiF_6$$

The alkali-gettering properties of phosphorous were assumed to make the sodium unavailable for the formation of such a complex.

The XPS results shown in figure 20 do not preclude interaction between Na, Si and F, but neither the F1s/FKLL nor the Na1s/NaKLL levels correspond to Na_2SiF_6.

Fedynyshyn et al.[112] measured silicon etch rates in a CF_4/O_2 plasma in the presence of an aluminium mask, a silver mask, and photoresist. They found that the etch rates were enhanced by aluminium, and even more so by silver, and proposed that both aluminium and silver catalyse the production of fluorine radicals, thereby enhancing the etch rate. Subsequently[113] they measured the etch rate of photoresist-masked silicon placed on aluminium, chromium and photoresist-masked plates, as well as pure copper and nickel plates. (These plates only covered part of the chamber electrode.) The local fluorine concentration was measured by OES with Ar actinometry. The silicon etch rates were enhanced, with respect to the photoresist plate, by an empty chamber, aluminium plate and chrome plate, and even more so by the

copper and nickel plates. The OES results correlated well with observed etch rates, confirming the proposed mechanism

The results presented in figure 26 demonstrate similar etch rates in the presence of aluminium and quartz cover plates with reduced etch rates in the presence of polythene (cf. photoresist), silver and nickel. Also, the OES results in figures 29 and 30 show similar atomic fluorine levels for quartz and aluminium and significantly reduced levels for polythene, nickel and silver in CF_4 and CF_4/O_2 plasmas. A more likely explanation is that aluminium does not in fact enhance silicon etch rates, rather polythene reduces them. This is in agreement with Coburn[114] who has noted that electrode materials such as silicon, carbon, PTFE, or polythene may be used to create fluorine-deficient fluorocarbon discharges as a way of increasing SiO_2-to-Si etch ratios.

Copper contamination of a silicon surface has been reported[115, 116] to enhance considerably thermal etching by molecular fluorine and NF_3, and to enhance slightly etching by fluorine atoms. The latter result is in agreement with that shown in figure 26 for a CF_4/10% O_2 plasma and copper cover-plate. Silver contamination also enhanced molecular fluorine etching of silicon, whereas other metals (including Al, Fe, Ni, Pb, and Pt) did not. Copper-catalysed dissociation of molecular fluorine was proposed as the most likely etch rate enhancement mechanism. This mechanism is also consistent with the slight enhancement found with fluorine-atom etching, where gas-phase recombination reactions might lead to a significant molecular fluorine concentration, but would appear inappropriate to our plasma system.

Thus, whilst it is recognised that these increases may result from more than one enhancement mechanism, it seems unlikely that the increases in etch rate seen in this work arise from the formation of favourable chemical precursors on the silicon surface.

(iii) Modification of the electronic properties of the silicon ("band bending") which may enhance silicon etching.

A more plausible mechanism for the alkali metal effects perhaps lies in the "band bending" mechanism suggested by Lee and Chen[117], and extensively developed by Winters and Haarer[118] (see also Yarmoff and McFeely[119]). This mechanism was devised to explain the higher etch rate of heavily doped n-type silicon relative to lightly doped or p-type silicon.

The presence of fluorine on the surface as negative ions (the most favoured state) causes the electronic bands in the silicon to bend upwards to an extent which depends on the thickness of the surface SiF_x layer and the electrical properties of the bulk silicon (i.e., the type of doping). In this interpretation, the band bending allows higher surface concentrations of negative ions on heavily doped n-type silicon, so increasing the etch rate. Winters and Haarer suggest that the presence of an alkali metal atom (with a low ionization potential) allows an extra negative ion on the surface without changing the electric field or Fermi level, again enhancing the etch rate. Ion bombardment decreases the thickness of the SiF_x layer, thereby increasing the etch rate and diminishing the influence of doping.

As lightly doped silicon in reactive-ion etch mode was used for this work, it is anticipated that band bending effects would be minimal in the absence of transferred metals. However, some support for modified electronic levels is shown in figure 50, which shows a reasonably close correlation between etch rate and binding energy of the Si2p levels in surface silicon (presumably fluorosilyl species).

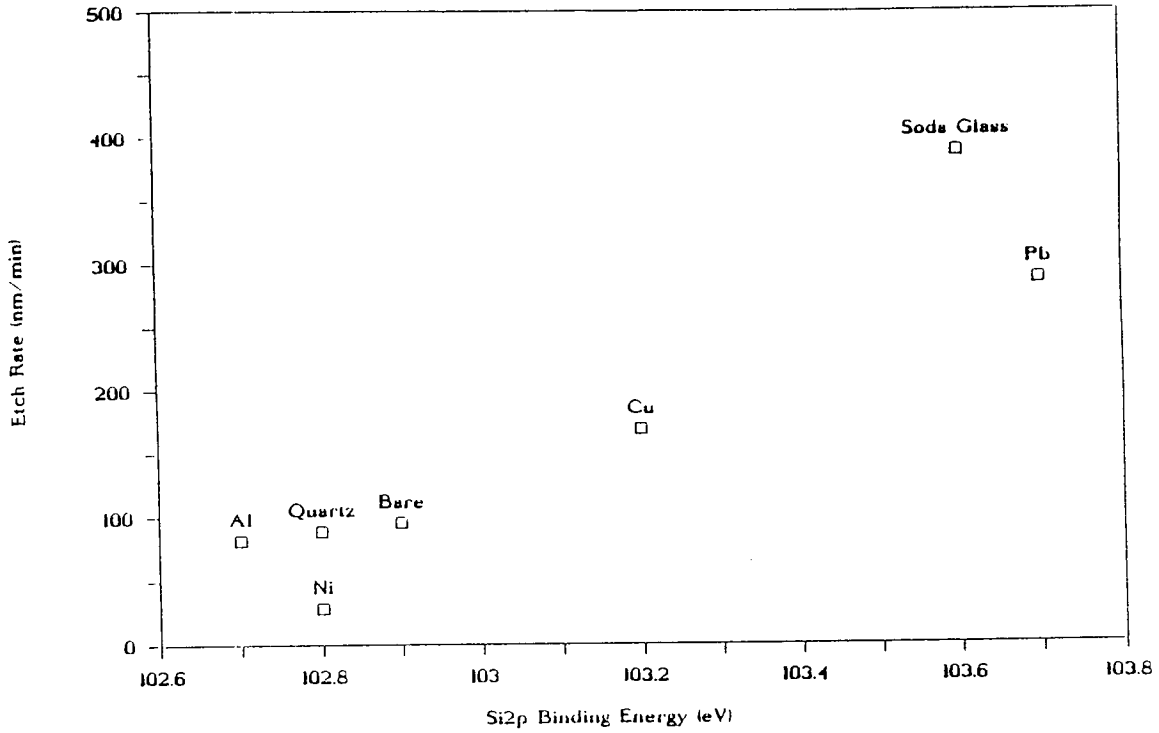

Figure 50. *Si etch rate vs. Si2p binding energy for various electrode cover-plate materials; CF_4/10% O_2 plasma.*

CHAPTER 6 - DISCUSSION: PLASMA POLYMERISATION

6.1 Introduction

The results contained in chapter 4 show a number of interesting features of fluorocarbon plasma polymerisation processes, and of the structure and properties of the resultant fluoropolymers. The principal results are summarised below.

The polymer deposition rate from pure C_3F_8, as a function of RF power, was shown to be proportional to the gas phase CF_2:F ratio (measured by optical emission spectroscopy). When hydrogen was present in the plasma, i.e. discharges of CHF_3, or CF_4, C_2F_6 and C_3F_8 with hydrogen additions, this simple relationship did not hold. Indeed, with increasing hydrogen additions to C_3F_8 the CF_2:F ratio fell whilst the deposition rate increased.

Reflection infrared spectra of polymers deposited onto aluminised surfaces showed two major bands corresponding to C=C and C-F stretch respectively. Surprisingly, the C-F band width was proportional to polymer film thickness irrespective of discharge chemistry (figure 38), whereas the C=C band width remained constant. The ratio of C=C:C-F band areas decreased with increasing film thickness for both plasma polymerised C_3F_8 and CHF_3. However, for a given film thickness the ratio was lower in C_3F_8 indicating a higher degree of saturation in these polymers. Increasing additions of hydrogen to C_3F_8 caused an increase in C=C:C-F ratio with film thickness, indicating that hydrogen increases polymer unsaturation (figure 39).

XPS analysis of the plasma fluoropolymers showed that they all contained carbon and fluorine in five chemical environments: $\underline{C}$, $\underline{C}$-CF, CF, CF_2 and CF_3 (figure 40). For

a given monomer the C:F ratio increased with increasing additions of hydrogen (table 27). This corresponded to a decrease in the CF_3 and CF_2 components and an increase in all other components (table 28).

All the polymers studied by thermal analysis were found to be unstable above ~200 °C in air. Thermogravimetric analysis showed that the temperature at which the maximum rate of polymer weight loss occured increased with increasing prior proportions of hydrogen in the plasma, e.g. C_3F_8, 294 °C; C_3F_8/50% H_2, 341 °C. With high proportions (50%) of hydrogen in the plasma a second weight loss peak appeared at 100 °C higher temperature. Differential scanning calorimetry showed that the plasma polymer decomposition reactions were all exothermic.

Thin films of plasma polymerised C_3F_8 and CHF_3 had a dielectric constant similar to PTFE. The a.c. resistivity of the C_3F_8 polymer was ~70% higher than that of the CHF_3-derived polymer.

The next section surveys the main features of polymerisation in fluorocarbon plasmas as currently understood. The rest of the chapter uses this material, with some original suggestions, to interpret the current results on plasma polymerisation rates and polymer structures.

6.2 Gas Phase Chemistry

As described in chapter 1, CF_2 radicals are most significant in plasma polymerisation, while F atoms mainly determine silicon etch rates. This section therefore concentrates on observations and interpretations relating to the CF_2:F ratio in fluorocarbon plasmas.

In a study of plasma deposited gold/fluorocarbon composite films in which C_3F_8 was used as the fluorocarbon monomer, the main dissociation products of C_3F_8 were considered to be CF_2, F and CF_3^+, with oligomers from CF_2 the primary polymer precursors and F a polymer etchant. Thus the polymer deposition rate is controlled by the gas phase CF_2:F ratio[120].

The relative concentrations of CF_2 and F in a C_3F_8 plasma both rose with increasing RF power, consistent with the findings of Millard and Kay[121]. However, the CF_2:F ratio passed through a maximum. In order to explain these observations in a qualitative fashion a **simplified** reaction scheme, based on those produced by d'Agostino et al. for CF_4 and C_2F_6[122], is proposed here. All the reactions are reversible, and the forward decomposition reactions are driven by electron impact dissociation.

$$C_3F_8 \downarrow +$$

(a)

$$\begin{array}{lll} & C_2F_5 \downarrow & \\ CF_3 & + & CF_2 \\ \downarrow & & \downarrow \\ CF_2 + F & & CF + F \\ \downarrow & & \\ CF + F & & \end{array}$$

$$CF_2 + CF_2 \rightarrow C_2F_4$$
$$CF_3 + CF_3 \rightarrow C_2F_6$$

(b)

$$\begin{array}{l} CF_3 \downarrow \\ CF_2 + F \downarrow \\ CF + F \end{array}$$

It can be seen that route (a) allows some production of CF_2 without the production of F. Further, this route is thermodynamically favoured as C-F bonds are ~20% weaker than C-C bonds. Thus, at low RF powers, the CF_2:F ratio would be expected to rise with increasing RF power. At high RF powers the extent of reaction will be greater, with increased C-F bond breaking via route (a) or route (b), causing the observed reduction in the CF_2:F ratio.

Table 35. Reaction enthalpies for CHF_3.

Reaction	ΔH (kJ.mol^{-1})
$CHF_3 \rightarrow CF_3 + H$	436
$CHF_3 \rightarrow CHF_2 + F$	473
$CHF_3 \rightarrow CF_2 + HF$	235

Examination of the enthalpies of formation of various radicals from CHF_3[123] (table 35) shows the formation of CF_2 by the elimination of HF to be the most energetically favoured reaction. The spectroscopic data obtained for CHF_3 showed a rise in both H and F-atom concentrations with RF power, consistent with the effects of increased HF concentrations and increased H-F bond cleavage. The CF_2 radical concentration remained near constant. Two possible explanations are offered for this:

(i) depletion of the gas phase CF_2 concentration by polymer formation on the chamber surfaces;

(ii) interaction of hydrogen with CF_2 to produce CF and further HF.

The latter explanation is favoured as it also accounts for the slower rise in atomic-H concentration relative to atomic-F.

The gas phase chemistry of fluorocarbon/hydrogen gas mixtures has been studied by Truesdale and Smolinsky[123] using mass spectroscopy, and by d'Agostino using both mass spectroscopy and actinometric optical emission spectroscopy. The changes in CF_2 radical and F-atom concentrations in CF_4, C_2F_6 and C_3F_8 plasmas as a function of percentage hydrogen addition, reported in chapter 4.4, are broadly comparable to those found by d'Agostino[124]. These changes include a fall then subsequent rise in F-atom concentration with increasing hydrogen additions in all three discharges, a substantial rise in CF_2 radical concentration for small percentage H_2 additions to CF_4 and C_2F_6, and a near invariance in CF_2 radical concentration in C_3F_8/H_2 plasmas. Differences in percentage hydrogen addition producing CF_2 radical concentration maxima most likely arise from variations in experimental arrangements and process conditions. For example, Truesdale and Smolinsky found that the discharge chemistry was sensitive to flow rate[123].

The initial rise in CF_2 and fall in F concentration is due to consumption of atomic fluorine by hydrogen to form the product HF, and the creation of CF_2 radicals from CF_3 (chapter 1, section 4.3):

$$F + H_2 \rightarrow HF + H$$

$$CF_3 + H \rightarrow CF_2 + HF$$

At higher hydrogen concentrations hydrogen is also available to abstract fluorine from gas phase fluorocarbon species, forming further HF. The HF thus produced may either redissociate or react with atomic hydrogen[124]:

$$HF + e \rightarrow H + F + e$$

$$H + HF \rightarrow H_2 + F$$

in either case a higher F-atom concentration results.

The fall in CF_2 concentrations may be due to a combination of several factors:

(i) dilution effects;

(ii) "loading" effects: i.e. preferential removal of CF_2 (to be discussed);

(iii) reaction with hydrogen: $CF_2 + H \rightarrow CF + HF$;

(iv) recombination reactions: e.g., $CF_2 + CF_2 \rightarrow C_2F_4$

(v) changes in the electron energy distribution function.

Changes in electron density and energy distribution on the addition of hydrogen to fluorocarbon plasmas have been considered in detail by d'Agostino[113], because of their influence on both the primary gas phase dissociation processes and more particularly the polymer growth mechanism. The emission intensities of two actinometers, N_2 (380.5 nm; 11.5 eV) and Ar (750.4 nm; 13.7 eV), were measured and the emission intensity ratio found to be constant. Thus the emission intensities were considered proportional to the electron density over a broad energy range. The addition of hydrogen to CF_4 caused a linear decrease in the actinometer signals whereas there was no change in the case of C_2F_6 or C_3F_8.

In this work a decrease in the Ar (750.4 nm) actinometer emission was found with hydrogen additions to each of CF_4, C_2F_6 and C_3F_8, albeit a more significant decrease with CF_4 than C_2F_6 or C_3F_8 (figure 51). It is not at first sight clear why hydrogen should have affected the electron density of CF_4 plasmas and not C_2F_6 or C_3F_8 in d'Agostino's work, and, indeed, he does not address this question.

A full understanding of the relative importance of each of the five proposed CF_2 concentration reduction mechanisms could only be gained from the additional knowledge

of CF radical concentration (not measured optically with this experimental arrangement), and essential corroborative information from both mass spectroscopy and direct measurement of the electron energy distribution function.

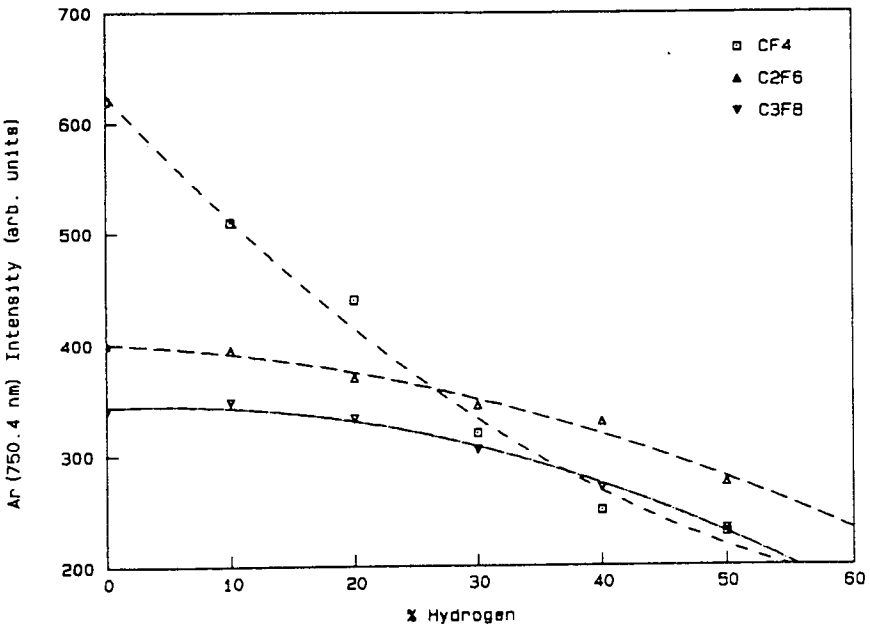

Figure 51. *Ar(750.4 nm) actinometer emission intensity vs. % H_2 in fluorocarbon plasmas.*

6.3 Polymer Deposition Rates

The observed polymer deposition rates may be put into perspective by considering the approximate percentage feed gas converted. With a CHF_3 plasma the polymer deposition rate was ~37 $nm.min^{-1}$ on the driven electrode, and ~12 $nm.min^{-1}$ on the ground electrode with operating conditions of 20 sccm flow, 200 mtorr pressure and 50W RF power. Assuming, as an upper limit, a similar deposition rate on the chamber walls to the ground electrode, and neglecting all other surfaces, this gives a total polymer deposition rate of 2.2×10^{-3} $cm^3.min^{-1}$ (see chapter 2.1 for chamber dimensions), corresponding to 4×10^{-3} $g.min^{-1}$ if the density of this material is similar to that of commercial PTFE. A feed gas flow of 20 sccm corresponds to a supply of 6×10^{-3} $g.min^{-1}$. Thus a mass balance indicates that 5-10% of the feed gas is deposited as polymer within the chamber. This figure could correspond to the majority of the feed dissociated. However, it should be noted that an experiment conducted at double the flow rate (40 sccm) gave a lower polymer deposition rate, indicating that the deposition rate was not limited by reactant supply.

d'Agostino has described an "activated growth model", based on work by Polak et al., to account for his observed fluoropolymer deposition rates[125]. In this model charged particles activate the surface sites for the growing polymer film. It is represented by:

$$R_g + (Pol)_n^* \xrightarrow{kp} (Pol)_{n+1}^* \qquad \text{(i)}$$

$$(e, I^-, I^+) + (Pol)_n \xrightarrow{ka} (Pol)_n^* \qquad \text{(ii)}$$

$$M + (Pol)_n^* \xrightarrow{kd} (Pol)_n + M \qquad \text{(iii)}$$

where R_g is a gas phase polymer precursor, $(Pol)_n^*$ is an activated surface site on the polymer, and e, I^- and I^+ are charged species in the plasma; equation (iii) represents the quenching step, i.e. the deactivation of the polymer surface.

Thus, from reaction (i) the polymer growth rate, r_p is

$$r_p = k_p[R_g]\theta_{act} \qquad (6.1)$$

where θ is the proportion of activated surface sites.

In the steady state, the rate of polymer activation (equation (ii) equals the rate of polymer deactivation (equation (iii)):

$$k_a f(n_e)(1 - \theta_{act}) = k_d[M]\theta_{act} \qquad (6.2)$$

where $f(n_e)$ is a function of the electron density, ion energy and flux. It was shown in the previous section that the actinometer emission signals were proportional to the electron (charged species) density.

$$\text{Thus, } r_p = \frac{k_p k_a}{k_d} \frac{[R_g] f(n_e)}{[M]} \qquad (6.3)$$

This equation, using either CF or CF_2 radical concentrations to represent R_g, satisfied the trends in deposition rate measured by d'Agostino.

More recently, Butler et al.[126] studied CF_4 plasma polymerisation rates as a function of both hydrogen additions and chamber pressure. They found that d'Agostino's representation of ion bombardment, $f(n_e)$, did not adequately account for their results. In a simple modification of the model they considered an ion flux derived from the Bohm criteria:

$$\text{Ion Flux} = 0.6\, n_e(kT_e/m_i)^{0.5} \qquad (6.4)$$

where n_e is the electron density, T_e the electron temperature and m_i the mass of the ion. At constant electron density the ion flux is proportional to electron temperature. The electron temperature may be estimated from changes in the emission intensity ratio of two actinometers, e.g. Ar (750.4 nm; emission threshold 13.7 eV) and N_2 (380.5 nm;

emission threshold 11.5 eV) (note that working at constant pressure d'Agostino found this ratio to be a constant).

However, neither version of the activated growth model can account for the results obtained in this work. For example, consider the results from studies of the C_3F_8/H_2 system: the polymer deposition rate rose with increasing H_2 concentration, whereas the CF_2 concentration remained constant, and the Ar actinometer signal declined. Thus the product of CF_2 concentration and Ar emission decreased with increasing H_2 concentration. Also, although not measured, there is no reason to believe that, operating at constant pressure and power, the plasma electron temperature could have risen whilst the Ar emission signal decined.

A **chemically activated growth model** is proposed to explain the fluorocarbon/hydrogen polymer deposition rates described in this work. Curiously, although d'Agostino et al. consider the influence of hydrogen on both fluorocarbon plasma chemistry and the structure of the resultant polymer, the potential role in the polymer growth mechanism is apparently ignored. Similarly, Butler et al. only consider the role of H_2^+ ions on polymer activation.

A portion of a fully saturated fluorocarbon surface is represented in two dimensions below. In both reaction schemes atomic hydrogen abstracts fluorine from the polymer surface with the formation of HF and "activated" surface sites. In reaction scheme (i) these sites are neighbouring allowing the possibility of C=C double bond formation. In reaction scheme (ii) polymer growth occurs by the incorporation of CF_2 radicals. Active sites of type (ii) may also convert to type (i) by F atom transfer. It follows that the degree of unsaturation increases with increasing H-atom concentration,

and that the polymer growth rate is dependent on both CF_x (represented by CF_2) radical and H-atom concentrations.

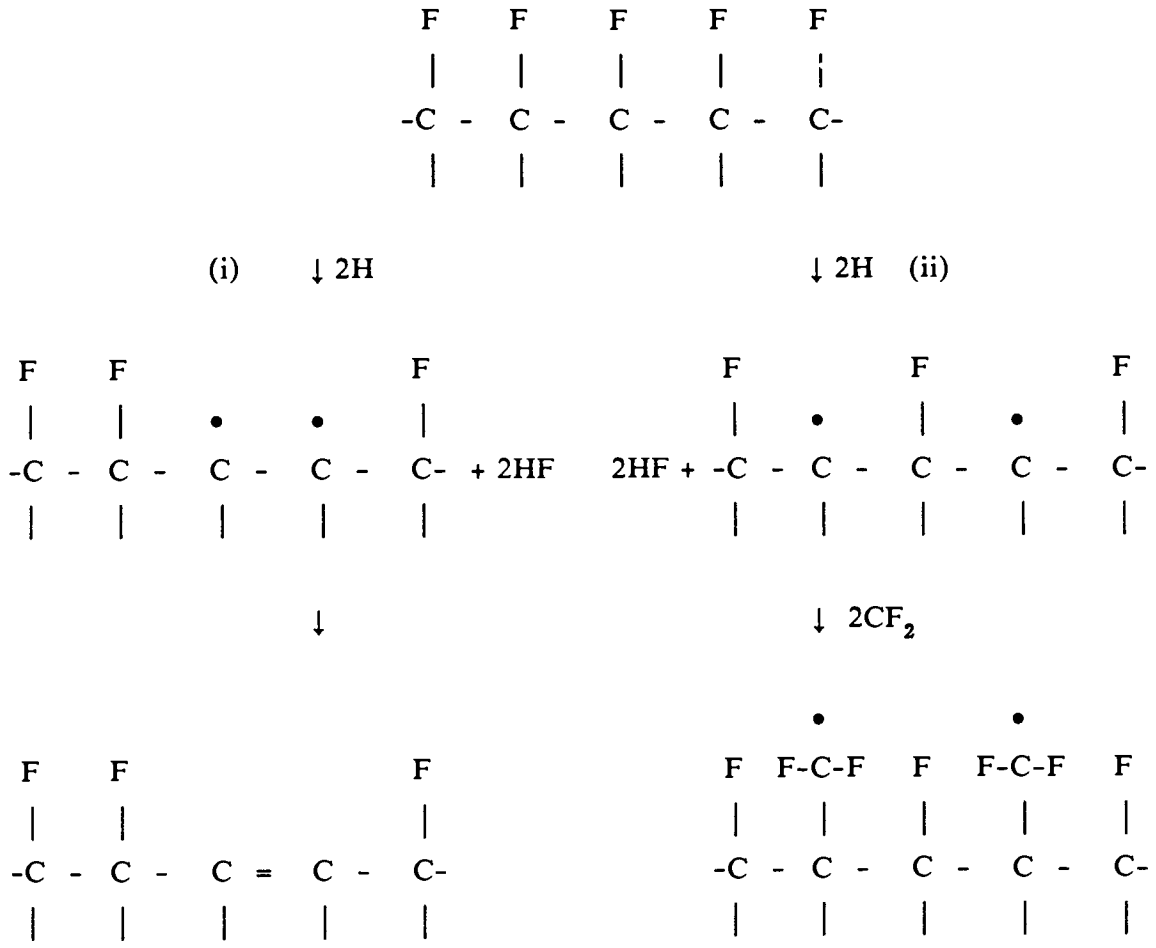

Further evidence that ion bombardment need not play a major role in plasma polymer growth is provided by Munro and Till[127]. They used X-ray photoelectron spectroscopy to characterise polymer films prepared by plasma polymerisation and uv irradiation of perfluorobenzene and a perfluorobenezene/benzene mixture. The films deposited by both methods were essentially the same, indicating that for this example

reaction mechanisms involving ions need not be considered for the plasma polymerisation process.

In order to test the proposition that the deposition rate is proportional to the product of the CF_2 radical and H atom concentrations, all the available data from this work for CF_4, C_2F_6 and C_3F_8 deposition rates as a function of percentage hydrogen, and CHF_3 deposition rates was fitted to a model of the form:

$$\text{Deposition Rate} = a[CF_2][H] \qquad (6.5)$$

(where a is a constant) using linear regression.

The results of the model are shown in figure 52 in the form of observed (actual) deposition rate vs. predicted (modelled) deposition rate. The general success of the model is apparent, but it can be seen that the C_3F_8/H_2 deposition rates are consistently underestimated by the model. It is therefore further proposed that CF_x radicals, i.e. C_1 species, are the predominant polymer precursors in CHF_3, CF_4/H_2 and C_2F_6/H_2 plasmas, but that both C_1- and C_2-species are significant in C_3F_8/H_2 plasma polymerisation processes. Although C_2 species might equally be expected to arise directly from C_2F_6, this proposition is consistent with C-C bond breaking being the primary plasma dissociation reaction for both C_2F_6 and C_3F_8 - due to the higher relative strengths of C-F to C-C bonds, as discussed.

Pure C_3F_8 also polymerises in a plasma. The model should therefore include a term for polymer growth at activated sites produced by methods other than hydrogen abstraction of fluorine, e.g. ion bombardment or uv irradiation. Finally, simultaneous fluoropolymer etching by fluorine or hydrogen, most likely ion assisted[128], should be allowed for. The revised model takes the form:

$$\text{Deposition Rate} = a[CF_2] + b[C_2F_x] + c[CF_2][H] + d[C_2F_x][H] - e[F]RF - f[H]RF \quad (6.6)$$

where a - f are constants,

$[C_2F_x]=[CF_2]$ for C_3F_8 (assumed)

$[C_2F_x]=0$ for CF_4, C_2F_6 and CHF_3 plasmas.

RF=applied RF power

All the available data was analysed using least squares regression analysis, and the model limited to significant terms (see chapter 3, section 2.1). The mathematically significant model is:

$$\text{Deposition Rate} = b[C_2F_x] + c[CF_2][H] + d[C_2F_x][H] + e[F]RF \quad (6.7)$$

and the values found for the constants are b=5.0, c=10.0, d=5.5 and e=-1.2.

The improvement in the model is immediately apparent from figure 53. Note that it accounts for a fifteen-fold variation in deposition rate from a wide range of gas chemistries, as well as, in the case of CHF_3, a twenty-fold variation in RF power. It must, however, be remembered that the model is based on very limited data, e.g. there are only four points each for C_3F_8/H_2 and CHF_3, and that no statistical design was employed. Although they are all of the expected sign, the absolute values of the constants should therefore be interpreted with some caution.

It is significant, however, that the $[C_2F_x]$ term, but not the $[CF_2]$ term, is retained in the model. The former accounts for C_3F_8 polymer growth from the pure monomer (C_3F_8, where $[C_2F_x]=[CF_2]$, was the only hydrogen-free deposition system). The absence of the latter implies that in the presence of hydrogen the proposed chemically activated growth mechanism is dominant.

It is recognised that the model may not account for changes in deposition rate with pressure - the studies were all carried out at a fixed chamber pressure, perhaps masking the effects of other polymer deposition mechanisms.

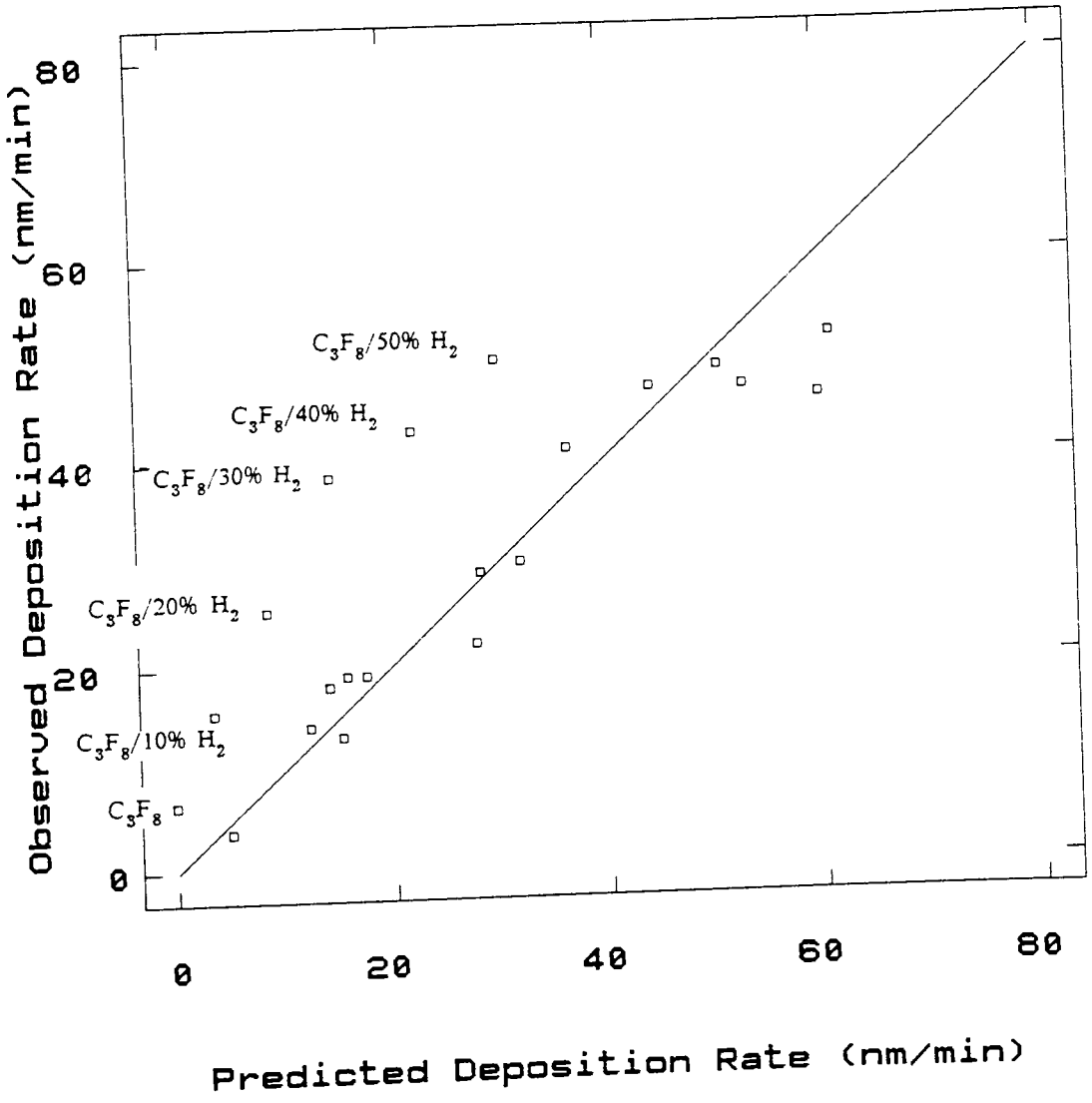

Figure 52. *Observed fluorocarbon plasma polymer deposition rate vs. deposition rate predicted by chemically activated growth model.*

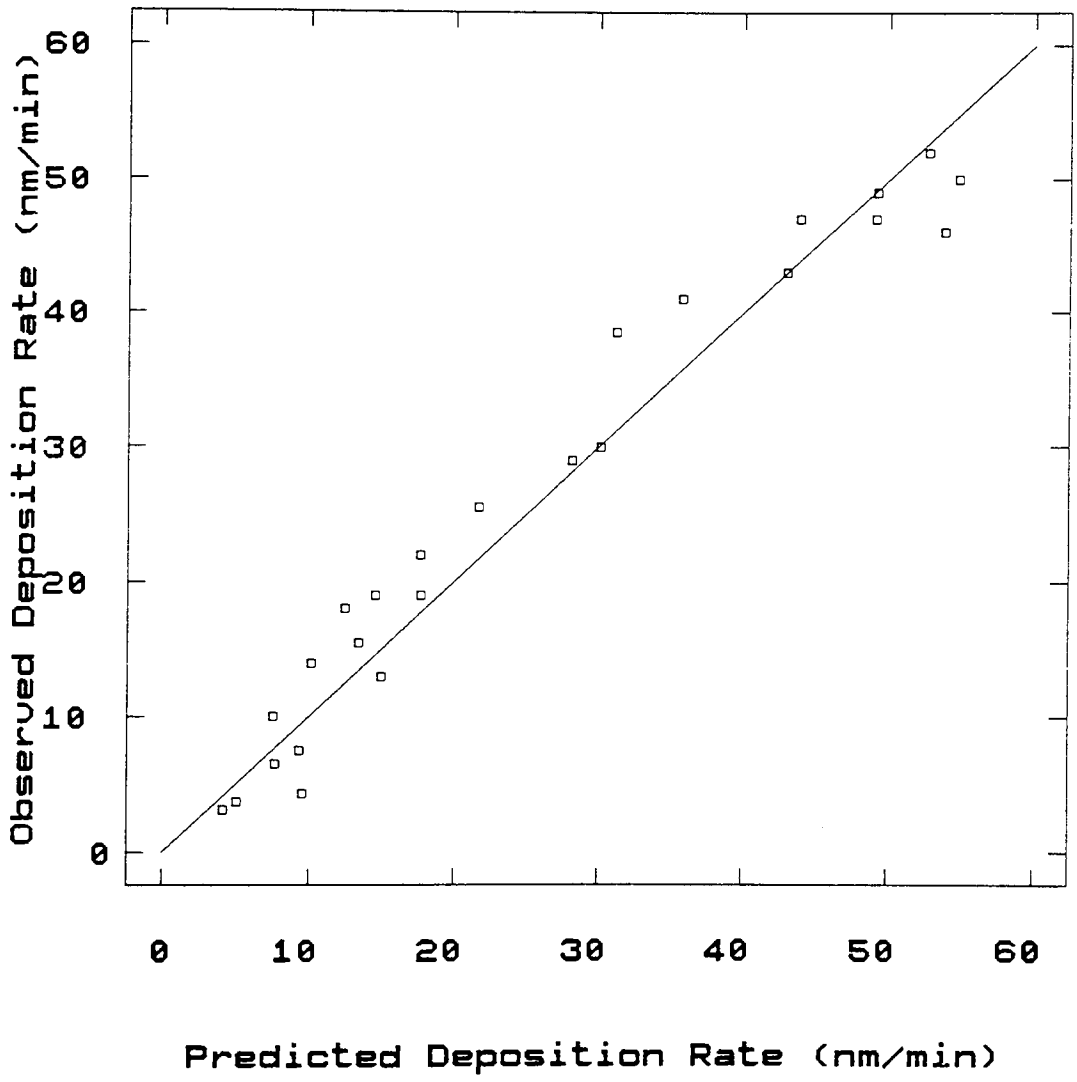

Figure 53. *Observed fluorocarbon plasma polymer deposition rate vs. deposition rate predicted by extended chemically activated growth model.*

6.4 Polymer Structure

The proposed chemically activated growth model predicts that the structure of the fluorocarbon polymers will be as affected by the presence of hydrogen in the feedstock as the deposition rate. Further, no hydrogen incorporation into the polymer structure is allowed for.

The results of the semi-quantitative analysis of reflection infrared spectra of many of the polymers are in full agreement with this hypothesis. Hydrogen was clearly shown to increase the degree of unsaturation, and, for the range of polymers studied, the degree of unsaturation was proportional to the percentage hydrogen in the feedstock. There was no evidence of bands due to C-H stretch, indicating that hydrogen was not incorporated into the polymer structure. This is in agreement with Arikado and Horiuchi[129] who studied polymer formation from CF_4/H_2 mixtures during the reactive ion etching of Si and SiO_2.

Quantitative information on the polymer structures came from analysis of XPS C(1s) spectra where C, C-CF, CF, CF_2 and CF_3 components were identified. It was seen that for a given fluorocarbon monomer, the CF_3 and CF_2 components decreased with increasing hydrogen additions whilst all other components (i.e. C-F, C-CF and C) increased. The percentage sum of CF_3 and CF_2 (representing percentage saturation) for the various polymers studied is shown in figure 54 plotted against the relative H-atom concentration in the source plasma. This clearly shows the strong dependence of polymer structure on H-atom concentration. Indeed, within experimental error, the structure appears almost independent of fluorocarbon gas used.

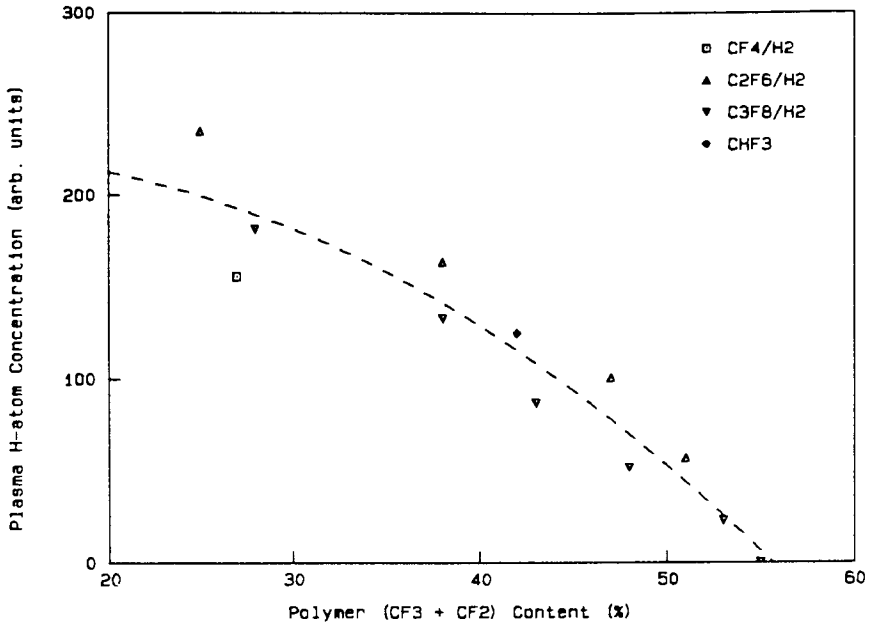

Figure 54. Plasma H-atom concentration vs. resultant percentage (CF_2 + CF_3) content of plasma fluoropolymers.

It is interesting to note that the maximum percentage saturation is only 55% (pure C_3F_8). All the polymers analysed by XPS were produced at 50 W RF power, and it would be reasonable to expect the polymer structure to be dependent on power level. However, for the range of conditions used in this work, the infrared results gave no such indication - for a given chemistry the C=C:C-F area ratio was a function of film thickness only, whether the film thickness was controlled by RF power (5-100 W) or deposition time. This again suggests that charged particle bombardment does not play a dominant role in controlling the deposition processes.

Astell-Burt et al.[37], with more limited XPS data (C_3F_8, C_3F_8/50% H_2 and CHF_3 plasma polymers only), also demonstrated increased polymer cross-linking when hydrogen was present in the discharge. They suggest that H atoms react with active sites on the polymer surface giving rise to C-H bonds, which may then interact with adjacent C-F bonds to eliminate HF and lead to cross-linking. (This is a similar mechanism to that proposed by Clark and Hutton[130] to account for the surface compositional changes causing defluorination of commercial PTFE in a hydrogen plasma.) However, the significant difference between their proposed cross-linking mechanism and this work is the requirement here for H atoms to generate, not consume, active sites.

Finally, extrapolation of the XPS and deposition rate data presented in chapter 4, indicates that at very high (~99%) hydrogen concentrations the production of purely carbonaceous material should be possible. It is interesting to note that similar chemistries are under investigation for diamond deposition[131].

6.5 Polymer Properties

6.5.1 Thermal

Kay et al.[132] have noted that conventional polymer characterisation methods such as differential scanning calorimetry (DSC) and thermogravimetric analysis (TGA) have been found to yield largely featureless spectra when applied to plasma polymers. However, the typical TGA trace shown in figure 42, and TGA and DSC results presented in tables 29 and 30 respectively, demonstrate that, in air, polymer characterisation is possible. Comparison of the TGA and DSC results showed that the polymer decomposition was an exothermic process, i.e., as expected, pyrolytic decomposition occurred. Although simultaneous analysis of the TGA or DSC exhaust gases, for example by mass specroscopy or gas chromatography, was not available, it is likely that the decomposition products were similar to those of conventional PTFE, i.e. CO, COF_2, HF, hexafluoroacetone[55].

The high thermal stability of commercial PTFE (table 29), relative to the plasma fluoropolymers, is noted. At first sight it is not clear why the C_3F_8 polymer, whose stoichiometry was closest to that of PTFE, was the least stable of the plasma polymers examined. Astell-Burt et al.[37] also deposited polymers from C_3F_8, C_3F_8/50% H_2 and CHF_3 discharges. In their parallel-plate system the electrodes were uncooled. The driven electrode reached ~200 °C whereas the temperature of the earthed electrode remained closer to room temperature. XPS analysis of the polymer from C_3F_8 showed that the polymer deposited on the earthed electrode was "PTFE-like", but the polymer on the driven electrode was carbonaceous in nature. In contrast, the C_3F_8/50 H_2% and CHF_3 polymers had similar structures when deposited on either electrode. This enhanced

thermal stability was attributed to the greater degree of cross-linking in the presence of hydrogen.

The more extensive results presented in this thesis (chapter 4: section 6, XPS; section 7, thermal analysis) fully corroborate these findings. It is not readily possible to define a relative molecular mass for a complex three-dimensional structure such as a plasma polymer. However, examination of the XPS C(1s) data in table 28 shows that the addition of hydrogen to a fluorocarbon polymer reduces the percentage of CF_3 (chain termination) groups in the resultant polymer. (This percentage is, of course, essentially zero in conventional PTFE.) This is always accompanied by a reduction in the CF_2 component. Thus, the addition of hydrogen to a fluorocarbon plasma may be regarded as causing an increase in an **effective** relative molecular mass of the resultant polymer, as evidenced by a reduction in chain termination groups (CF_3) and increased cross-linking (C, C-CF, CF). In the present work, conditions have not been identified under which polymers may be produced with a low CF_3 concentration and high CF_2 concentration, i.e. an optimised PTFE structure. As already discussed in the previous section, increasing hydrogen additions to the plasma will ultimately lead to a purely carbonaceous material, due to abstraction of fluorine from the polymer surface by hydrogen. Potential evidence of the onset of this comes from the appearance of a second peak (at ~475 °C) in the TGA and DSC traces of the C_2F_6/50% H_2 and C_3F_8/50% H_2 polymers. It should be noted, however, that combustion of lampblack occurs at ~600 °C; combustion at ~475 °C is more typical of a partially hydrogenated material[133].

6.5.2 Electrical

The electrical characteristics of plasma polymerised C_3F_8 and CHF_3 over the frequency range 1-100 kHz are summarised in tables 31 and 32 respectively. It should be remembered that the values of resistance and capacitance obtained are for an **equivalent parallel circuit**. The true values of resistance and capacitance will only equal the calculated values if this model holds.

The polymer resistivities at or below 100 Hz were too high for measurement with the experimental arrangement used, i.e. $>10^{10}$ Ωm. Laurent et al.[134] measured the d.c. resistivity of plasma polymerised C_2F_4 and found it to be $\sim10^{14}$ Ωm (10^{16} Ωcm). Conduction was deduced from current-voltage studies to be by a Poole-Frenkel mechanism - the emission of trapped electrons (or holes) from localised centers or potential wells within the dielectric.

However, the resistivities of both polymers fell rapidly with increasing frequency in the range studied, whereas the capacitance remained near constant. Even so, the resistivities remained sufficiently high for the circuit impedance to be dominated by the reactance term. The higher C_3F_8 polymer resistivity relative to the CHF_3 polymer is attributed to the higher degree of saturation of the former, as evidenced by XPS. These results are in agreement with Hetzler and Kay[135] who studied the a.c. conductivity and capacitance of plasma polymerised C_2F_4. At room temperature, they found that the conductivity was linearly proportional to the log of the frequency over a similar frequency range, and that the capacitance remained essentially constant. The conductivity at a given frequency was about an order of magnitude lower than the equivalent values from tables 31 and 32, and was independent of film thickness for films in the range 0.5-2.0 μm. It was attributed to hopping conductivity.

The dielectric properties of insulators are strongly dependent on their polarisability. Polarisation may occur in three ways[136]:

(i) Electronic. All materials consist of ions surrounded by electron clouds. As electrons are very light they have a rapid response to field changes.

(ii) Molecular. Bonds between atoms are stretched by applied electric fields when the lattice ions are charged.

(iii) Orientational. This occurs when whole molecules, having a pemanent or induced dipole moment, move into line with the applied field.

Most materials are polarisable in a combination of these ways depending on the frequency of the applied field. The dielectric constant may therefore vary in a complex fashion with frequency.

In general, plasma polymers have dielectric constants comparable to their conventional counterparts. Their dissipation factors, the ratio of energy stored to energy lost, though, are often an order of magnitude higher. This is indeed the case for the plasma polymerised C_3F_8 and CHF_3. Their dielectric constants were, within experimental error, identical to that of PTFE (~2.2) but their dissipation factors were at least an order of magnitude higher than the conventional polymer[137]. This is due to the fact that plasma polymers contain a certain number of polar groups independent of whether the monomer used was polar or nonpolar.

CHAPTER 7 - CONCLUSIONS

(a) Silicon etching in SF_6 and CF_4

Statistically designed experiments were used to investigate the reactive ion etching of Si and SiO_2 in SF_6 and CF_4 discharges as a function of flow, pressure and RF power. The corresponding relative gas phase concentration of atomic fluorine (etchant) and other species was monitored by optical emission spectroscopy with argon actinometry. For a given set of process conditions, the F-atom concentrations in SF_6 were higher (×4) than those in CF_4, whereas the Si etch rates were considerably higher (×20). However, the d.c. self-biases, which would be expected to enhance etching, produced by SF_6 were lower than those in CF_4.

Enhanced etching in SF_6 by SF_x species, through dissociative chemisorption[94, 95], and/or inhibited etching in CF_4 due to involatile film formation by fluorocarbon species[98-100] (mainly CF_2) may account for the observed results. The Si etch rates in the two systems were best modelled by:

SF_6: Si etch rate = $45[F]^{0.78}$ (7.1)

CF_4: Si etch rate = $0.061[F]^{0.46}$ × d.c. self-bias (7.2)

Equation (7.1) is consistent with a purely chemical etch mechanism, and (7.2) an ion-assisted mechanism.

Si etch rates in SF_6/CF_4 mixtures could only be accounted for if the SF_6 model was applied to both the pure SF_6 and the SF_6/CF_4 mixtures (10-90% CF_4), and the CF_4 model to pure CF_4 only.

(b) Silicon etching in fluorocarbon/additive mixtures

Si etch rates were measured in CF_4, C_2F_6 and CHF_3 as a function of the addition of each of O_2, N_2O and CO_2. The corresponding relative gas phase concentrations of F, O and CF_2 were measured also. The etch rates were accounted for by a model of the form:

$$\text{Silicon etch rate} = a + I_{Ar} \times (b[F] + c[O] + d[CF_2]) \qquad (7.3)$$

where I_{Ar} is the Ar (750.4 nm) intensity, used to represent ion flux to the substrate; a-d are constants - a=38, b=0.0043, c=-0.026, and d=-0.00054. Note that for pure CF_4 only a ~4% reduction in etch rate due to CF_2 is predicted by the model.

(c) Etching of silicon dioxide

In fluorocarbon discharges, many species, e.g. F[41, 42], CF_2[43, 44], CF_3^+[45], HF[37, 46], have variously been considered active oxide etchants. In this work studies of SiO_2 etching in CF_4 and SF_6 as a function of flow, pressure and RF power showed that the etch rates were predominantly dependent on RF power level. In the case of CF_4, the variation in SiO_2 etch rate with power and pressure showed some correlation with the product of ion flux (estimated from argon actinometry results) and d.c. bias. In the case of SF_6 the oxide etch rates were almost directly proportional to RF power. A degree of correlation was found between etch rate and the product of F-atom concentration and d.c. bias. This result, taken with that for CF_4, is in agreement with the views of Steinbruchel and Curtis[49] that at low F-atom concentrations (CF_4) direct reactive ion etching dominates, whereas at high F-atom concentrations (SF_6) the etching is ion enhanced with F-atoms as the main neutral reactants.

SiO_2 etch rates were also measured in Ar, CF_4/SF_6 mixtures and SF_6/additive (Ar, O_2, CO_2, H_2, CH_4) mixtures at various power levels. A wide range of F-atom concentrations and d.c. self-biases were obtained. The results of these experiments indicated, for the range of process parameters studied, that:

(i) RF power (ion density) has a dominant influence on oxide etch rates;

(ii) for a given RF power level, d.c. bias (ion energy) has a secondary influence on oxide etch rates;

(iii) fluorine/fluorinated species are required for etching to proceed, but their attack on the oxide is not the rate determining step;

(iv) the presence of CF_x/carbonaceous species has no chemical influence on oxide etch rates.

(d) Influence of electrode materials

It was found that the silicon etch rate in a CF_4 plasma was considerably enhanced, relative to an anodised aluminium electrode, in the presence of soda glass or sodium or potassium "doped" quartz. The effect was even more pronounced in a CF_4/O_2 discharge. In the latter system lead and copper electrodes also enhanced the silicon etch rate. These results could not be accounted for by a corresponding rise in atomic fluorine concentration, or by changes in the electrical characteristics of the plasma. Thus the observed variations in silicon etch rate must be predominantly due to chemical effects. XPS confirmed that sodium had been transferred from the soda glass electrode onto the silicon surface. Similarly, nickel, copper and lead were detected on the surface of silicon samples after etching on the respective cover-plates. The same range of electrode materials had little effect on the relative etch rates of SiO_2. Three etch enhancement mechanisms have been identified:

(i) Inhibition or enhanced removal of fluorocarbon films, which inhibit etching, by the transferred metals. This mechanism is consistent with the results presented in conclusion (a). However, studies of net polymer deposition and bulk polymer etching were unable to confirm it.

(ii) Direct enhancement of silicon etching by the formation of favourable intermediates. Several authors[111-113, 115, 116] ascribe their observations of enhanced silicon etching in the presence of a variety of metals to this mechanism, but it appears inappropriate to the results presented in this thesis.

(iii) Modification of the electronic properties of the silicon ("band bending") which may enhance silicon etching. Some support for this is given by XPS results which show a reasonably close correlation between etch rate and binding energy of the Si2p levels in surface silicon.

(d) Fluorocarbon plasma polymerisation

Fluorocarbon polymer deposition was studied as a function of fluorocarbon source gas (CF_4, C_2F_6, C_3F_8 and CHF_3), process time, RF power and percentage hydrogen addition. Gas phase concentrations of F, H and CF_2 were measured by optical emission spectroscopy, and the resultant polymer structure determined by x-ray photoelectron spectroscopy and infrared spectroscopy. Thermal and electrical properties were measured also.

The polymer deposition rate from pure C_3F_8, as a function of RF power, was shown to be proportional to the gas phase CF_2:F ratio. When hydrogen was present in the plasma, i.e. discharges of CHF_3, or CF_4, C_2F_6 and C_3F_8 with hydrogen additions, this simple relationship did not hold. Indeed, with increasing hydrogen additions to C_3F_8 the

CF_2:F ratio fell whilst the deposition rate increased. An "activated growth model"[125], in which charged particles activate the surface sites for the growing film, did not adequately describe these results.

A chemically activated growth model is therefore proposed to explain the fluorocarbon/hydrogen polymer deposition rates described in this work. In this model atomic hydrogen abstracts fluorine from the polymer surface with the formation of HF and "activated" surface sites. Polymer growth occurs by the incorporation of CF_2 radicals at these sites. There is also the possibility of C=C double bond formation if two sites are adjacent. It follows that the degree of unsaturation increases with increasing H-atom concentration, as evidenced by XPS and infrared spectroscopy results, and that the polymer growth rate is dependent on both CF_x (represented by CF_2) radical and H-atom concentrations.

A model of the form:

$$\text{Deposition Rate} = a[CF_2][H] \qquad (7.4)$$

(where a is a constant) underestimated the C_3F_8/H_2 deposition rates. It is therefore proposed that both C_1- and C_2-species are significant in C_3F_8/H_2 plasma polymerisation, and that both species are present in equal proportions. A revised model, also allowing for ion-assisted etching, is:

$$\text{Deposition Rate} = a[CF_2] + b[C_2F_x] + c[CF_2][H] + d[C_2F_x][H] - e[F]RF - f[H]RF \quad (7.5)$$

where a - f are constants,

$[C_2F_x]$=$[CF_2]$ for C_3F_8 (assumed)

$[C_2F_x]$=0 for CF_4, C_2F_6 and CHF_3 plasmas.

RF=applied RF power

All the available data was analysed using least squares regression analysis, and the model limited to significant terms. The mathematically significant model is:

$$\text{Deposition Rate} = b[C_2F_x] + c[CF_2][H] + d[C_2F_x][H] + e[F]RF \quad (7.6)$$

and the values found for the constants are b=5.0, c=10.0, d=5.5 and e=-1.2.

The model accounts for a fifteen-fold variation in deposition rate from a wide range of gas chemistries, as well as, in the case of CHF_3, a twenty-fold variation in RF power. It must, however, be remembered that the model is based on very limited data. It is significant, though, that the $[C_2F_x]$ term, but not the $[CF_2]$ term, is retained in the model. The former accounts for C_3F_8 polymer growth from the pure monomer (C_3F_8, where $[C_2F_x]$=$[CF_2]$, was the only hydrogen-free deposition system). The absence of the latter implies that in the presence of hydrogen the proposed chemically activated growth mechanism is dominant.

All the polymers studied by thermal analysis were found to be unstable above ~200 °C in air. Thermogravimetric analysis showed that the temperature at which the maximum rate of polymer weight loss occured increased with increasing prior proportions of hydrogen in the plasma, e.g. C_3F_8, 294 °C; C_3F_8/50% H_2, 341 °C. With

high proportions (50%) of hydrogen in the plasma a second weight loss peak appeared at 100 °C higher temperature. Differential scanning calorimetry showed that the plasma polymer decomposition reactions were all exothermic.

Thin films of plasma polymerised C_3F_8 and CHF_3 had a dielectric constant similar to PTFE. The a.c. resistivity of the C_3F_8 polymer was ~70% higher than that of the CHF_3-derived polymer.

REFERENCES

1. S. Marshall (Ed.), "The transistor...the first 40 years...", Solid State Technology, 30 (12), 67-89 (December 1987).

2. J.D. Meindl, "Microelectronic circuit elements", Scientific American, 70-81 (September 1977).

3. Harwell Computing Centre "Facts", Harwell Laboratory, Oxfordshire (1987).

4. D. Gross, *A Silicon Primer*, L. Messel and Co., London (1986), p. 9.

5. L. Clifford, "Half-micron technology in pipeline", Electronics Weekly, No. 1492, 6 (24 January 1990).

6. M. Cross, "Battle to win the world's greatest memory contest", New Scientist, 35 (22 July 1989).

7. J. Speight in *The Chemistry of the Semiconductor Industry*, edited by S.J. Moss and A. Ledwith, Blackie, Glasgow (1987), p. 4.

8. D.B. Graves, "Plasma processing in microelectronics manufacturing", AIChE Journal, 35, 1-29 (1989).

9. C.G. Willson in *Introduction to Microlithography*, edited by L.F. Thompson, C.G. Willson and M.J. Bowden, ACS Symposium Series 219 (1983), pp. 87-160.

10. T.R. Pampalone, "Novolac resins used in positive resist systems", Solid State Technology, 27 (11), 115-20 (June 1984).

11. B. Chapman, *Glow Discharge Processes*, Wiley, New York (1980).

12. M.R. Wertheimer and M. Moisan, "Comparison of microwave and lower frequency plasmas for thin film deposition and etching", J. Vac. Sci. Technol. A, 3, 2643-9 (1985).

13. R.A. Morgan, *Plasma Etching in Semiconductor Fabrication*, Elsevier, Amsterdam (1985), pp. 111-42.

14. J.W. Coburn and H.F. Winters, "Plasma-assisted etching in microfabrication", Ann. Rev. Mater. Sci., **13**, 91-116 (1983).

15. J. Pelletier and M.J. Cooke, "Microwave plasma etching of Si and SiO_2 in halogen mixtures: Interpretation of etching mechanisms", J. Vac. Sci. Technol B, 7, 59-67 (1989).

16. E.B. Smith, *Basic Chemical Thermodynamics*, Oxford University Press, Oxford (1973), pp. 42-4.

17. *Handbook of Chemistry and Physics, 57th Edition*, edited by R.W. Feast, Chemical Rubber Company Press (1976).

18. M. Nakamura, T. Kurimoto, K. Iizuaka and H. Yano, "Temperature effect on reactive ion etching", CIPG 89, Le Vide, les Couches Minces, **246** (Supplement), 74-81 (1989).

19. D.J. Oostra, A. Haring and A.E. de Vries, "Sputtering of SiO_2 in a XeF_2 and Cl_2 atmosphere", J. Vac. Sci. Technol. B, **4**, 1278-82 (1986).

20. J.W. Coburn and H.F. Winters, "Plasma etching - a discussion of mechanisms", J. Vac. Sci. Technol., **16**, 391-403 (1979).

21. E. Kay, "Reactive ion etching and related polymerization processes", Society of Chemical Industry: Plasma Etching and Deposition, Symposium at Harwell Laboratory, 15th April 1986.

22. J.A. Yarmoff and F.R. McFeely, "Mechanism of ion-assisted etching of silicon by fluorine atoms", Surface Science, **184**, 389-400 (1987).

23. D.L. Flamm, V.M. Donnelly and J.A. Mucha, "The reaction of fluorine atoms with silicon", J. Appl. Phys., 52, 3633-9 (1981).

24. D.L. Flamm, D.E. Ibbotson, J.A. Mucha and V.M. Donnelly, "XeF_2 and F-atom reactions with Si: their significance for plasma etching", Solid State Technology, 117-21 (April 1983).

25. J. Pelletier, "A model for the halogen-based plasma etching of silicon", J. Phys. D: Appl. Phys., **20**, 858-69 (1987).

26. I.C. Plumb and K.R. Ryan, "Gas-phase reactions of CF_3 and CF_2 with atomic and molecular fluorine: their significance in plasma etching", Plasma Chem. Plasma Process., **6**, 11-25 (1986).

27. E. Kay, "Reactive ion etching and related polymerization processes", Society of Chemical Industry: Plasma Etching and Deposition, Symposium at Harwell Laboratory, 15th April 1986.

28. K.R. Ryan and I.C. Plumb, "Gas-phase reactions of CF_2 with O(3p) to produce COF: their significance for plasma etching", Plasma Chem. Plasma Process., **4**, 271-83 (1984).

29. C.J. Mogab, A.C. Adams and D.L. Flamm, "Plasma etching of Si and SiO_2 - the effect of oxygen additions to CF_4 plasmas", J. Appl. Phys., **49**, 3796-803 (1978).

30. J.P. Booth, G. Hancock, N.D. Perry, D.C.W. Blaikley, J.A. Cairns and R. Smailes, "Laser induced fluorescence and optical emission studies of fluorocarbon plasmas", Mat. Res. Symp. Proc., **98**, 135 (1987).

31. Y.H. Lee and M.-M. Chen, "Silicon etching mechanism and anisotropy in CF_4 + O_2 plasma", J. Appl. Phys., **54**, 5966-73 (1983).

32. H. Kawata, T. Shibano, K. Murata and K. Nagami, "A study of Si plasma etching in CF_4-O_2 gas with a planar-type reactor", J. Appl. Phys., **54**, 2720-6 (1983).

33. G.S. Oehrlein, S.W. Robey and J.L. Lindstrom, "Surface processes in CF_4/O_2 reactive etching of silicon", Appl. Phys. Lett., **52**, 1170-2 (1988).

34. F.H.M. Sanders, J.H.J. van Dommelen, J.A.M. Sanders, C.I.M. Beenakker and J. Dieleman, "The role of carbon dioxide in halocarbon etch plasmas", Proc. of the 1st Symp. on Plasma Processing, **81**, 155-66 (1981).

35. Y. Tzeng and T.H. Lin, "Plasma etching with tetrafluoromethane and nitrous oxide. The role of oxygen in the etching of silicon materials", J. Electrochem. Soc., **133**, 1443-8 (1986).

36. Y. Tzeng and T.H. Lin, "Dry etching of silicon materials in SF_6-based plasmas, J. Electrochem. Soc.", **134**, 2305-9 (1987).

37. P.J. Astell-Burt, J.A. Cairns, A.K. Cheetham and R.M. Hazel, "A study of the deposition of polymeric material onto surfaces from fluorocarbon RF plasmas", Plasma Chem. Plasma Process., 6, 417 (1986).

38. L.M. Ephrath, "Selective etching of silicon dioxide using reactive ion etching with CF_4-H_2", J. Electrochem. Soc., **126**, 1419-21 (1979).

39. G.S. Oehrlein and Y.H. Lee, "Reactive ion etching related Si surface residues and subsurface damage: their relationship to fundamental etching mechanisms", J. Vac. Sci. Technol. A, **5**, 1585-94 (1987).

40. R.A.H. Heinecke, "Control of relative etch rates of SiO_2 and Si in plasma etching", Solid State Electron., **18**, 1146-7 (1975).

41. C.J. Mogab, A.C. Adams and D.L. Flamm, "Plasma etching of Si and SiO_2 - the effect of oxygen additions to CF_4 plasmas", J. Appl. Phys., **49**, 3796-803 (1978).

42. R. d'Agostino, V. Colaprico and F. Cramarossa, "The use of "actinometer" gases in optical diagnostics of plasma etching mixtures: SF_6-O_2", Plasma Chem. Plasma Process., **1**, 365-75 (1981).

43. A.J. van Roosmalen, "Review: dry etching of silicon oxide", Vacuum, **34**, 429-36 (1984).

44. E.M. van Veldhyizen, Th. Bisschops, E.J.W. van Vliemberger and J.H.M.C. van Wolput, "Absolute reaction densities of reaction products from plasma etching of quartz", J. Vac. Sci. Technol. A, 3, 2205-8 (1985).

45. H. Norstrom, R. Buchta, F. Runovc and P. Wiklund, "RIE of SiO_2 in doped and undoped fluorocarbon plasmas", Vacuum, 32, 737-45 (1982).

46. Ch. Steinbruchel, H.W. Lehman and K. Frick, "Mechanism of dry etching of silicon dioxide", J. Electrochem. Soc., 132, 180-6 (1985).

47. R.G. Frieser and J. Nogay, "Optical spectroscopy applied to the study of plasma etching", Appl. Spec., 34, 31-3 (1980).

48. G. Smolinsky, T.M. Mayer and E.A. Truesdale, "The reactive ion etching of silicon oxides with ammonia and trifluoromethane. Plasma etching of silicon and silicon dioxide with hydrogen fluoride mixtures", J. Electrochem. Soc., 129, 1770-2 (1982).

49. Ch. Steinbruchel and B.J. Curtis, "The role of F atoms in the reactive sputter etching of silicon dioxide: Langmuir probe and optical actinometry measurements", Mat. Res. Symp. Proc., 76, 179-83 (1987).

50. H. Grunwald, H. Suhr and H.S. Munro, "Plasma deposition of polymers with chemically reactive groups", Plasma Technology Conference, Brighton, Proceedings Pg.109 (1987).

51. H.V. Boenig, *Plasma Science and Technology*, Cornell University Press, Ithaca (1982).

52. R.F. Brady, "Fluoropolymers", Chemistry in Britain, 427-30 (May 1990).

53. M.E.B. Jones in *Basic Organic Chemistry, Part 5 Industrial Products*, edited by J.M. Tedder, A. Nechtvatal and A.H. Jubb, Wiley, London (1975), pp. 224-5.

54. P. Burgraff (Senior Editor), Industry News, Semiconductor International, 12(9), 26 (August 1989).

55. Teflon AF, Du Pont, Speciality Polymers Division, USA, Information pack (January 1990).

56. L. Holland, "Plasma deposition of optical thin films for infrared use", SPIE, **197**, 319-23 (1979).

57. H. Biederman, "Deposition of polymer films in low pressure reactive plasmas", Thin Solid Films, **86**, 125-35 (1981).

58. *Plasma News Report*, edited by T.M. Mayer, Research Institute of Plasma Chemistry and Technology, Carlsbad, USA (1990).

59. P. Burggraaf, "Solutions for 'pump damaging' etch and CVD processes", Semiconductor International, 66-71 (October 1986).

60. P. Duval, "Problems in pumping aggressive, poisonous and explosive gases", Vacuum, **38**, 651-8 (1988).

61. B. Emslie and P. May, "Oil free vacuum pumping system for semiconductor processes", CIPG 87, Antibes, France, Conference proceedings pp. 93-7 (1987).

62. R.W. Dreyfuss, J.M. Jasinski, R.E. Walkup and G.S. Selwyn, "Optical diagnostics of low pressure plasmas", Pure and Appl. Chem., **57**, 1265-76 (1985).

63. R.A. Gottscho and T.A. Miller, "Optical techniques in plasma diagnostics", Pure and Appl. Chem., **56**, 189-208 (1984).

64. P.M. Banks, "Plasma temperatures during reactive ion etching", Microelectronic Engineering, **11**, 603-6 (1990).

65. R.A. Gottscho and V.M. Donnelly, "Optical emission actinometry and spectral line shapes in rf glow discharges", J. Appl. Phys., **56**, 245-50 (1984).

66. W.R. Harshbarger, R.A. Porter, T.A. Miller and P. Norton, "A study of the optical emission from an RF plasma during semiconductor etching", Appl. Spect., **31**, 201-7 (1977).

67. J.W. Coburn and M. Chen, "Optical emission spectroscopy of reactive plasmas: a method for correlating emission intensities to reactive particle density", J. Appl. Phys., **51**, 3134-6 (1980).

68. R. d'Agostino, F. Cramarossa, S. De Benedictis and G. Ferraro, "Spectroscopic diagnostics of CF_4-O_2 plasmas during Si and SiO_2 etching processes", J. Appl. Phys., **52**, 1259-65 (1981).

69. R. d'Agostino, F. Cramarossa and S. De Benedictis, "Diagnostics and decomposition mechanism in radio-frequency discharges of fluorocarbons utilised for plasma etching or polymerisation", Plasma Chem. Plasma Process., **2**, 213-31 (1982).

70. R. Walkup, K. Saenger and G.S. Selwyn, "Studies of O atom concentration by two-photon laser induced fluorescence and optical emission spectroscopy", Mat. Res. Symp. Proc., **38**, 69-76 (1985).

71. J.W. Coburn and M. Chen, "Dependence of F atom density on pressure and flow rate in CF_4 glow discharges as determined by emission spectroscopy", J. Vac. Sci. Technol., **18**, 353-6 (1981).

72. S. Walker in *Spectroscopy, Volume Three*, edited by B.P. Straughan and S. Walker, Chapman and Hall, London (1976), pp. 26-49.

73. Application note number 5.0, "Plasma diagnostics", Monolight Instruments Ltd. (1990).

74. A.N. Zaidel', V.K. Prokof'ev, and S.M. Raiskii, *Tables of Spectrum Lines*, Pergamon Press, London (1961).

75. R.W.B. Pearse and A.G. Gaydon, *The Identification of Molecular Spectra*, Chapman and Hall, London (1976).

76. D. Field, D.F. Klemperer and I.T. Wade, "Spectroscopic studies of fluorescent emission in plasma etching of silicon nitride", J. Vac. Sci. Technol. B, **26**, 551-8 (1988).

77. W. Kemp, *Organic Spectroscopy*, Macmillan, London (1978) pp. 8-36.

78. *An Infrared Spectroscopy Atlas for the Coatings Industry*, edited by J.T. Vandeberg (chairman), Federation of Societies for Coatings Technology, Philadelphia (1980), pp. 49-58.

79. Materials Characterisation Service, Harwell Laboratory.

80. E. Kay and A. Dilks, "Metal-containing fluoropolymer films produced by simultaneous plasma etching and polymerisation: the series C_nF_{2n+2} (n=1,2,3,4)", Thin Solid Films, **78**, 309-18 (1981).

81. J.H. Thomas, X. Chun Mu and S.J. Fonash, "An X-ray photoelecron spectroscopy study of CF_4/H_2 reactive ion etching residue on silicon", J. Electrochem Soc., **134**, 3122-5 (1987).

82. A. Hooper, *The Application of a.c. Measurement and Analysis Techniques to Materials Research*, U.K.A.E.A. report no. AERE-R 9757 (1980).

83. Y.H. Lee and M.R. Polcari in *Properties of Silicon*, EMIS Datareviews Series No. 4, INSPEC (1988), pp. 855-84.

84. M.W. Jenkins, M.T. Mocella, K.D. Allen and H.H. Sawin, "The modelling of plasma etching processes using response surface methodology", Solid State Technology, **29** (4), 175-82 (April 1986).

85. P.E. Riley, V.D. Kulkarni and S.H. Bishop, "Examination of fluorocarbon-based plasmas used in the selective and uniform etching of silicon dioxide by response-surface methodology: Effects of helium addition", J. Vac. Sci. Technol. B, 7, 24-34 (1989).

86. D.W. Daniel, R. Bloom and J.E. Reece, "Identifying an etch process window using response surface methodology", Solid State Technology, **31** (9), 117-20 (September 1988).

87. D.A.O. Hope, D. Lowe, A.J. Hydes, V.G.I. Deshmukh, T.I. Cox and A.D. Wilson, "Parametric modelling of oxygen reactive ion etching of polymers", CIPG 89, Le Vide, les Couches Minces, **246** (Supplement), 93-5 (1989).

88. G.E.P. Box, W.G. Hunter and J.S. Hunter, *Statistics for Experimenters*, Wiley, New York (1978).

89. Statgraphics (Version 3.0), Statistical Graphics Corporation (1988).

90. H.U. Poll, D. Hinze and H. Schlemm, "In situ analysis of fluorinated gases in plasma etching by infrared spectroscopy", Applied Spectroscopy, **36**, 445-51 (1982).

91. K. Ninomiya, K. Suzuki, S. Nishimatsu and O. Okada, "Role of sulfur atoms in microwave plasma etching of Silicon", J. Appl. Phys., **62**, 1459-68 (1987).

92. P. Brault, P. Ranson, H. Estrade-Szwarckopf and B. Rousseau, "Analysis of SF_6 and F_2 plasma etched silicon surfaces: An X-ray photoelectron spectroscopy investigation", Appl. Phys. Lett., 57, 2649-50 (1990).

93. K.R. Ryan and I.C. Plumb, "A model for the etching of silicon in SF_6/O_2 plasmas", Plasma Chem. Plasma Process., **10**, 207-29 (1990).

94. Y.-J. Lii, J. Jorné, K.C. Cadien and J.E. Schoenholtz, "Plasma etching of silicon in SF_6: Experimental and reactor modelling studies", J. Electrochem. Soc. ,**137**, 3633-9 (1990).

95. H.M. Anderson, J.A. Merson and R.W. Light, "A kinetic model for plasma etching silicon in a SF_6/O_2 discharge", IEEE Trans. Plasma. Sci., **PS-14**, 156-64 (1986).

96. C.C. Tang and D.W. Hess, "Tungsten etching in CF_4 and SF_6 discharges", J. Electrochem. Soc., **131**, 115-20 (1984).

97. E. Gogolides, J.-P. Nicolai and H.H. Sawin, "Comparison of experimental measurements and model predictions for radio-frequency Ar and SF_6 discharges", J. Vac. Sci. Technol. A, 7, 1001-6 (1989).

98. D.J. Thomson and C.R. Helms, "A surface spectroscopic study of reactive ion bombardment of silicon", Surf. Sci., **236**, 41-7 (1990).

99. C. Lejeune, E. Collard, J.P. Grandchamp, P. Scheiblin and J.P. Gilles, "C-F incorporated overlayer growth on silicon exposed to a d.c.-excited CF_4 plasma", Thin Solid Films, **193/194**, 1008-16 (1990).

100. G.S. Oehrlein and H.L. Williams, "Silicon etching mechanisms in a CF_4/H_2 glow discharge", J. Appl. Phys., **62**, 662-72 (1987).

101. I.C. Plumb and K.R. Ryan, "A model for the etching of Si in CF_4 plasmas: Comparison with experimental measurements", Plasma Chem. Plasma Process., **6**, 231-46.

102. M.A. Carter and G.F. Goldspink, "Reactive and chemically assisted ion beam etching of Si and SiO_2", Vaccum, **38**, 5-10 (1988).

103. R. d'Agostino, F. Cramarossa and S. De Benedictis, "Chemical mechanisms in C_3F_8-H_2 radio frequency discharges", Plasma Chem. Plasma Process., **4**, 21-32 (1984).

104. T.I. Cox, V.G.I. Deshmukh, D.A.O. Hope, A.J. Hydes, N.StJ. Braithwaite and N.M.P. Benjamin, "The use of Langmuir probes and optical emission spectroscopy to measure electron energy distribution functions in RF-generated argon plasmas", J. Phys. D: Appl. Phys, **20**, 820-31 (1987).

105. N. Nakamura, T. Kurimoto, K. Iizuka and H. Yano, "Temperature effect on reactive ion etching", CIPG 89, Le Vides, les Couches Minces, No. 246 (Supplement), 74-81 (1989).

106. P. Burggraaf (Ed.), "Carbon Stimulates SiO_2 etching", Semiconductor International, 41 (February 1989).

107. D.C.W. Blaikley, J.A. Cairns, C.M. Kemp and S.J. Moss, "The enhancement of silicon etch rates", CIPG 89, Le Vides, les Couches Minces, No. 246 (Supplement), 48 (1989).

108. D.W. McKee, *Chemistry and Physics of Carbon*, Vol. 16, edited by P.L. Walker and P.A. Thrower (Dekker Inc., New York, 1980), p. 2.

109. M. Copel, R.M. Tromp, S.W. Robey and G.S. Oehrlein, "Medium energy ion scattering analysis of reactive ion etched Si(001) surfaces", Appl. Phys. Lett., **53**, 2317-19 (1988).

110. T. Makino, H. Nakamura and M. Asano, "Acceleration of plasma etch rate caused by alkaline residues", J. Electrochem. Soc., **128**, 103-6 (1981).

111. L.K. White and J.-S. Maa, "Etch rate enhancement of silicon in CF_4-O_2 plasmas", Appl. Phys. Lett., **46**, 1050 (1985).

112. T.H. Fedynyshyn, G.W. Grynkewich and R.H. Dumas, "Mask dependent etch rates III: The effect of a silver mask on the plasma etch rate of silicon", J. Electrochem. Soc., **135**, 268-9 (1988).

113. T.H. Fedynyshyn, G.W. Grynkewich, B.A. Chen and T.P. Ma, "The effect of metal masks on the plasma etch rate of silicon", J. Electrochem. Soc., **136**, 1799-804 (1989).

114. J.W. Coburn, "Plasma-assisted etching", Plasma Chem. Plasma Process., **2**, 1-41 (1982).

115. N. Selamoglu, J.A. Mucha, D.L. Flamm and D.E. Ibbottson, "Catalysed gaseous etching of silicon", Mat. Res. Symp. Proc. 75, 459-65 (1987).

116. N. Selamoglu, J.A. Mucha, D.L. Flamm and D.E. Ibbottson, "Copper-catalysed etching of silicon by F_2: Kinetics and feature morphology", J. Appl. Phys., **64**, 1494-8 (1988).

117. Y.H. Lee and M.-M. Chen, "Silicon doping effects in reactive plasma etching", J. Vac. Sci. Technol. B, **4**, 468-75 (1986).

118. H.F. Winters and D. Haarer, "Influence of doping on the etching of Si(111)", Physical Review B, **36**, 6613-23 (1987).

119. J.A. Yarmoff and F.R. McFeely, "Effect of sample doping level during etching of silicon by fluorine atoms", Physical Review B, **38**, 2057-62 (1988).

120. J. Perrin, B. Despax, V. Hanchett and E. Kay, "Microstructure and electrical conductivity of plasma deposited gold/fluorocarbon composite films", J. Vac. Sci. Technol A, **4**, 46-51 (1986).

121. M.M. Millard and E. Kay, "Difluorocarbene emission spectra from fluorocarbon plasmas and its relationship to fluorocarbon polymer formation", J. Electrochem. Soc., **129**, 160-5 (1982).

122. R. d'Agostino, F. Cramarossa and S. De Benedictis, "Diagnostics and decomposition mechanism in radio-frequency discharges of fluorocarbons utilised for plasma etching or polymerisation", Plasma Chem. Plasma Process., **2**, 213-31 (1982).

123. E.A. Truesdale and G. Smolinsky, "The effect of added hydrogen on the rf discharge chemistry of CF_4, CF_3H, and C_2F_6", J. Appl. Phys., **50**, 6594-9 (1979).

124. R. d'Agostino, S. De Benedictis and F. Cramarossa, "Radiofrequency plasma decomposition of C_nF_{2n+2}-H_2 and CF_4-C_2F_4 mixtures during Si etching or fluoropolymer deposition", Plasma Chem. Plasma Process., **4**, 1-14 (1984).

125. R. d'Agostino, F. Cramarossa, V. Colaprico and R. d'Ettole, "Mechanisms of etching and polymerisation in radiofrequency discharges of CF_4-H_2, CF_4-C_2F_4, C_2F_6-H_2, C_3F_8-H_2", J. Appl. Phys., **54**, 1284-8 (1983).

126. S.W. Butler, I. Trachtenberg and T.F. Edgar, "Mechanisms and modelling of plasma polymerization", ECS Spring Meeting, Symposium on Plasma Processing, Montreal (1990).

127. H.S. Munro and C. Till, "The surface photopolymerization of perfluorobenzene and photocopolymerization of perfluorobenzene/benzene: a possible model for plasma polymerization", J. Polym. Sci.: Part A: Polym. Chem., **26**, 2873-80 (1988).

128. A.J. Bariya, H. Shan, C.W. Frank, S.A. Self and J.P. McVittie, "The etching of CHF_3 plasma polymer in fluorine-containing discharges", J. Vac. Sci. Technol. B, **9**, 1-7 (1991).

129. T. Arikado and S. Horiuchi, "Etching mechanism of SiO_2 in CF_4/H_2 mixed gas plasma", Proc. of the lst. Symp. on Plasma Processing, Electrochem. Soc. proceedings vol. V81(1), 66-74 (1981).

130. D.T. Clark and D.R. Hutton, "Surface modification by plasma techniques. I. The interactions of a hydrogen plasma with fluoropolymer surfaces", J. Polym. Sci.: Part A: Polym. Chem., **25**, 2643-64 (1987).

131. "'New chemistry' overcomes problems of diamond films", R&D News, R&D Magazine, 24 (January 1991).

132. E. Kay, J. Coburn and A. Dilks, "Plasma chemistry of fluorocarbons as related to plasma etching and plasma polymerisation", *Plasma Chemistry 3*, edited by S. Veprek, Topics in Current Chemistry, **94**, 1-42 (1980).

133. M.J. Davies, Catalyst Unit, Harwell Laboratory, private communication (1991).

134. C. Laurent, E. Kay and N. Souag, "Dielectric breakdown of polymer films containing metal clusters", J. Appl. Phys., **64**, 336-43 (1988).

135. U. Hetzler and E. Kay, "Conduction mechanism in plasma-polymerised tetrafluoroethylene films", J. Appl. Phys., **49**, 5617-23 (1978).

136. L. Solymar and D. Walsh, *Lectures on the Electrical Properties of Materials (third edition)*, Oxford University Press, Oxford (1984), pp. 262-7.

137. H. Yasuda, *Plasma Polymerisation*, Academic Press, London (1985), pp. 370-3.

138. J.P. Booth, O. Joubert and J. Pelletier, "Oxygen atom actinometry reinvestigated: Comparison with absolute measurements by resonance absorption at 130 nm", J. Appl. Phys., **69**, 618-26 (1991).

139. G. Hancock and M.J. Toogood, "Laser-induced fluorescence of oxygen atoms in a plasma reactor", Appl. Phys. Lett, **60**, 35-7 (1992).

140. G. Baravian, Y. Chouan, A. Ricard and G. Sultan, "Doppler-broadened H_α line shapes in a rf low-pressure H_2 discharge", J. Appl. Phys., **61**, 5249-53 (1987).

141. G. Hancock, J.P. Sucksmith and M.J. Toogood, "Plasma kinetic measurements using time-resolved actinometry: Comparisons with laser-induced fluorescence", J. Phys. Chem., **94**, 3269-72 (1990).

Appendix 1

Possible limitations of the technique of optical emission spectroscopy with argon actinometry.

The application of argon actinometry to optical emission spectroscopy (OES) to yield quantitative data on the relative concentrations of gas phase species in plasma discharges was described in chapter 2 (section 2.2).

Harshbarger et al.[66] first used OES to study silicon and silicon nitride etching in CF_4-O_2 mixtures. They found that oxygen additions to a CF_4 plasma enhanced the etch rate of these materials by the liberation of atomic fluorine. Their results, though, were qualitative as the emission intensity of an excited species is a function of both its ground state concentration and the electron energy distribution function (eedf) of the plasma. The eedf may vary with changes in the plasma parameters. In order to overcome this problem, Coburn and Chen[67] devised a method, referred to as "actinometry", for correlating emission intensities to reactive particle density. It involves the deliberate addition of a small constant amount of a noble gas, the actinometer, to a plasma and monitoring the noble gas emissions concurrently with those of the reactive particle. If the excited state responsible for the noble gas emission matches closely in energy with the level of the reactive particle, then the same group of electrons will be responsible for the excitation of both levels. By comparing the emission intensities from the actinometer and reactive particle, the relative changes in ground state concentration of the latter can be assessed. Ideally the excited states should also be produced by direct electron impact only, and decay exclusively by photoemission. Coburn and Chen applied their method to atomic-F (703.7 nm; 14.5 eV) with argon as an actinometer (750.4 nm; 13.5 eV).

In practice, actinometry has been applied even when the above conditions are violated. For example, d'Agostino et al.[68] studying the CF_4-O_2 system validated the use of argon actinometry for the measurement of F, O, CO and CO_2 concentrations from emitting levels in the range 8-20 eV by comparing two actinometers Ar (750.4 nm; 13.5 eV) and N_2 (380.5 nm; 11.5 eV). The trends in the two actinometers were coincident, implying that their relative emission intensities were proportional to the electron density in a broad energy range. The technique was similarly extended to CF_2 (4.5 eV)[69].

However, whilst the technique has proved extremely popular, mainly due to its ease of application, there is increasing doubt as to its validity. The principle area of concern is the production of the emitting excited states by routes other than direct electron impact, e.g dissociative excitation or dissociative ionization. A number of papers pertinant to species discussed in this thesis are described below.

(a) O-atoms.

Argon actinometry for the determination of O-atom concentrations in CF_4-O_2 plasmas has been tested directly using two-photon laser induced fluorescence (LIF) by Walkup et al.[70]. They found that at high O_2 concentrations (not studied in this thesis) the O(844.6 nm)/Ar(750.4 nm) intensity ratio followed the changes in O-atom concentration observed by LIF but the O(777.4 nm)/Ar(750.4 nm) ratio did not. Both O(777.4 nm) and O(844.6 nm) are produced by direct electron impact excitation of atomic oxygen and dissociative excitation of molecular oxygen. However, the O(844.6 nm) emission line is a much better indicator of O-atom concentration than the O(777.4 nm) emission line because the cross section for direct excitation of O(844.6 nm) is much

larger than that for O(777.4 nm) whereas the opposite is true for the dissociative excitation cross sections.

Booth et al.[138] measured oxygen atom concentrations in SF_6/O_2 discharges by resonance absorption at 130 nm, as a function of percentage SF_6, and compared the results to those obtained by optical emission actinometry measurements. They found that the addition of 10% SF_6 to a pure oxygen discharge increased the O-atom concentration by a factor of 4.5, whereas the actinometry signal only increased by 20% giving clear evidence of dissociative excitation of O_2. At higher SF_6 concentrations the O(844 nm) actinometry signal was well correlated with [O]. They propose, however, that a high proportion of the O(844 nm) emission still comes from dissociative excitation of O_2. The concentrations of both O_2 and atomic oxygen will decrease due to dilution with increasing proportions of SF_6, and thus also the contributions to the O(844 nm) actinometry signal from the dissociative excitation and the direct electron impact mechanisms respectively. The correlation between I_O/I_{Ar} and [O] is therefore fortuitous.

Most recently, Hancock and Toogood[139] used two-photon laser induced fluorescence to measure oxygen atom concentrations in a 90.25% O_2, 4.75% CF_4, 5% Ar discharge as a function of RF power to test the validity of the actinometry technique directly. In agreement with the previous workers, they found that both excitation of O-atoms and dissociative excitation of O_2 contributed to the O(844 nm) emission. They also found that the actinometric technique was particularly inaccurate when conditions are changed so that the fraction of O_2 dissociated alters markedly, e.g. by increasing the RF power.

(b) H-atoms

Doppler broadening of H_α emissions in a pure hydrogen discharge was studied by Baravian et al.[140] using high resolution (0.004 nm) emission spectroscopy. The line was found to consist of a central peak emerging from a pedestal of two plateaus, and by large wings. They attribute the form of this complex line shape to the several mechanisms responsible for the production of H atoms in the excited state n=3 which lead to the H_α emission:

(i) the dissociative excitation of H_2

$$e + H_2 \rightarrow e + H_2^*$$

$$H_2 \rightarrow H^*(n=3) + H$$

(ii) the dissociative ionization of H_2

$$e + H_2 \rightarrow 2e + H_2^+$$

$$H_2^+ \rightarrow H^*(n=3) + H^+$$

(iii) the electron-impact excitation of H atoms

$$e + H \rightarrow H^*(n=3) + e$$

The H_α emission is then produced by the reaction:

$$H^*(n=3) \rightarrow H^*(n=2) + h\nu(H_\alpha)$$

The photons produced from processes (i) and (ii) are denoted the "molecular H_α", and from process (iii) the "atomic H_α". Baravian et al. have calculated the ratio atomic H_α to molecular H_α and found it to be greater than unity for electronic temperatures greater than 3 eV, i.e. temperatures typically found in RF discharges.

(c) CF_2 radicals

Hancock et al.[141] used laser-induced fluorescence (LIF) to test the validity of the actinometric technique for CF_2 radicals in a CF_4 plasma. They varied the ground state concentration of CF_2 by changing the applied RF power between 10 and 200 W, at three pressures - 50, 100 and 200 mtorr - and compared the LIF and actinometric signals (figure 55). It can be seen that at high pressures and powers the correlation between the two signals is poor. The discontinuity in the 200 mtorr data is mainly a result of a change in the optical emission signal from CF_2. (N.B. no such discontinuity was seen in this work for a C_3F_8 discharge under similar conditions (figure 31).)

As already stated, if the excited state responsible for the actinometer emission matches closely in energy with the level of the reactive particle, then the same group of electrons will be responsible for the excitation of both levels. However, CF_2 and Ar have widely differing electronic excitation thresholds (5 and 14 eV respectively). Hancock et al. also added a second actinometer, neon, to the system, and compared the emissions from Ne (excitation threshold 18 eV) to those from Ar as a function of RF power. Their results indicated that an increase in power caused a larger increase in the fraction of electrons with energy greater than 18 eV than those with energy greater than 14 eV. They note that the change in electron energy distribution function itself is sufficient to question the use of actinometry for CF_2 because of the large difference between threshold energy of this species and those of the rare gas actinometers.

Conclusion

Optical emission spectroscopy with argon actinometry was the chosen/available plasma gas-phase diagnostic technique for the work contained within this thesis. It was used to measure the relative concentrations of various species as a function of process gas composition and operating conditions. Although it is a popular and readily applied, non-invasive technique, a growing body of literature has cast some doubt on its validity. The principle causes for concern are:

(i) the production of the emitting excited states by routes other than direct electron impact, e.g dissociative excitation or dissociative ionization;

(ii) the presence of large differences in excitation threshold between the actinometer and the species of interest, particularly under plasma conditions likely to lead to variations in the electron energy distribution function.

Nonetheless, perhaps fortuitously, actinometry has generally predicted the correct trends in relative concentrations of gas phase species.

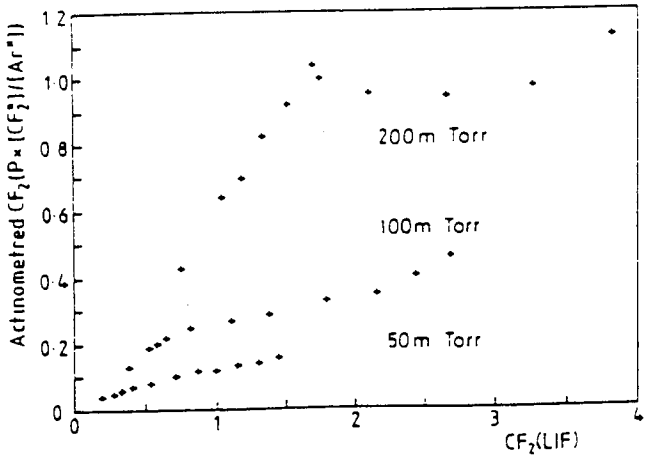

Figure 55 Variation of the signal from electronically excited CF_2 (CF_2^*, measured by actinometered optical emission) with that from CF_2 (measured by LIF) at pressures P = 50, 100, and 200 mTorr, varying the power from 10 to 200 W to change the radical concentration. The factor P allows the actinometered CF_2^* signal to be corrected for changes in concentration of Ar as pressure is varied.

Appendix 2

Optical Emission Spectra

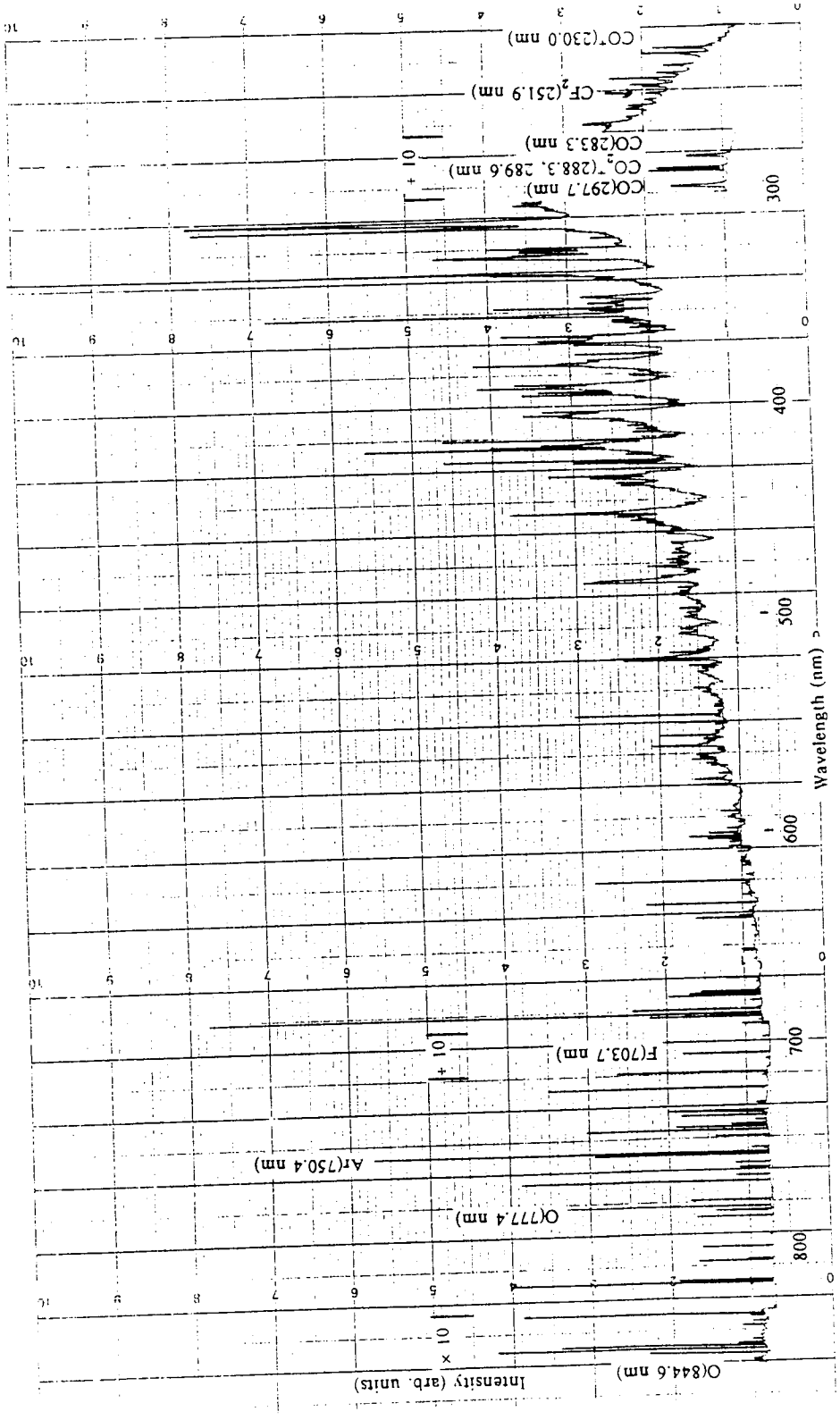

Figure 56. Optical emission spectrum; CF_4, 10% O_2, 5%Ar plasma.

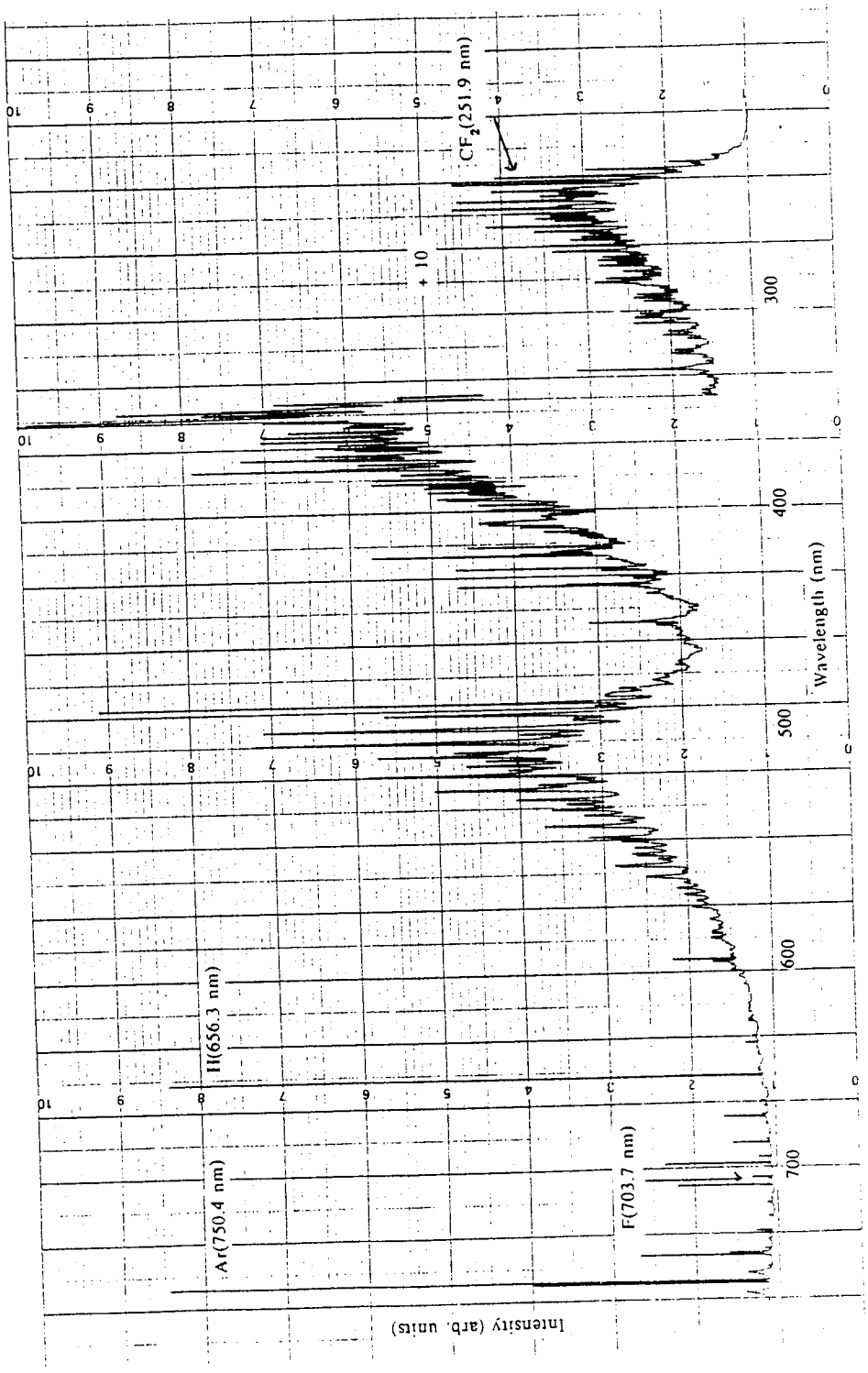

Figure 57. Optical emission spectrum. CHF_3, 5% Ar plasma.